(2)

Annual Technical Progress Report[1]

Covering period:
Nov. 1, 1991 - Oct. 31, 1992

Contract N00014-91-J-1461

Principal Investigators:
Dr. Yih-Fang Huang and Ruey-wen Liu

Department of
ELECTRICAL ENGINEERING

UNIVERSITY OF NOTRE DAME, NOTRE DAME, INDIANA

Annual Technical Progress Report[1]

Covering period:
Nov. 1, 1991 - Oct. 31, 1992

Contract N00014-91-J-1461

Principal Investigators:
Dr. Yih-Fang Huang and Ruey-wen Liu

[1]This report is a reproduction of Dr. Victor C. Soon's Ph.D. Dissertation submitted in August, 1992, to the Graduate School of the University of Notre Dame, Notre Dame, IN. Distribution of this report is unlimited.

ARRAY SIGNAL PROCESSING UNDER MODEL ERRORS WITH APPLICATION TO SPEECH SEPARATION

Abstract

by

Victor C. Soon

In recent years there have been increasing interest in eigenstructure based array signal processing techniques especially in the areas of radar and sonar processing and in signal separation applications as found in communications or speech acquisition/enhancement. However, model errors are not accounted for in these methods. Unfortunately, the problem of model error is a ubiquitous part of real systems: they arise from such phenomena as non-ideal sensor characteristics (eg., sensor calibration errors in phase and gain, etc.), unknown source characteristics and locations, etc. This report is broadly divided into two parts. The first part examines the effects of model errors on the performance of existing eigenstructure based methods in array signal processing. A statistical analysis of the ESPRIT (Estimation of Signal Parameters via Invariance Techniques) algorithm under random model errors is performed. The analysis provides interesting insight into the sensitivity of ESPRIT to model errors: in particular, for uniform linear arrays of sensors, it is found that the mean square error of DOA (direction of arrival) estimates found using ESPRIT is almost totally dependent on errors in sensor phases and not that of sensor gains. The second part of the report deals with the development of algorithms that take model errors into account. Two approaches are proposed. The first is based on a signal subspace constraint on the possible set of model parameters as determined from the array covariance. This constraint is incorporated into an iterative procedure which calibrates

the array under model errors and unknown source signals. The second approach incorporates blind identification and clustering for the source estimation problem under model errors or uncertainties. The proposed approach is shown to be robust to the *silmutaneous* presence of such uncertainties such as unknown sensor and channel gains, unknown combinations of near-field and far-field sources, unknown combinations of narrowband and wideband sources, unknown source spectral characteristics and unknown number of sources.

Contents

List of Figures

ACKNOWLEDGEMENTS

This dissertation has been supported in part by the Office of Naval Research under contract N00014-J-91-1461.

I have been extremely lucky thus far in life - I have had the opportunity to study here at Notre Dame and to live with and to know a lot of good people, both within the academic setting and within the community. I do not believe it to be an exaggeration to say that my decision years ago to come here for graduate school was one of the best choices I have ever made.

I wish to thank my advisor Dr. Yih-Fang Huang: I am grateful for his guidance and assistance throughout the years here and I regard him as a friend. I wish also to thank Dr. Ruey-wen Liu for his help and for being on my committee. Thanks also to the other committee members, Dr. Peter Bauer and Dr. Ken Sauer, to Dr. Daniel J. Costello for serving on my thesis proposal committee and to Dr. John J. Uhran for his kind help. I salute a friend who I had shared an office with and throughout the years, had shared both research directions and countless arguments about life: Dr. Lang Tong.

Grace (in as far as I understand the term) is given to someone regardless of the particular merits of the person. This is at least true for me, for I feel that unmerited grace is the sole reason for my good fortune in knowing the people that I do here. Of all of them, I owe the biggest debt to two friends: Shawn Murphy-Allan and John Perna. Friendship with them has been and continue to be life-giving and my debt to them is larger than I (or they) will ever know. My gratitude goes out to all the friends that have made life here both fulfilling and invigorating. One hardly knows how to thank the source of such grace but hopefully one lives a life that resonates such an awareness and gratitude for the mystery.

1

INTRODUCTION

The processing of signals obtained from arrays of sensors is of interest in a wide range of problems in radar and sonar processing where the presence or absence of source signals, their direction-of-arrivals (DOA), signal power, etc. are of interest (see eg. [53, 50, 83], in speech recognition and teleconference applications where source signals from spatially distributed locations are to be separated from mixed measurements (the so called "cocktail party problem"), see eg. [25, 36, 32, 12, 16, 57, 22]. In communications one may be interested in extracting a desired signal from jammer-contaminated measurements, see eg., [11]. In biomedical signal processing a set of measurements taken from an array of electrodes may be processed to extract signals from individual neuronal firings, etc. The rapidly expanding demand for mobile communications such as in cellular telephone technology provides an interesting area of possible application for array signal processing techniques where their capability of resolving signals based on their spatial locations may make it possible to increase channel capacity, see eg., [66]. In radio astronomy, arrays of radio observatories are used in obtaining higher resolution maps of galaxies and quasars. Radar imaging is also one application where array signal processing is used.

In most of these applications a common model is assumed to adequately model the

physical processes in the applications. When assumptions of the techniques in array signal processing are satisfied, these techniques are capable of providing superior performance as compared to conventional methods. This is the case in DOA estimation where the modern eigenstructure based methods are capable of resolving DOA angles separations that are much smaller than the conventional (classical) beamforming method which is limited to the Rayleigh resolution limit. These techniques however are dependent on model assumptions that may not be true in actual systems, i.e., model errors are not accounted for in these methods. Unfortunately, the problem of model error is a ubiquitous part of real systems: they arise from such phenomena as non-ideal sensor characteristics (eg., sensor calibration errors in phase and gain, etc.), errors in the locations and orientation of the sensors within the array, source characteristics that deviate from the assumed source model (eg., sources are not ideal point sources, intensity of sources may favor certain direction of propagation resulting in unequal intensities observed at different sensors), channel inhomogenities, sources *in the near-field, etc.*

The goal of this report is thus to study the problem of array signal processing under model uncertainties. A performance analysis of the ESPRIT (Estimation of Signal Parameters via Rotational Invariance Techniques) , a popular eigenstructure based method, under random model uncertainties is undertaken to further understand its robustness to model errors. Two techniques are then proposed for this problem: the first is based on a signal subspace constraint on the possible sets of model errors and DOA angles while the second is based on the incorporation of blind identification techniques with clustering techniques. The integration of these techniques and ideas may make it possible to apply array signal processing under less ideal conditions.

Chapter 2 presents the model formulation for the array signal processing problem and its areas of application. Chapter 3 covers the basic mathematical machinery

needed for the study in the report. Chapter 4 gives a broad overview of various aspects of array signal processing, from conventional methods to eigenstructure based methods and other aspects such as model order estimation and extensions for coherent and wideband situations. Chapter 5 presents the performance analysis of ESPRIT under random model errors. Chapter 6 contains the signal subspace approach to array signal processing under model errors. Chapter 7 presents an approach based on the incorporation of blind identification and clustering techniques to solve the problem.

2

MODEL FORMULATION

In this chapter, we shall cover the basic model formulation of the array signal processing problem. Narrowband and wideband formulations are then discussed. Model parameters such as time delays, direction-of-arrival angles of source signals and channel coefficients are then looked at. In the final section areas of application for array signal processing methods are examined.

2.1 Notations and Preliminaries

Throughout this thesis, we assume the following notational convention: All matrix quantities will be denoted by upper case bold faced symbols while vector quantites will be denoted by lower case bold faced symbols. Also,

- $(.)^t$ - Transpose of (.)
- $(.)^\dagger$ - Complex conjugate transpose of (.)
- $(.)^{-1}$ - Inverse of (.)
- $(.)^\#$ - Pseudo-inverse of (.)
- $\| \mathbf{M} \|_F$ — Frobenius norm of $\mathbf{M}$

- $\| \mathbf{v} \|$ — Euclidean norm of the vector $\mathbf{v}$.
- $\| \mathbf{M} \|_2$ - 2-norm of matrix $\mathbf{M}$
- m — Number of sensors within array
- n — Number of sources
- (μ_i, ν_i) — Location of i-th sensor in array
- τ_{ik} — Time delay of k-th source signal at i-th sensor.
- θ_k — Direction-of-arrival of k-th source signal measured relative to ν-axis.

We write the general formulation of the problem in the following manner. Let the i-th sensor output be denoted by

General Model

$$x_i(t) = \sum_{k=1}^{n} a_{ik} s_k(t - \tau_{ik}) + \eta_i(t), \; i = 1, 2, \cdots, m. \tag{2.1}$$

where

a_{ik} : channel coefficient

s_k : k-th source signal

$\eta_i(t)$: additive noise at i-th sensor.

τ_{ik} : Time delay at i-the sensor of k-th source.

Fig. 2.1 shows the model.

The channel coefficients are the result of the sensor and source characteristics - i.e. the sensors and sources directionality, sensitivity, gains, phases, etc. and channel parameters, inhomogeneities, etc. The time delays are due to the spatial distribution of the sensors and locations of the source signals - they are functions of sensor

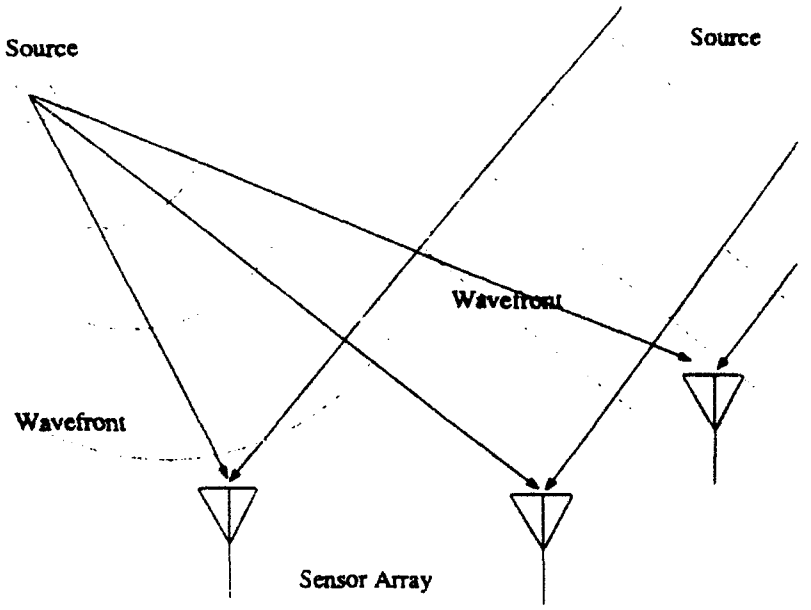

Figure 2.1: Array Signal Processing Model

locations, source locations, distance between sensors, etc. Propagation of the signals through the channel can be far-field or near field or any combination thereof.

The general problem which is wideband in form is such that the channel and signal components cannot be separated in the time-domain. However, under narrowband conditions (which will be discussed in the next section), $s_k(t)$ may be assumed to be **baseband** and the model written as:

Narrowband Model

$$\mathbf{x}(t) = \mathbf{A}\mathbf{s}(t) + \eta(t) \tag{2.2}$$

$$\mathbf{A} = \begin{bmatrix} a_{11}e^{-j\omega_0\tau_{11}} & \cdots & a_{1n}e^{-j\omega_0\tau_{1n}} \\ a_{21}e^{-j\omega_0\tau_{21}} & \cdots & a_{2n}e^{-j\omega_0\tau_{2n}} \\ \vdots & \cdots & \vdots \\ a_{m1}e^{-j\omega_0\tau_{m1}} & \cdots & a_{mn}e^{-j\omega_0\tau_{mn}} \end{bmatrix} \tag{2.3}$$

where ω_0 is the **center frequency** of the signals.

The specific form of the parameterization of the time delays will be elaborated on in the sequel.

The following assumptions will be assumed to hold for all the coming discussions in this thesis.

Assumptions

(A1) The matrix **A** in Eqn. (2.3) has full column rank.

(A2) $\mathbf{s}(t)$ is zero mean stationary with a positive definite covariance matrix.

(A3) $\eta(t)$ is additive white Gaussian noise, mutually uncorrelated with $\mathbf{s}(t)$.

(A4) The number of sources, n is assumed known or estimated previously.

2.2 Narrowband and Wideband Formulations

As from Eqn. (2.1)

$$x_i(t) = \sum_{k=1}^{n} a_{ik} s_k(t - \tau_{ik}),\ i = 1, 2, \cdots, m. \tag{2.4}$$

If $s_k(t)$ is **bandlimited** with center frequency ω_0, we write

$$s_k(t) = \tilde{s}_k(t) \cos(\omega_0 t + \phi_k(t))$$

where $\tilde{s}_k(t)$ denotes the envelope of $s_k(t)$ and $\phi_k(t)$ denotes the phase associated with $s_k(t)$.

Under **narrowband** assumptions on $s_k(t)$, the time delays τ_{ik} are small enough such that $\tilde{s}_k(t) \simeq \tilde{s}_k(t - \tau_{ik})$ and $\phi_k(t) \simeq \phi_k(t - \tau_{ik})$.

Definition: A baseband signal $\tilde{s}_k(t)$ is said to be *narrowband* if the reciprocal of its highest frequency component is much larger than the maximum delay time of the signal propagating through the sensor array in question, see also [78].

The signal is said to be *wideband* if it is not narrowband.

Thus by demodulating the received signal at the $i-th$ sensor down to the baseband level through a quadrature demodulator and passing the results through low pass filters, we can write the outputs as:

$$\text{In} - \text{Phase} - \text{Component} : x_i(t) = \sum_{k=1}^{n} a_{ik} cos(\omega_0 \tau_{ik} + \phi_k(t)) \tilde{s}_k(t) \tag{2.5}$$

$$\text{Quadrature} - \text{Phase} - \text{Component} : x_i(t) = -\sum_{k=1}^{n} a_{ik} sin(\omega_0 \tau_{ik} + \phi_k(t)) \tilde{s}_k(t) \tag{2.6}$$

Combining both the in-phase and quadrature-phase components we can write the complex valued i-th sensor output as

$$x_i(t) = -\sum_{k=1}^{n} a_{ik} e^{-j\omega_0 \tau_{ik}} \tilde{s}_k(t) e^{-\phi_k(t)} \tag{2.7}$$

Remark: The result of the quadrature de-modulation of a real valued white gaussian noise is circular complex valued uncorrelated gaussian noise, see [35].

Writing the array observations as a vector, we get Eqn.(2.2)

$$\mathbf{x}(t) = \mathbf{A}\mathbf{s}(t) + \eta(t) \tag{2.8}$$

Here $\mathbf{s}(t) = [\tilde{s}_1(t)e^{-j\phi_1(t)} \cdots \tilde{s}_n(t)e^{-j\phi_n(t)}]^T$ is the source signal vector and $\eta(t) = [\eta_1(t) \cdots \eta_m(t)]$ is the additive observation noise vector. Also,

$$\mathbf{A} = \begin{bmatrix} a_{11}e^{-j\omega_0\tau_{11}} & \cdots & a_{1n}e^{-j\omega_0\tau_{1n}} \\ a_{21}e^{-j\omega_0\tau_{21}} & \cdots & a_{2n}e^{-j\omega_0\tau_{2n}} \\ \vdots & \cdots & \vdots \\ a_{m1}e^{-j\omega_0\tau_{m1}} & \cdots & a_{mn}e^{-j\omega_0\tau_{mn}} \end{bmatrix} \tag{2.9}$$

where ω_0 is the **center frequency** of the signals. Fig.2.2 shows a block figure diagram of the quadrature demodulator.

Under wideband conditions, the assumption $\tilde{s}_k(t) \simeq \tilde{s}_k(t-\tau_{ik})$ and $\phi_k(t) \simeq \phi_k(t-\tau_{ik})$ are no longer valid and the array observations may no longer be written in the

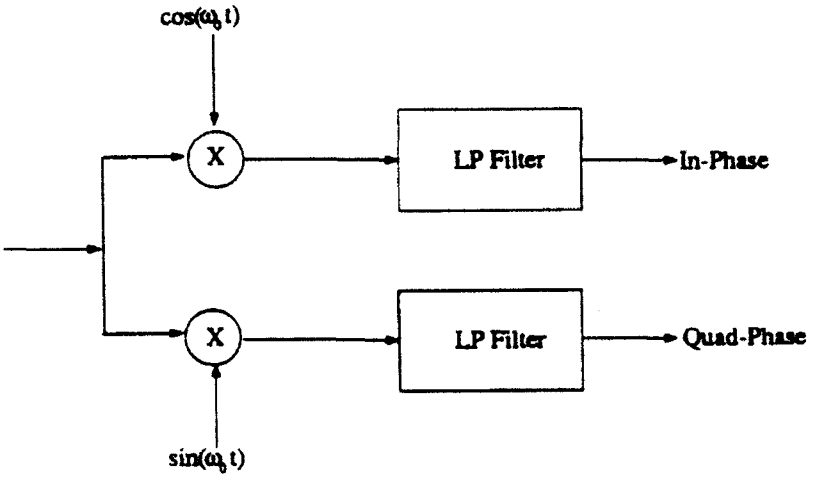

Figure 2.2: Quadrature Demodulator Block Diagram

form of Eqn. (2.8), at least not in the time-domain. However, by taking the Fourier Transform of the general array observations, we get

$$\mathbf{x}(\omega) = \mathbf{A}(\omega)\mathbf{s}(\omega) + \eta(\omega) \tag{2.10}$$

$$\mathbf{A} = \begin{bmatrix} a_{11}e^{-j\omega\tau_{11}} & \cdots & a_{1n}e^{-j\omega\tau_{1n}} \\ a_{21}e^{-j\omega\tau_{21}} & \cdots & a_{2n}e^{-j\omega\tau_{2n}} \\ \vdots & \cdots & \vdots \\ a_{m1}e^{-j\omega\tau_{m1}} & \cdots & a_{mn}e^{-j\omega\tau_{mn}} \end{bmatrix} \tag{2.11}$$

where ω denotes frequency in radians. The matrix $\mathbf{A}$ is usually referred to as the steering matrix in the literature.

2.3 Time delays, τ_{ik} and Direction-of-arrivals (DOA), θ_k Relations

In this section, the form of the time delays τ_{ik} will be discussed. Due to the spatial distributions of the sources and sensors, different sensors will observe the same signal

at different time delays. Thus, by selecting the location of the reference sensor as $(0,0)$, the k-th source signal will be observed at the time delay value τ_{ik} at the i-th sensor. The direction of arrival of the k-th source, denoted by θ_k, is defined with reference to the vertical (ν) axis at the reference sensor. Without any loss of generality one can select the reference sensor location as the origin.

There are two cases of interest.

Far-Field: Consider the far-field case, i.e., the plane wave propagation assumption is valid, see Fig. 2.3. From Fig.2.3, it can be easily shown through simple analytical geometry that,

$$\tau_{ik} = \frac{1}{c}\{\nu_i \cos\theta_k + \mu_i \sin\theta_k\} \tag{2.12}$$

where c denotes the velocity of propagation of the signal.

Example (Uniform Linear Array): The uniform linear array (ULA) is an important special case in array signal processing. It corresponds to the case where ther sensors are aligned in a single axis and spaced with equal distance d between adjacent sensors, see Fig.2.4. In this case, the time delays may be written as:

$$\tau_{ik} = \frac{(i-1)d\sin\theta_k}{c} \tag{2.13}$$

When the channel coefficients a_{ik} are all equal to 1.0, the form of the steering matrix $\mathbf{A}$ from (2.11) is written as

$$\mathbf{A} = \begin{bmatrix} e^{-j\omega\tau_1(0)} & \cdots & e^{-j\omega\tau_n(0)} \\ e^{-j\omega\tau_1(1)} & \cdots & e^{-j\omega\tau_n(1)} \\ \vdots & \cdots & \vdots \\ e^{-j\omega\tau_1(m-1)} & \cdots & e^{-j\omega\tau_n(m-1)} \end{bmatrix} \tag{2.14}$$

where $\tau_k \equiv \frac{d\sin\theta_k}{c}$. The steering matrix $\mathbf{A}$ in this case has a special form called *Vandermonde*. It has been shown that it has full column rank when the $\{\tau_k\}$ terms are distinct.

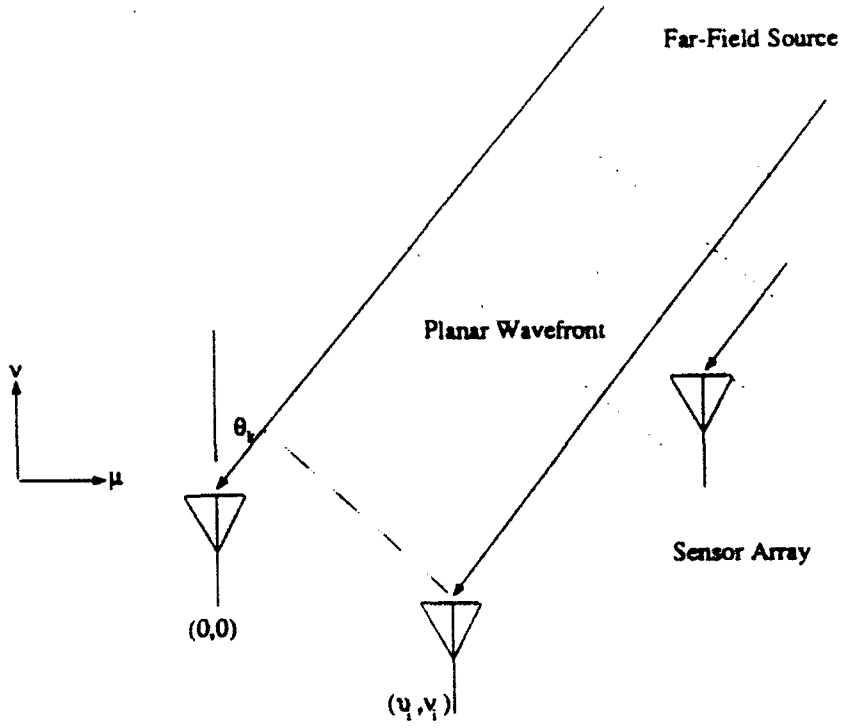

Figure 2.3: Far-Field Propogation

Near-Field: For the case where the far-field assumption does not hold the wavefronts cannot be assumed to be planar but rather are spherical. Fig. 2.5 shows the situation in the near field. The form for the time delay is then written as

$$\tau_{ik} = \tau_{ik}(\text{far} - \text{field}) - \frac{1}{2Rc}\{(\mu_i \sin\theta_k + \nu_i \cos\theta_k)^2 - \frac{1}{2Rc}(\nu_i^2 + \mu_i^2)\} \qquad (2.15)$$

where $\tau_{ik}(\text{far} - \text{field})$ is the time delay assuming far-field propagation and R is the range or distance of the source signal from the reference sensor, see also [17]. From Eqn.(2.15) it can be seen that the near-field time delay has a correction term $(1/R)$ due to the curvature of the propagating wave. It is obvious that as the range gets very large, the time delay approaches the far-field form.

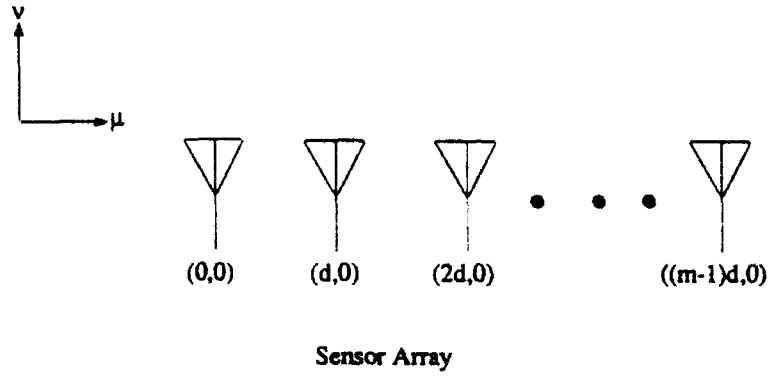

Figure 2.4: Uniform Linear Array (ULA)

2.4 Channel Coefficients Relations

The channel coefficients a_{ik} terms are a result of the combined effects of the channel attenuation characteristics, the sensor characteristics gains and the geometrical attenuation due to wave propagation.

Channel Attenuation: The channel attenuation characteristics are dependent on the type of channel in question, for example it may be the atmospheric channel for radar, underwater sea channel for sonar or the air sound channel for speech applications. The physical process by which a source signal is attenuated through these channels are often highly complex and difficult to model. In underwater sonar channels, signal attenuation is caused by a combination of molecular relaxation processes (such as chemical relaxation in salt water) and frictional heat losses due to the

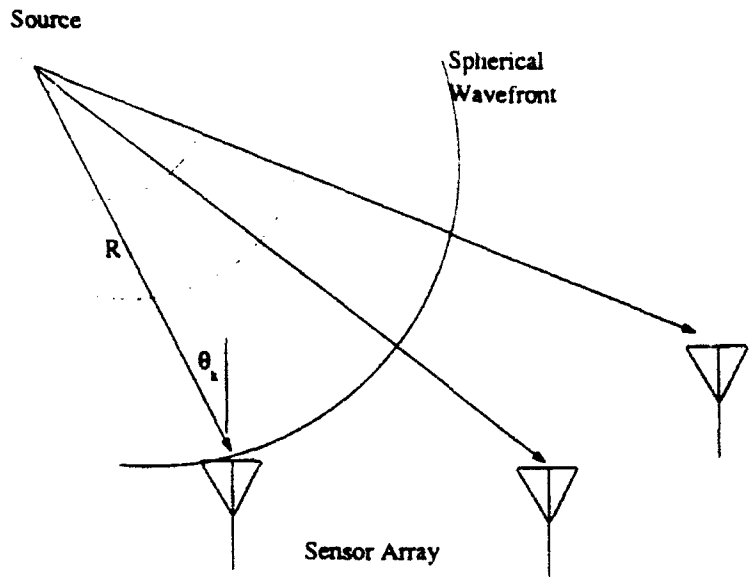

Figure 2.5: Near-Field Propagation

relative motion of portions of the transmission medium, see [9, 49].

Sensor Gains: The sensor gains are due to the combined effects of the sensor receiving characteristics, the gains of the amplifiers and the subsequent conditioning done on the signals such as quadrature de-modulating, etc.

Geometrical Attenuation: The physics of wave propagation in electromagnetic and acoustic theory is governed by the wave equation (a d'Alembertian equation), with vector quantities in electromagnetism and scalar quantities in acoustics. When a spherical propagation mode is assumed in the wave equation, the intensity of the k-th signal at the i-th sensor is inversely proportional to R_{ik} which is the radial distance of the k-th source to the i-th sensor, see for example [55, 49]. Thus the channel coefficient a_{ik} are inversely proportional to R_{ik}. Generally, it is clear that the channel coefficients are not equal to each other since R_{ik} s are not the same. However, in the case where the dimensions of the array are small in comparison to the distances R_{ik}, the geometrical attenuations may be assumed to be approximately equal.

2.5 Areas of Interest and Application of Model

The general model and the narrowband model of Eqns.(2.10),(2.8) and the associated parameters are a focus of interest in many applications. For example, the time delays and DOAs of the various source signals are of interest in radar and sonar processing while the source signals themselves are of interest in communications applications.

2.5.1 Array Signal Processing for DOA Estimation

In this application, the DOA of various source signals are of interest. When the channel coefficients are known , or normalized to unity, or the sensors in the array are identical the models can be further simplified to the following.

Wideband Model

$$\mathbf{x}(\omega) = \mathbf{A}(\omega)\mathbf{s}(\omega) + \eta(\omega) \tag{2.16}$$

$$\mathbf{A} = \begin{bmatrix} e^{-j\omega\tau_{11}} & \dots & e^{-j\omega\tau_{1n}} \\ e^{-j\omega\tau_{21}} & \dots & e^{-j\omega\tau_{2n}} \\ \vdots & \dots & \vdots \\ e^{-j\omega\tau_{m1}} & \dots & e^{-j\omega\tau_{mn}} \end{bmatrix} \tag{2.17}$$

where ω denotes frequency in radians.

Narrowband Model

$$\mathbf{x}(t) = \mathbf{A}\mathbf{s}(t) + \eta(t) \tag{2.18}$$

$$\mathbf{A} = \begin{bmatrix} e^{-j\omega_0\tau_{11}} & \dots & e^{-j\omega_0\tau_{1n}} \\ e^{-j\omega_0\tau_{21}} & \dots & e^{-j\omega_0\tau_{2n}} \\ \vdots & \dots & \vdots \\ e^{-j\omega_0\tau_{m1}} & \dots & e^{-j\omega_0\tau_{mn}} \end{bmatrix} \tag{2.19}$$

where ω_0 is the **center frequency** of the signals.

Thus given the observation of $\mathbf{x}(t)$ over N snapshots or samples, the objective is to estimate the DOA angles θ_k, for $k = 1, .., n$.

2.5.2 Spectrum Estimation

There is a duality between the estimation of multiple complex sinusoids in noise and the estimation of DOAs using uniform linear arrays. The scalar observation can be written as

$$x(t) = \sum_{i=1}^{n} e^{-j(\omega_i t + \phi_i)} s_i + \eta(t) \tag{2.20}$$

where ω_i denotes the frequency (in radians) of the i-th sinusoid, ϕ_i denotes the phase of the i-th sinusoid and s_i denotes the intensity of the i-th sinusoid. Assuming that the observation is sampled uniformly at the sampling frequency of f_s, the discrete scalar observation is written as

$$x(k) = \sum_{i=1}^{n} e^{-j\omega_i((k-1)/f_s + \phi_i)} s_i + \eta(k) \tag{2.21}$$

By collecting m consecutive discrete observations into a column vector form we get

$$\mathbf{x}(k) = \mathbf{A}\mathbf{s}(k) + \eta(k) \tag{2.22}$$

where $s \equiv [s_1 e^{j\phi_1} \; s_2 e^{j\phi_2} \cdots s_n e^{j\phi_n}]^t$, $\eta(k) \equiv [\eta(k) \; \eta(k-1) \cdots \eta(k-m+1)]^t$ and

$$\mathbf{A} = \begin{bmatrix} e^{-j\omega_1(0)/f_s} & \cdots & e^{-j\omega_n(0)/f_s} \\ e^{-j\omega_1(2)/f_s} & \cdots & e^{-j\omega_n(2)/f_s} \\ \vdots & \cdots & \vdots \\ e^{-j\omega_1(m-1)/f_s} & \cdots & e^{-j\omega_n(m-1)/f_s} \end{bmatrix} \tag{2.23}$$

Thus the matrix $\mathbf{A}$ is in the same form as in the uniform linear array case discussed in a previous section, i.e., it is Vandermonde.

2.5.3 Signal Separation Applications

The extraction of certain desired source signals from contaminated or jammed observations can be found in areas such as speech or tele-conferencing processing where

individual speech signals must be extracted from an environment with background and other noise sources, in communications where sources of interference may degrade the received signals and in EMG medical processing where the evoked potentials from various neurons must be separated. The model may be either narrowband or wideband depending on the specific application of interest. Certainly in communications systems which employ narrowband signals, the narrowband model is appropriate. In speech applications however, the wideband model is a better representation of the problem since speech signals are wideband in nature.

Remark: Note that the emphasis in signal applications is on the extraction of individual signals from observations where they are mixed. This requires the estimation of the channel coefficients $\{a_{ik}\}$ and time delays $\{\tau_{ik}\}$.

2.5.4 Echo Resolution of Signals with Known Shapes

The problem of resolving echoes of multiple signals of known shape may also be framed to fit the model of (2.18). This is achieved by a suitable parameterization of the matrix $\mathbf{A}$ in terms of the known shapes, see [7]. Suppose that a signal $g(t)$ of known shape is used to probe a medium with n scatterers. n echoes of this signal would be reflected back to the receiving sensor and we write the received sensor output as

$$x(t) = \sum_{i=1}^{n} s_i g(t - \tau_i) + \eta(t) \tag{2.24}$$

where $\{s_i\}$ models the random gains due to channel propagation and scatterer characteristics and τ_i denotes the time delay of the i-th echo. Next, suppose that the signal $g(t)$ is sent to probe the channel repetitively, say N times and assume that the echo returns would have died out at the beginning of each probe period. Then there

is an ensemble of N sensor observation periods, which is written as

$$\left\{ x(t) = \sum_{i=1}^{n} s_i(k) g(t - \tau_i) + \eta(t) \right\}_k , k = 1, 2, \cdots, N \text{ and } t = 1, 2, \cdots, m \qquad (2.25)$$

where $s_i(k)$ denotes the i-th echo's random gain during the k-th observation interval and t denotes the discrete time index.

By re-writing the scalar observation into a vector form, we get

$$\mathbf{x}(k) = \mathbf{A}\mathbf{s}(k) + \eta(k) \qquad (2.26)$$

where $\mathbf{x} = [x(1)\ x(2)\ \cdots x(m)]^t$, $\mathbf{s} = [s_1\ s_2\ \cdots s_n]^t$, $\eta = [\eta(1)\ \eta(2)\ \cdots \eta(m)]^t$. Here define the 'steering matrix' $\mathbf{A} = [\mathbf{g}(t - \tau_1) \mid \mathbf{g}(t - \tau_2) \mid \cdots \mid \mathbf{g}(t - \tau_n)]$, with $\mathbf{g}(t) = [g(1)\ g(2)\ \cdots g(m)]^t$. Thus the model in this case fits the narrowband model with the steering matrix $\mathbf{A}$ parameterized in terms of the signal $g(t)$ of known shape.

3

MATHEMATICAL PRELIMINARIES

In this chapter the basic mathematical results of matrix and perturbation theory is presented. Two matrix decompositions are covered: the eigenvalue eigenvector decomposition (EED) and the singular value decomposition (SVD). Orthogonal projectors and solutions to the deterministic least square problem are presented. The chapter ends with basic perturbation results on the perturbations of eigenvalues and eigenvectors of a Hermitian covariance matrix and the perturbation of a pseudoinverse.

3.1 Matrix and Vector Norms

Throughout this thesis we will utilize the following norms for vectors and matrices.

Definitions: The Euclidean norm of a column vector $\mathbf{v}$ of dimension m is defined as

$$\| \mathbf{v} \| = (\sum_{i=1}^{m} | v_i |^2)^{1/2} \tag{3.1}$$

Thus the Euclidean norm is nothing but the length of the vector $\mathbf{v}$.

The 2-norm of the matrix $\mathbf{M}$ is defined as that induced by the Euclidean vector

norm as in the following

$$\| \mathbf{M} \|_2 = sup \| \mathbf{Mv} \| \tag{3.2}$$

where the supremum is taken over all vectors $\mathbf{v}$ of unit norm.

Finally, the Frobenius norm of a matrix $\mathbf{M} \equiv [m_{ik}]$ is defined as

$$\| \mathbf{M} \|_F = (\sum_{i=1}^{m} \sum_{k=1}^{m} | m_{ik} |^2)^{1/2} \tag{3.3}$$

The norms defined above are also *consistent*, i.e.,

$$\| \mathbf{MN} \| \leq \| \mathbf{M} \| \| \mathbf{N} \| \tag{3.4}$$

$$\| \mathbf{Mv} \| \leq \| \mathbf{M} \| \| \mathbf{v} \| \tag{3.5}$$

Next we state certain observations regarding the matrix theory.

3.2 Eigenstructure Decompositions

In array signal processing, the decomposition of a covariance matrix is frequently of interest. The covariance matrix is defined as $\mathbf{R} = E\{\mathbf{x}\mathbf{x}^\dagger\}$. Thus it is Hermitian and positive semi-definite.

Given a Hermitian matrix $\mathbf{R}$, there are several different decompositions that are available. In this thesis, we will be concerned with the Eigenvalue-Eigenvector Decompostion (EED) and the Singular Value Decomposition (SVD), see [15].

Eigenvalue-Eigenvector Decomposition: Given a Hermitian matrix $\mathbf{R}$ of size m-by-m and rank n, where $m > n$, there exists a decomposition of $\mathbf{R}$ in the following manner

$$\mathbf{R} = \mathbf{U}\mathbf{\Lambda}\mathbf{U}^\dagger \tag{3.6}$$

where $\mathbf{U}$ is a unitary matrix (i.e., $\mathbf{U}\mathbf{U}^\dagger = \mathbf{U}^\dagger\mathbf{U} = \mathbf{I}$) and $\mathbf{\Lambda}$ is a diagonal matrix consisting of the real-valued eigenvalues of $\mathbf{R}$, i.e.,

$$\mathbf{\Lambda} = \begin{bmatrix} \lambda_1 & & \mathbf{0} \\ & \ddots & \\ \mathbf{0} & & \lambda_m \end{bmatrix} \tag{3.7}$$

Example: Consider the covariance matrix of the observation vector as found in the narrowband model of Eq.(2.8) and apply assumptions A1-A4 of the previous chapter. Thus

$$\mathbf{R} = E\{\mathbf{x}\mathbf{x}^\dagger\} = \mathbf{A}\mathbf{Q}\mathbf{A}^\dagger + \sigma^2\mathbf{I} \tag{3.8}$$

where $\mathbf{A}$ has full column rank (from assumption A1), $\mathbf{Q}$ is the positive definite covariance matrix of the source signals (from assumption A2) and σ^2 is the variance of the additive white Gaussian noise vector (from assumption A3).

Its eigenvalue-eigenvector decomposition can then be found as

$$\mathbf{R} = \mathbf{U}_s\mathbf{\Lambda}_s\mathbf{U}_s^\dagger + \sigma^2\mathbf{U}_n\mathbf{U}_n^\dagger \tag{3.9}$$

where $\mathbf{U} = [\mathbf{U}_s\mathbf{U}_n]$ is unitary, $\mathbf{\Lambda}_s$ is an n-by-n diagonal matrix of eigenvalues greater than σ^2. The subspaces spanned by the column vectors of $\mathbf{U}_s$, $\mathbf{U}_n$ are referred to as *signal* and *null (or noise)* subspace, respectively.

Similarly, in the case of the wideband model of Eq.(2.10)

$$\begin{aligned} \mathbf{R}(\omega) &= E\{\mathbf{x}(\omega)\mathbf{x}^\dagger(\omega)\} \\ &= \mathbf{A}(\omega)\mathbf{Q}(\omega)\mathbf{A}^\dagger(\omega) + \sigma^2(\omega)\mathbf{I} \\ &= \mathbf{U}_s(\omega)\mathbf{\Lambda}_s(\omega)\mathbf{U}_s^\dagger(\omega) + \sigma^2(\omega)\mathbf{U}_n(\omega)\mathbf{U}_n^\dagger(\omega) \end{aligned} \tag{3.10}$$

Singular Value Decomposition: *Given a rectangular matrix* $\mathbf{A}$ of size m-by-n and rank n, where $m > n$, the Singular Value Decomposition of $\mathbf{A}$ is:

$$\mathbf{A} = \mathbf{U}\mathbf{\Sigma}\mathbf{V}^\dagger \tag{3.11}$$

where $\mathbf{U}$, $\mathbf{V}$ are unitary matrices of sizes m-by-m and n-by-n, respectively and $\mathbf{\Sigma}$ is

$$\mathbf{\Sigma} = \begin{bmatrix} \sigma_1 & & \\ & \ddots & \\ & & \sigma_n \\ -- & -- & -- \\ & \mathbf{O} & \end{bmatrix} \tag{3.12}$$

where $\sigma_i, i = 1, 2, ..., n$ are real.

Remark: The SVD and EED of a positive definite Hermitian matrix (i.e., conjugate symmetric) matrix are the same.

3.3 Orthogonal Projectors

Definition: A square matrix P is said to be an *orthogonal projector* onto the subspace $\mathcal{S}$ if it satisfies the following:

(I) $P^2 = P$, it is *idempotent*

(II) $Range(P) = \mathcal{S}$

(III) $P^\dagger = P$, it is Hermitian.

Remarks:

(i) An orthogonal projector onto a given subspace is unique, see [15].

(ii) The orthogonal projector $\mathbf{P}^\perp$ which projects onto the subspace orthogonal to that of $\mathbf{P}$ satisfies $\mathbf{P}^\perp + \mathbf{P} = \mathbf{I}$.

Example: Consider the covariance matrix $\mathbf{R} = E\{\mathbf{x}\mathbf{x}^\dagger\} = \mathbf{A}\mathbf{Q}\mathbf{A}^\dagger + \sigma^2\mathbf{I}$ as in Eq.(3.8). Its eigenvalue-eigenvector decomposition is then

$$\mathbf{R} = \mathbf{U}_s\mathbf{\Lambda}_s\mathbf{U}_s^\dagger + \sigma^2\mathbf{U}_n\mathbf{U}_n^\dagger \tag{3.13}$$

where $\mathbf{U} = [\mathbf{U}_s\mathbf{U}_n]$ is unitary, and $\mathbf{\Lambda}_s$ is an n-by-n diagonal matrix of eigenvalues greater than σ^2. The subspaces spanned by the column vectors of $\mathbf{U}_s$, $\mathbf{U}_n$ are referred

to as *signal* and *null (or noise)* subspace, respectively. The orthogonal projector for the signal subspace may be defined as:

$$\mathbf{P}_s = \mathbf{U}_s\mathbf{U}_s^\dagger \tag{3.14}$$

The above projector may be shown to satisfy conditions (I-III) above. Similarly the orthogonal projector for the noise subspace may be shown to be

$$\mathbf{P}_n = \mathbf{U}_n\mathbf{U}_n^\dagger \tag{3.15}$$

Since the eigenvector matrix $\mathbf{U}$ is unitary, it follows that the signal subspace orthogonal projector is also *orthogonal* to the noise subspace orthogonal projector, (i.e., $\mathbf{P}_s \perp \mathbf{P}_n$) and that

$$\mathbf{P}_s + \mathbf{P}_n = \mathbf{I} \tag{3.16}$$

Example: Consider a matrix $\mathbf{A}$ of full column rank and dimensions m-by-n. The orthogonal projector $\mathbf{P}_A$ for the subspace spanned by the column vectors of $\mathbf{A}$ can be shown to be

$$\mathbf{P}_A = \mathbf{A}(\mathbf{A}^\dagger\mathbf{A})^{-1}\mathbf{A}^\dagger \tag{3.17}$$

Pre-multiplying a vector $\mathbf{x}$ by $\mathbf{P}_A$ is equivalent to projecting the vector $\mathbf{x}$ onto the subspace spanned by $\mathbf{A}$. Thus the result $\hat{\mathbf{x}} = \mathbf{P}_A\mathbf{x}$ lies entirely in the subspace of $\mathbf{A}$ and the difference (or error) vector $(\hat{\mathbf{x}} - \mathbf{x})$ lies in the subspace orthogonal to $\mathbf{A}$, see also Remark (ii) above.

3.4 Least Squares Solutions

In this section we will be looking at the deterministic linear equation problem of

$$\mathbf{x} = \mathbf{A}\mathbf{s} + \eta \tag{3.18}$$

Given that $\mathbf{x}$ and $\mathbf{A}$ is known, the problem is to estimate $\mathbf{s}$ such that the squared error $Tr\{(\mathbf{x}-\mathbf{A}\hat{\mathbf{s}})(\mathbf{x}-\mathbf{A}\hat{\mathbf{s}})^{\dagger}\}$ is minimized for some estimate $\hat{\mathbf{s}}$.

When $\mathbf{A}$ is a square matrix and non-singular, the least squares solution may be found by inverting $\mathbf{A}$. Thus,

$$\hat{\mathbf{s}} = \mathbf{A}^{-1}x. \tag{3.19}$$

However, when $\mathbf{A}$ is not a square matrix but is rectangular, then the least squares solution is found by using the pseudo-inverse of $\mathbf{A}$. Thus,

$$\hat{\mathbf{s}} = \mathbf{A}^{\#}x. \tag{3.20}$$

where $\mathbf{A}^{\#}$ is the pseudo-inverse of $\mathbf{A}$. The pseudo-inverse of $\mathbf{A}$ fulfills the following conditions, see [15, 51].

(I) $\mathbf{A}^{\#}\mathbf{A} = \mathbf{I}$

(II) $\mathbf{A}\mathbf{A}^{\#} = \mathbf{P}_A$, the orthogonal projector onto the subspace of $\mathbf{A}$.

(III) $\mathbf{A}\mathbf{A}^{\#}\mathbf{A} = \mathbf{A}$

(IV) $\mathbf{A}^{\#}\mathbf{A}\mathbf{A}^{\#} = \mathbf{A}^{\#}$

When $\mathbf{A}$ has rank n and is of dimension m-by-n, (ie., it has full column rank), we can write the pseudo-inverse of $\mathbf{A}$ as

$$\mathbf{A}^{\#} = (\mathbf{A}^{\dagger}\mathbf{A})^{-1}\mathbf{A}^{\dagger}. \tag{3.21}$$

Thus the least squares solution for $\mathbf{s}$ as found from Eq. (3.20) is $\hat{\mathbf{s}} = (\mathbf{A}^{\dagger}\mathbf{A})^{-1}\mathbf{A}^{\dagger}\mathbf{x}$.

An equivalent formulation of the least squares problem would be to find the closest estimate $\hat{\mathbf{x}}$ which lie within the subspace spanned by $\mathbf{A}$ to the actual observation $\mathbf{x}$. Then the solution for $\hat{\mathbf{x}}$ would be the projection of the actual observation $\mathbf{x}$ onto the subspace of $\mathbf{A}$, i.e.,

$$\hat{\mathbf{x}} = \mathbf{P}_A\mathbf{x}$$

$$= \mathbf{A}(\mathbf{A}^\dagger\mathbf{A})^{-1}\mathbf{A}^\dagger\mathbf{x} \tag{3.22}$$

The source signal estimate corresponding to this estimated observation is observed to be the same as in Eq.(3.20).

3.5 Matrix Perturbation Theory Results

In this section we will state first-order perturbation results for the eigenvectors and eigenvalues and pseudo-inverse of a matrix perturbed from a nominal matrix.

3.5.1 Perturbation of Eigenvalues and Eigenvectors of a Hermitian matrix

Given a Hermitian matrix $\hat{\mathbf{R}} = \mathbf{R} + \mathbf{E}$ where $\mathbf{R}$ has eigenvalues $\{\lambda_k\}, k = 1,2,..,m$ and eigenvectors $\{\mathbf{u}_k\}, k = 1,2,...,m$, and the perturbation matrix $\mathbf{E}$ is Hermitian and small enough, see [15], then the eigenvalues and eigenvectors of the perturbed matrix can be written to first order as

$$\hat{\lambda}_k \simeq \lambda_k + \mathbf{u}_k^\dagger\mathbf{E}\mathbf{u}_k \tag{3.23}$$

$$\hat{\mathbf{u}}_k \simeq \mathbf{u}_k + \sum_{i\neq k}^{m} \frac{\mathbf{u}_i^\dagger\mathbf{E}\mathbf{u}_k}{\lambda_k - \lambda_i} \tag{3.24}$$

In practice, at least in statistical signal processing applications, the covariance matrix $\mathbf{R}$ is often unknown and hence have to be estimated from finite data. Thus, assuming that the data is wide-sense stationary and that there are N available samples or snapshots of the observation array, the estimated covariance matrix is

$$\hat{\mathbf{R}} = \frac{1}{N}\sum_{i=1}^{N}\mathbf{x}(i)\mathbf{x}(i)^\dagger \tag{3.25}$$

When the observation vector $\mathbf{x}(i)$ is assumed to have a zero-mean gaussian distribution, asymptotically (for large N)

$$E\{\hat{\lambda}_i\} = \lambda_i + O(N^{-1}) \tag{3.26}$$

$$Cov\{\hat{\lambda}_i, \hat{\lambda}_k\} = \frac{\lambda_i^2}{N}\delta_{ik} + O(N^{-1}) \tag{3.27}$$

where δ_{ik} denotes the dirac function which is unity for $i = k$ and zero otherwise.

$$E\{\hat{\mathbf{u}}_i\} = \mathbf{u}_i + O(N^{-1}) \tag{3.28}$$

$$Cov\{\hat{\mathbf{u}}_i, \hat{\mathbf{u}}_k\} = \delta_{ik}\frac{\lambda_i}{N}\sum_{l\neq i}^{m}\frac{\lambda_l}{(\lambda_l - \lambda_1)^2}\mathbf{u}_l\mathbf{u}_l^\dagger + O(N^{-1}) \tag{3.29}$$

See [23].

3.5.2 Perturbations in Pseudo-Inverse

Given a matrix $\mathbf{A}$ of full column rank n, we have seen in the previous section that its pseudo-inverse may be written as $\mathbf{A}^\# = (\mathbf{A}^\dagger\mathbf{A})^{-1}\mathbf{A}^\dagger$. Suppose that instead of $\mathbf{A}$, one is given a perturbed matrix $\hat{\mathbf{A}} = \mathbf{A} + \mathbf{\Delta A}$. Then a first-order approximation for the pseudo-inverse of $\hat{\mathbf{A}}$ may be written, see [19], as

$$\hat{\mathbf{A}}^\# = \mathbf{A}^\# + (\mathbf{A}^\dagger\mathbf{A})^{-1}\mathbf{\Delta A}^\dagger(\mathbf{I} - \mathbf{A}\mathbf{A}^\#) - \mathbf{A}^\#\mathbf{\Delta A}\mathbf{A}^\# \tag{3.30}$$

3.6 Complex Differentiation

Array signal processing involves the computation of complex quantitie. Since there will be a need to take the derivatives or gradient of certain function with respect to complex quantities, this section presents a summary of the operation, see [18].

Let the complex quantity z be written as $z = z_r + jz_i$, where z_r, z_i denotes the real and imaginary parts of z respectively. Then the derivative operators with respect to z and z^* are

$$\frac{\partial}{\partial z} = \frac{\partial}{\partial z_r} + j\frac{\partial}{\partial z_i} \tag{3.31}$$

$$\frac{\partial}{\partial z^*} = \frac{\partial}{\partial z_r} - j\frac{\partial}{\partial z_i} \tag{3.32}$$

This operation is extended to the vector gradient operation in the following manner. Suppose that $\mathbf{w}$ is a complex column vector, with $\mathbf{w} = [w_1\ w_2\ \cdots w_m]^t$. Then the gradient operator is defined to be $\frac{\partial}{\partial \mathbf{w}} = [\frac{\partial}{\partial w_1}\ \frac{\partial}{\partial w_2}\ \cdots \frac{\partial}{\partial w_m}]^t$.

Thus

$$\frac{\partial(\mathbf{c}^t\mathbf{w})}{\partial \mathbf{w}} = \mathbf{0} \tag{3.33}$$

$$\frac{\partial(\mathbf{w}^t\mathbf{c})}{\partial \mathbf{w}} = 2\mathbf{c} \tag{3.34}$$

$$\frac{\partial(\mathbf{w}^t\mathbf{R}\mathbf{w})}{\partial \mathbf{w}} = 2\mathbf{R}\mathbf{w} \tag{3.35}$$

4

ASPECTS OF ARRAY SIGNAL PROCESSING

In this chapter we will cover several conventional methods for array processing such as beamforming, adaptive beamforming, eigenstructure based methods such as MUSIC and ESPRIT and maximum likelihood methods (assuming gaussian distribution for the observation vector). Also, the estimation of the number of sources using information theoretic criteria such as the Akaike Information Criterion (AIC) and the Minimum Description Length (MDL) will be discussed. The conventional methods are first discussed in the narrowband model case, and where the signal sources are not coherent with one another (i.e., the source signal covariance matrix is non-singular). Extensions of these methods to the case where the signal sources are coherent through the use of spatial averaging using sub-arrays is covered. Finally, the extension to the wideband case is also discussed.

4.1 Beamforming Approaches

Beamforming is a spatial filtering approaches to array processing. Given that a desired source signal is to be extracted from a desired DOA angle, the outputs of the observation array are delayed and summed in such a manner as to direct a narrow

beam of sensitivity for signals coming from the desired DOA and suppressing others. Since time delays may be equivalently represented as phase shifts, the output of a beam-former may also be viewed as the result of an inner product of the complex valued beamformer weight vector and the array observation vector, as in

$$y = \mathbf{w}^{\dagger}\mathbf{x} \tag{4.1}$$

where the column vector $\mathbf{w}$ denotes the beamformer weight vector. Note that the weight vector $\mathbf{w}$ must be a function of the desired DOA angle. It may or may not be dependent on the statistics of the observation vector $\mathbf{x}$ and this is the manner by which the different types of beamforming approaches may be classified, see [83]. Beamforming approaches where the weight vector is selected independent of the observations are classified as *data independent*, while beamforming approaches whose weight vectors are dependent on the statistics of the observation data are classified as *statistically optimum*.

4.1.1 Conventional Beamformer

The conventional beamformer approach, also known as the delay and sum beamformer is one of the earliest approach used for array signal processing. This approach is classified in the data independent category of beamformers as the beamformer weights are not dependent on the observed data or its statistics.

Intuitively, the idea is to time delay the different array sensor outputs and sum them in such a manner that the source signal emitted from the desired DOA would add coherently while those of the interfering and noise signals would add incoherently. Thus, the resulting beamformer output would increase the SNR of the desired source signal relative to the other signals, including noise.

This approach can be illustrated easily for a ULA with a single source signal, at

DOA angle θ_1. Assume that the channel gains a_{ik} are all unity. Thus, the i-th sensor output is

$$x_i(k) = e^{-j\frac{2\pi d}{\lambda}(k-1)sin\theta_1} s_1 \tag{4.2}$$

Thus if the beamformer is steered towards a DOA angle of θ, its weight vector $\mathbf{w}$ is defined such that

$$\mathbf{w} = [1.0\ e^{-j\frac{2\pi d}{\lambda}2sin\theta} \ldots e^{-j\frac{2\pi d}{\lambda}(m-1)sin\theta}]^t \tag{4.3}$$

Thus the output of the beamformer is

$$y = \mathbf{w}^\dagger \mathbf{x} = s_1 \left(\sum_{k=1}^{m} e^{-j\frac{2\pi d}{\lambda}(k-1)(sin\theta_1 - sin\theta)} \right) \tag{4.4}$$

Looking at the power of the beamformer output, we have

$$|\ y\ |^2 = |\ s_1\ |^2 \left(\frac{sin\{\frac{\pi dm}{\lambda}(sin\theta_1 - sin\theta)\}}{sin\{\frac{\pi d}{\lambda}(sin\theta_1 - sin\theta)\}} \right)^2 \tag{4.5}$$

Looking at the above expression for the beamformer output power, it is clear that it has a 'sinc-like' behavior with respect to the argument $(sin\theta_1 - sin\theta)$. The maximum power is found when the beamformer is steered towards the source signal at the DOA $\theta = \theta_1$, and that it has a main lobe width of $\frac{2\lambda}{md}$. The conventional beamformer would therefore not be able to resolve a case there are two source signals with DOA angles such that their separation is less than half the main lobe width. Fig. 4.1 shows an example of a sensitivity plot for a ULA with ten sensors spaced half a wavelength apart with the beam steered towards 30 degrees. Note that any two signals with DOA angles that fall within the main lobe would not be resolvable. The *Rayleigh resolution limit* for the ULA array is $\frac{\lambda}{md}$ (in radians). Note that this inability of the conventional beamformer to resolve two signals with close DOA angles is related to the array aperture size and not due to the amount of observation data available.

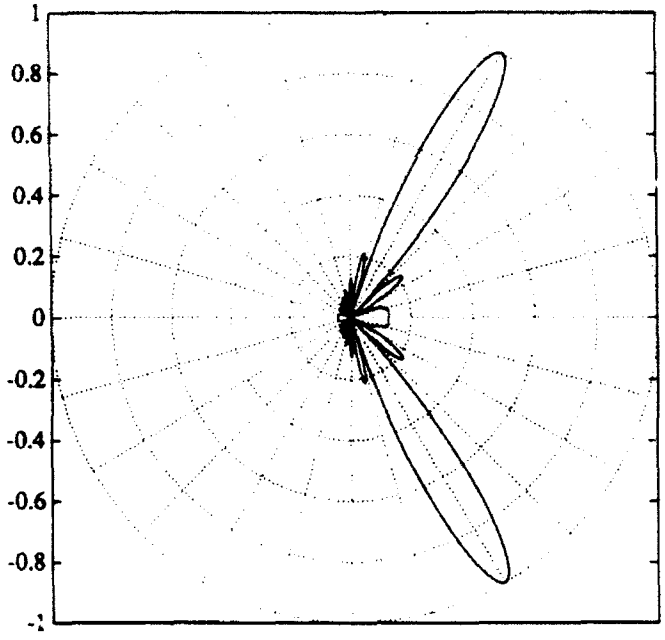

Figure 4.1: Conventional Beamformer Example

When a general array geometry is assumed instead of the ULA in the discussion above, the beamformer weight vector is defined accordingly as

$$\mathbf{w} = [1.0 \; e^{-j\omega_0\tau_2} \cdots e^{-j\omega_0\tau_m}]^t \tag{4.6}$$

where the delays τ_i are defined as in Eq.(2.12).

When N samples or snapshots of the array observations are available, the smoothed beamformer power estimate is:

$$\begin{aligned} \hat{P(\theta)} &= \frac{1}{N}\sum_{k=1}^{N} \mid y(k) \mid^2 \\ &= \mathbf{w}^\dagger \hat{\mathbf{R}} \mathbf{w} \end{aligned} \tag{4.7}$$

where $\hat{\mathbf{R}} = \frac{1}{N}\sum_{k=1}^{N} \mathbf{x}\mathbf{x}^\dagger(k)$.

The conventional beamformer approach is thus summarized as follows:

1. Estimate $\mathbf{R} = E\{\mathbf{x}\mathbf{x}^\dagger\}$.

2. $P(\theta) = \mathbf{w}^\dagger\mathbf{R}\mathbf{w}$, where $\mathbf{w}(\theta) = [1\ exp(-j\omega_0\tau_1), \cdots . exp(-j\omega_0\tau_{m-1})]^T$.

DOA angle estimates are found from peaks of $P(\theta)$.

Remarks:

(i) As can be seen from Eq.(4.4), the conventional beamformer may be implemented as a FFT in the ULA case. Thus it is an attractive approach due to its simplicity of implementation.

(ii) Conventional beamformers suffer from the problem of resolution, i.e., source signals that are situated close to one another in DOA angles cannot be resolved.

(iii) In general, conventional beamformer performance is degraded by the presence of multiple sources. It performs well however for a single source or for widely separated sources.

(iv) 'Leakages' or spurious signal power may arise due to the relatively high sidelobe levels of the conventional beamformer. The sidelobe levels may be reduced by using 'window' functions (also known as taper weights) in the beamformer weight vector. This is achieved at the expense of reduced resolution capability however due to increased main lobe width.

4.1.2 Linearly Constrained Minimum Variance Beamformer

The linearly Constrained Minimum Variance (LCMV) beamforming approach is based on minimizing the beamformer output power subject to certain linear constraints, [83]. Thus interfering signals disjoint from the source signal of interest would have their power minimized. These constraints may consists of point constraints such as constraining the signals from certain DOA angles be passed through the beamformer with specified gains and/or phases, or, that certain inferference signals from certain

DOA angles be suppressed. Derivative constraints may also be used to control the beamformer response over a specified range of DOA angles. The LCMV beamformer problem is stated as follows.

$$\min_{\mathbf{w}} \mathbf{w}^\dagger \mathbf{R} \mathbf{w} \text{ such that } \mathbf{C}^\dagger \mathbf{w} = \mathbf{f} \tag{4.8}$$

$\mathbf{C}$ is the m-by-p constraint matrix and $\mathbf{f}$ is the p-by-1 specified response vector (there are p linear contraints on the problem). Using Lagrange multipliers for the constraints, we write the minimization problem as

$$\xi = \mathbf{w}^\dagger \mathbf{R} \mathbf{w} + (\mathbf{f} - \mathbf{C}^\dagger \mathbf{w})^\dagger \lambda \tag{4.9}$$

where $\lambda = [\lambda_1 \ \lambda_2 \ \cdots \lambda_p]^t$ is vector of Lagrange multipliers.

Taking the gradient of ξ with respect to the beamformer weight vector and setting it to zero (a necessary condition for the minimum), we get

$$\mathbf{w} = \mathbf{R}^{-1} \mathbf{C} \lambda \tag{4.10}$$

Using the constraint relation $\mathbf{C}^\dagger \mathbf{w} = \mathbf{f}$ and assuming that the constraint matrix $\mathbf{C}$ has full column rank and the covariance matrix $\mathbf{R}$ is invertible, we get

$$\text{Beamformer Weight Vector: } \mathbf{w} = \mathbf{R}^{-1} \mathbf{C} (\mathbf{C}^\dagger \mathbf{R}^{-1} \mathbf{C})^{-1} \mathbf{f} \tag{4.11}$$

$$\text{Beamformer Power: } \mathbf{w}^\dagger \mathbf{R} \mathbf{w} = \mathbf{f}^\dagger (\mathbf{C}^\dagger \mathbf{R}^{-1} \mathbf{C})^{-1} \mathbf{f} \tag{4.12}$$

It is clear that the beamformer weight vector $\mathbf{w}$ is dependent on the covariance of the observation vector $\mathbf{R}$ and is therefore classified in the statistically optimum category of beamformers.

The LCMV beamformer weight vector $\mathbf{w}$ may be decomposed into a sum of two orthogonal vectors $\mathbf{w}_C$ and $\mathbf{w}_{\bar{C}}$ which are their projections onto the subspace spanned by $\mathbf{C}$ and its orthogonal complement, see [83]. From Eq.(3.17) in the previous chapter,

we have that the orthogonal projector onto the subspace spanned by the constraint matrix $\mathbf{C} = \mathbf{C}(\mathbf{C}^\dagger\mathbf{C})^{-1}\mathbf{C}^\dagger$, and thus

$$\begin{aligned} \mathbf{w}_C &= \mathbf{P}_C\mathbf{w} \\ &= \mathbf{C}(\mathbf{C}^\dagger\mathbf{C})^{-1}\mathbf{f} \end{aligned} \tag{4.13}$$

where $\mathbf{w}_C$ is *independent of the observation data*! Thus the only component of $\mathbf{w}$ which is dependent on the observation data statistics is $\mathbf{w}_C^\perp = \mathbf{P}_C^\perp\mathbf{w}$. Since $\mathbf{w}_C^\perp$ is orthogonal to $\mathbf{C}$, we may write it as

$$\mathbf{w}_C^\perp = \mathbf{D}\mathbf{b} \tag{4.14}$$

where $\mathbf{D}$ is a m-by-$(m-p)$ matrix orthogonal to $\mathbf{C}$ (it can be found by applying an SVD decomposition to $\mathbf{C}$) and $\mathbf{b}$ is a $(m-p)$ column vector. Note that constrained minimization of Eq.(4.8) is reduced to the un-constrained minimization as below

$$\min_{\mathbf{b}}(\mathbf{w}_C + \mathbf{D}\mathbf{b})^\dagger\mathbf{R}(\mathbf{w}_C + \mathbf{D}\mathbf{b}) \tag{4.15}$$

since $\mathbf{C}^\dagger\mathbf{w} = \mathbf{C}^\dagger(\mathbf{w}_C + \mathbf{C}^\dagger\mathbf{D}\mathbf{b} = \mathbf{f}$. Solving for $\mathbf{b}$, we get

$$\mathbf{b} = -(\mathbf{D}^\dagger\mathbf{R}\mathbf{D})^{-1}\mathbf{D}^\dagger\mathbf{R}\mathbf{w}_C \tag{4.16}$$

Thus the LCMV beamformer may be implemented with a combination of a data independent component and a data dependent component as in Fig. 4.2.

This equivalent formulation of the LCMV beamformer is important in the adaptive versions of the LCMV beamformer as will be shown next.

4.1.3 Adaptive Beamforming

Statistically optimum beamformers as in the LCMV beamformer above require an estimate of the observation covariance. Since the statistics of the data may vary with

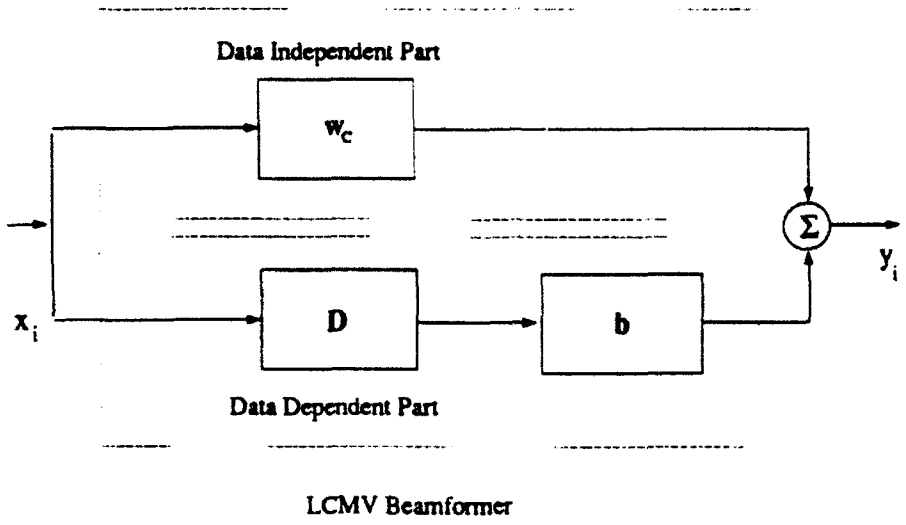

Figure 4.2: Block Diagram of LCMV Beamformer

time, adaptive beamformers have been proposed that will track such changes. The problem may be stated as follows, see [83]:

$$\begin{aligned} \min_{\mathbf{w}} \xi(\mathbf{w}) &= \min_{\mathbf{w}} E\{\mid z - \mathbf{w}^\dagger \mathbf{u} \mid^2\} \\ &= \min_{\mathbf{w}} \left\{\sigma_z^2 - \mathbf{w}^\dagger \mathbf{r}_{uz} - \mathbf{r}_{uz}^\dagger \mathbf{w} + \mathbf{w}^\dagger \mathbf{R}_u \mathbf{w}\right\} \end{aligned} \tag{4.17}$$

Here z is the desired respones, $\mathbf{u}$ is an input data vector and $\mathbf{w}$ is the beamformer weight vector. σ_z^2 is the power of the desired output, $\mathbf{r}_{uz} = E\{\mathbf{u}z^*\}$ and $\mathbf{R}_u = E\{\mathbf{u}\mathbf{u}^\dagger\}$. The solution for Eq.(4.17) can be shown to be

$$\mathbf{w} = \mathbf{R}_u^{-1} \mathbf{r}_{uz} \tag{4.18}$$

Adaptive methods for the estimation of $\mathbf{w}$ may be implemented using a whole host of techniques from adaptive filter theory, see [11, 18]. Note for example that the Recursive Least Squares method or the Least Mean Squares method may be used, [18, 11].

Using the Least Mean Squares (LMS) algorithm to allow for the adaptive updating

of the beamformer weight vector estimate, we have

$$\mathbf{w}_{k+1} = \mathbf{w}_k + \alpha \mathbf{u}(k) e^*(k) \tag{4.19}$$

where $e(k) = z(k) - \mathbf{w}^\dagger(k)\mathbf{u}$ and α is the step size or gain constant.

Example (Adaptive LCMV Beamformer): The LCMV beamformer consists of a data independent component $\mathbf{w}_C$ which may be computed beforehand and a data dependent component $\mathbf{w}_{\bar{C}}$which is dependent on the second order statistics of the data, see Eqs.(4.13),(4.16). Thus the adaptive version of the LCMV beamformer may be accomplished by defining the quantities

$$\begin{aligned} \text{Solution Vector: } \mathbf{w} &= \mathbf{b} \\ \text{Desired Response: } z &= \mathbf{w}_C^\dagger \mathbf{x} \\ \text{Input Vector: } \mathbf{u} &= \mathbf{D}^\dagger \mathbf{x} \end{aligned}$$

where the quantities $\mathbf{b}$, $\mathbf{w}_C$ and $\mathbf{D}$ are as defined in the previous section on LCMV beamformers.

4.2 Eigenstructure Based Approaches

In the past two decades there have been increasing interest in eigenstructure based approaches for array signal processing. Unlike the conventional beamforming approach or the LCMV beamforming approach, the eigenstructure based approaches are capable of (theoretically) resolving very closely separated source signals. This has led to these methods being called *high resolution* or *super resolution* methods, since they are capable of resolving source signals with DOA separation of less than the Rayleigh resolution limit as found in a conventional beamformer.

The two eigenstructure based methods that will be covered in this section are called MUltiple SIgnal Classification (MUSIC) and Estimation of Signals Parameters

via Rotational Invariance Techniques (ESPRIT), see [52, 50]. Before we proceed to a discussion of these two methods, we shall first discuss the basic subspace relations upon which these two methods rest.

Consider the narrowband observation covariance as in Eq. (3.8) and its EED decomposition

$$\begin{aligned} \mathbf{R} &= E\{\mathbf{x}\mathbf{x}^\dagger\} = \mathbf{A}\mathbf{Q}\mathbf{A}^\dagger + \sigma^2\mathbf{I} \\ &= \mathbf{U}_s\mathbf{\Lambda}_s\mathbf{U}_s^\dagger + \sigma^2\mathbf{U}_n\mathbf{U}_n^\dagger \end{aligned} \tag{4.20}$$

Here $\mathbf{U}_s$ of dimension m-by-n,$\mathbf{U}_n$ of dimension m-by-$(m-n)$ are the signal subspace and noise subspace eigenvector matrix respectively. The signal subspace eigenvector matrix $\mathbf{U}_s$ spans the column vectors of the steering matrix $\mathbf{A}$ and thus there exists a non-singular matrix $\mathbf{T}$ such that

$$\mathbf{U}_s = \mathbf{A}\mathbf{T} \tag{4.21}$$

This is easily shown by considering the following. Suppose that there is no noise, and thus $\sigma^2 = 0$. Then we have

$$\mathbf{U}_s\mathbf{\Lambda}_s\mathbf{U}_s^\dagger = \mathbf{A}\mathbf{Q}\mathbf{A}^\dagger \tag{4.22}$$

Then by post multiplying both sides of the equation above with $\mathbf{U}_s\mathbf{\Lambda}_s^{-1}$, we get Eq. (4.21), where $\mathbf{T} = \mathbf{Q}\mathbf{A}^\dagger\mathbf{U}_s\mathbf{\Lambda}_s^{-1}$. Note that $\mathbf{T}$ is square and of full rank (it is non-singular). It is also straightforward show that

$$\mathbf{U}_s\mathbf{U}_s^\dagger\mathbf{A} = \mathbf{A} \tag{4.23}$$

It is also clear that the noise subspace eigenvector matrix $\mathbf{U}_n$ is orthogonal to the steering matrix $\mathbf{A}$, i.e., $\mathbf{U}_n \perp \mathbf{A}$, since

$$\begin{aligned} \mathbf{R}\mathbf{U}_n &= \mathbf{A}\mathbf{Q}\mathbf{A}^\dagger\mathbf{U}_n + \sigma^2\mathbf{U}_n \\ &= \sigma^2\mathbf{U}_n \end{aligned} \tag{4.24}$$

This implies that

$$\mathbf{A}^{\dagger}\mathbf{U}_n = \mathbf{0} \tag{4.25}$$

These relations comprise the backbone of most eigenstructure based algorithms such as MUSIC or ESPRIT. The signal subspace relation of Eq. (4.21) is used in the development of ESPRIT while the orthogonality of the noise subspace to the steering matrix as in Eq.(4.25) is used in MUSIC.

4.2.1 MUltiple SIgnal Classification (MUSIC)

MUSIC was proposed by Schmidt in, see [52, 53], and independently by Reddi, see [45]. It exploits the orthogonality of the noise subspace to the steering matrix by defining a cost which measures the "closeness" to orthogonality of an estimated steering matrix relative to the noise subspace. From Eq.(4.25), it is clear that

$$\mathbf{U_n}^{\dagger}\mathbf{a}(\theta) = \mathbf{0},\ \theta = \theta_k \text{ for } k = 1, 2, \cdots, n \tag{4.26}$$

where $\mathbf{a}(\theta)$ is a steering vector.

The MUSIC cost function is thus defined to be

$$P(\theta) = \frac{1}{\| \mathbf{U}_n^{\dagger}\mathbf{a}(\theta) \|^2} \tag{4.27}$$

When the *array manifold* is known, i.e., the collection of all possible steering vectors $\mathbf{a}(\theta)$ for all possible DOA angles is known, the n DOA estimates may be found from the n highest peaks of the cost function $P(\theta)$ as the DOA angle parameter is swept. Thus MUSIC replaces the multidimensional search as implied in Eq.(4.25) with a one dimensional search over the range of possible DOA angles.

Remark: MUSIC requires the array manifold to be known or measured (calibrated) beforehand. Thus, while it has the attractive feature that it is an one-dimensional search procedure, it does require a calibration table (a lookup table) of

the array manifold values which may prove costly in terms of memory size (depending on the grid size of measured calibration values).

In theory the orthogonality relation in Eq.(4.26) should hold regardless of how close the angle separation of the DOA of any pairs of source signals are. Thus MUSIC is capable of resolving source signals with DOA separation that are much smaller than that of the conventional beamformer. Under finite though large sample conditions, however, it has been shown that MUSIC does exhibit a resolution threshold behavior, [23].

In general, a one dimensional search is necessary in the implementation of MUSIC to the array signal processing problem. In the case of ULA with identical sensors however, as may have been noticed by the reader by now, an elegant method may be used instead of searching for the DOA angles. In this case, a variant of MUSIC called Root-MUSIC can be applied. Note that the steering vector $\mathbf{a}(z)(\theta)$ is Vandermonde and may be written as $\mathbf{a}(\theta) = [1.0\ z^1\ \cdots z^{(m-1)}]^t$, where $z \equiv e^{\{-j\frac{2\pi}{\lambda}sin\theta\}}$. Then Eq.(4.26) may be written as

$$\mathbf{U}_n^{\dagger}\mathbf{a}(z) = \mathbf{0},\ \text{at}\ z = e^{\{-j\frac{2\pi}{\lambda}sin\theta\}_k} \tag{4.28}$$

Form the polynomial

$$D(z) = \| \mathbf{U}_n^{\dagger}\mathbf{a}(z) \|^2 \tag{4.29}$$

The polynomial $D(z) = 0$ for $z = e^{\{-j\frac{2\pi}{\lambda}sin\theta_k\}}$, i.e., it has zeros on the unit circle corresponding to the true DOA angles. Thus the Root-MUSIC method, see [3], forms the polynomial $D(z)$ from the estimate of the noise subspace eigenvector matrix and solves for roots lying on the unit circle.

In the past few years, the performance analyses of MUSIC and its variants have been a subject of intense interest. Of particular note is the work found in [23], which is one of the first papers to analyze MUSIC. See also [62, 63, 43]. What is clear from

these analyses is that MUSIC provides DOA estimates that are asymptotically unbiased, gaussian distributed and in general is not equivalent to Maximum-Likelihood estimates, see next section and also [64, 62]. In the case of uncorrelated source signals however, MUSIC and ML methods are asymptotically equal in MSE. The Root-MUSIC and MUSIC methods are asymptotically equivalent as has been shown in [43].

4.2.2 Estimation of Signal Parameters via Rotational Invariance Techniques (ESPRIT)

In contrast to MUSIC which utilizes the noise subspace relation of Eq.(4.25), ESPRIT exploits the signal subspace relation of Eq.(4.21), namely the fact that the steering matrix **A** is spanned by the signal subspace eigenvector matrix. The rotational invariance component comes into play here because ESPRIT assumes that **A** has a certain special invariance structure, see [50]. Specifically, **A** must have the structure that it may be partitioned in the following manner.

$$\mathbf{A} = \begin{bmatrix} \mathbf{B} \\ \mathbf{B}\mathbf{\Phi} \end{bmatrix} \tag{4.30}$$

where **B** is a steering sub-matrix and $\mathbf{\Phi}$ is a diagonal matrix such that

$$\mathbf{\Phi} = \begin{bmatrix} e^{\{-j\frac{2\pi d}{\lambda}\sin\theta_1\}} & & \bigcirc \\ & \ddots & \\ \bigcirc & & e^{\{-j\frac{2\pi d}{\lambda}\sin\theta_n\}} \end{bmatrix} \tag{4.31}$$

Here ESPRIT assumes an array structure composed of two sub-arrays we shall call X and Y sub-arrays, where each sensor in X is matched (identical) to its pair in Y and spaced at a distance d from each other, see Fig. 4.3 for example. Note that only the sensor pairs (also known as doublets) need to be matched and different sensor characteristics for different pairs are allowed. Using simple geometry to calculate the time delay difference between the sensors of a sensor pair, we can see that the

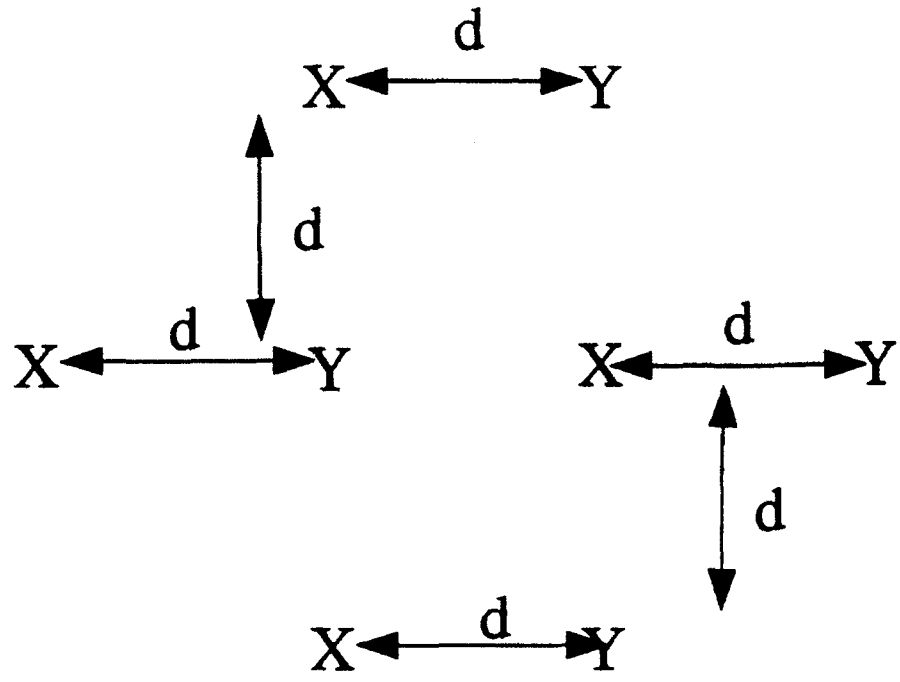

Figure 4.3: Esprit Subarrays Example

difference in time delay for a signal coming from DOA angle θ_k at the i-th sensor in X and its pair in Y is $\Delta\tau_{ik} = \frac{d}{c}sin\theta_k$. Thus if the observation column vector is arranged by concatenating the observations from the X sub-array on top of the observations from the Y sub-array, then the steering matrix **A** which results will fulfill the required rotational invariance as in Eq.(4.30). From the fact that the steering matrix **A** is spanned by the signal subspace eigenvector matrix, see Eq. (4.21), there exists a non-singular matrix **T** such that

$$\begin{aligned} \mathbf{AT} &= \mathbf{U}_s \\ &= \begin{bmatrix} \mathbf{B} \\ \mathbf{B\Phi} \end{bmatrix} \mathbf{T} \\ &= \begin{bmatrix} \mathbf{E}_X \\ \mathbf{E}_Y \end{bmatrix} \mathbf{T} \end{aligned} \tag{4.32}$$

where $\mathbf{E}_X, \mathbf{E}_Y$ are matrices partitioned from $\mathbf{U}_s$ with dimensions corresponding to the size of the X and Y sub-matrices. Furthermore, the matrices $\mathbf{E}_X, \mathbf{E}_Y$ both span

the same subspace due to the structure of the steering matrix $\mathbf{A}$. Thus, there exists a matrix $\mathbf{\Psi}$ such that

$$\mathbf{E}_X\mathbf{\Psi} = \mathbf{E}_Y \tag{4.33}$$

Notice however that due from Eq.(4.32)

$$\mathbf{BT\Psi} = \mathbf{B\Phi T} \tag{4.34}$$

Since $\mathbf{T}$ is non-singular and $\mathbf{B}$ has full column rank this implies that *the eigenvalues of* $\mathbf{\Psi}$ *are exactly the diagonal terms in* $\mathbf{\Phi}$! Thus the ESPRIT algorithm comprises primarily the estimation of the signal subspace eigenvector, its partitioning into submatrices $\mathbf{E}_X, \mathbf{E}_Y$ solving for $\mathbf{\Psi}$ from Eq.(4.33) and finally the extraction of the eigenvalues of $\mathbf{\Psi}$. The DOA angles may thus be extracted from the phase terms in the eigenvalues.

Remarks:

(i) $\mathbf{\Psi}$ may be solved from Eq.(4.33) by using either Total Least Squares (see [50, 15]) in which case the algorithm is called TLS-ESPRIT or by ordinary least squares in which case it is called LS-ESPRIT.

(ii) ESPRIT circumvents the need for a search procedure and for knowledge of/or calibration of the array manifold. Thus it is an attractive alternative to MUSIC. It requires however the special rotational invariance structure of the array which entails matched sensor pairs (matched in terms of characteristics and alignments).

Performance analysis of ESPRIT have been conducted by Stoica et., al, [63], Rao et., al, [44], Ottersten et., al, [35]. One interesting result of Stoica/Nehorai is that the performance of MUSIC is aymptotically better than that of ESPRIT. The DOA estimates have been shown to be zero mean, gaussian distibuted, see for example [35]. It has also been shown that asymptotically, TLS-ESPRIT and LS-ESPRIT are

equivalent, although simulations have suggests that TLS-ESPRIT is superior in low SNR and small snapshot size cases, see [50, 44].

4.3 Maximum Likelihood (ML) Methods

There are two formulations for maximum likelihood methods for the narrowband array signal processing problem, the so called *stochastic maximum likelihood* formulation and the *deterministic maximum likelihood* formulation. The deterministic tag here refers to the assumption that the source signals themselves are deterministic, the observations however are still random since the additive noise is AWGN. Maximum Likelihood methods are of interest in all facets of estimation theory since under certain conditions, ML estimates have mean square errors that are asymptotically equal to the Cramer-Rao lower bounds, see [29].

4.3.1 Stochastic Maximum Likelihood

In the stochastic ML formulation the source signals have zero mean, temporally white gaussian distributions such that

$$E\{\mathbf{s}(t)\mathbf{s}^{\dagger}(\xi)\} = \mathbf{Q}\delta_{t\xi} \tag{4.35}$$

$$E\{\mathbf{s}(t)\mathbf{s}^{t}(\xi)\} = \mathbf{0} \tag{4.36}$$

Writing the probability density function for N snapshots of the observation array, we get

$$f_{\boldsymbol{\Theta}}(\mathbf{x}_1, \cdots, \mathbf{x}_N) = \frac{1}{(2\pi)^{N/2}\sqrt{det(\mathbf{R})}} exp\left\{-\frac{1}{2}\sum_{k=1}^{N}\mathbf{x}_k^{\dagger}\mathbf{R}^{-1}\mathbf{x}_k\right\} \tag{4.37}$$

where $\boldsymbol{\Theta}$ is a column vector of the parameters to be estimated which includes the n DOA angles, the entries of the source covariance matrix $\mathbf{Q}$ and the noise variance σ^2. The maximum likelihood method entails finding the estimate of the parameter vector

Θ such that the probability density function in Eq.(4.37) is maximized. Taking the negative log of the pdf (since the log function is monotonic) this is equivalent to

$$\hat{\Theta} = \min_{\Theta} \left\{ log(det(\mathbf{R})) + \sum_{k=1}^{N} \mathbf{x}_k^{\dagger} \mathbf{R}^{-1} \mathbf{x}_k \right\} \tag{4.38}$$

Allowing for the fact that the source covariance matrix is Hermitian, the total number of parameters that must be estimated is n DOA angles+m^2 real and imaginary parts of source covariance matrix+1 noise variance. This minimization is thus often computationaly expensive as it essentially means that a multi-dimensional (specifically $(n + m^2 + 1)$) search must be conducted. The non-linearity of the minimization criterion of Eq.(4.38) further compounds the problem due to the likely existence of local minima solutions.

For methods proposed to solve for the estimates of the stochastic ML estimates, see [34] and the references therein. For performance analysis, see [34] – the stochastic ML method is asymptotically efficient if the global minimum of Eq.(4.38) is found. See also [64, 62].

4.3.2 Deterministic Maximum Likelihood

In the deterministic ML formulation, the source signals are assumed to be *deterministic* signals, i.e., they are not random processes. The observations however would still be gaussian distributed due to the additive white gaussian noise component. Assuming that there are N snapshots of the observation array vector, we can write the probability density function of the observations as

$$f_{\Theta}(\mathbf{x}_1, \cdots, \mathbf{x}_N) = \frac{1}{(2\pi\sigma^2)^{mN/2}} exp\left\{ -\frac{1}{2\sigma^2} \sum_{k=1}^{N} (\mathbf{x}_k - \mathbf{A}\mathbf{s}_k)^{\dagger} (\mathbf{x}_k - \mathbf{A}\mathbf{s}_k) \right\} \tag{4.39}$$

where $\mathbf{s}_k, k = 1, \cdots, N$ are the deterministic source signal vectors and $\mathbf{A}$ is the steering matrix. The parameters within the parameter vector Θ that must be estimated are

the n DOA angles, the N signal source vectors and the noise variance, σ^2. The pdf of Eq.(4.39) may also be viewed as a conditional pdf (conditioned on N realization of the source signal vector). Taking the negative log of Eq.(4.39), we get

$$\{\hat{\mathbf{x}}_k\}, \{\hat{\theta}_k\}, \{\hat{\sigma^2}\} = \min_{\{\mathbf{x}_k\},\{\theta_k\}} \left\{ mN \log \sigma^2 + \frac{1}{\sigma^2} \sum_{k=1}^{N} (\mathbf{x}_k - \mathbf{A}\mathbf{s}_k)^\dagger (\mathbf{x}_k - \mathbf{A}\mathbf{s}_k) \right\} \quad (4.40)$$

Taking the derivative with respect to the noise variance σ^2 and setting to zero, we can solve for its ML estimate as

$$\sigma^2 = \frac{1}{mN} \sum_{k=1}^{N} (\mathbf{x}_k - \mathbf{A}\mathbf{s}_k)^\dagger (\mathbf{x}_k - \mathbf{A}\mathbf{s}_k) \quad (4.41)$$

Next, taking the derivative of the log likelihood function with respect to the deterministic source signal vector $\mathbf{s}_k$ and setting to zero, find that their ML estimates are

$$\mathbf{s}_k = (\mathbf{A}^\dagger \mathbf{A})^{-1} \mathbf{A}^\dagger \mathbf{x} \quad (4.42)$$

Plugging these ML estimates for the noise variance and source signal vectors into the minmization of Eq.(4.40), we get the compressed deterministic ML problem

$$\{\hat{\theta}_k\} = \min_{\{\theta_k\}} Tr\{\mathbf{P}_A^\perp \hat{\mathbf{R}}\} \quad (4.43)$$

where $\mathbf{P}_A^\perp = \mathbf{I} - \mathbf{P}_A$ and $\hat{\mathbf{R}} = \frac{1}{N} \sum_{k=1}^{N} \mathbf{x}_k \mathbf{x}_k^\dagger$.

Remark: The deterministic ML problem is a nonlinear minimization problem and thus computationally expensive. Various methods have been proposed for this problem, see [4, 84]. Statistical performance analysis have been conducted, see [64, 62, 34] etc.

4.4 Cramer Rao (CR) Bounds

Given *any* unbiased estimator of the parameter vector Θ, the error covariance matrix of its estimated parameter vector is lower bounded by the Cramer Rao bound.

Specifically, given any estimate $\hat{\Theta}$ such that

$$\begin{aligned} E\{\hat{\Theta}\} &= \Theta \\ \text{and } \mathbf{C} &= E\{(\hat{\Theta}-\Theta)(\hat{\Theta}-\Theta)^t\} \end{aligned}$$

then the error covariance matrix $\mathbf{C}$ is lower bounded such that

$$\mathbf{C} \geq \mathbf{J}^{-1} \tag{4.44}$$

where $\mathbf{J}$ is the so-called Fisher Information matrix and the inequality is taken to mean that $\mathbf{C}-\mathbf{J}^{-1} \geq \mathbf{0}$, i.e., it is non-negative definite. Let the pdf of the observation vector be denoted by $f_\Theta(\mathbf{x})$. Then the Fisher Information matrix is defined as

$$\mathbf{J} = E\left\{\frac{\partial}{\partial\Theta}f_\Theta(\mathbf{x})\left(\frac{\partial}{\partial\Theta}f_\Theta(\mathbf{x})\right)^t\right\} \tag{4.45}$$

$$= -E\left\{\frac{\partial}{\partial\Theta}\left(\frac{\partial}{\partial\Theta}f_\Theta(\mathbf{x})\right)^t\right\} \tag{4.46}$$

The CR bound thus provides a benchmark by which the 'goodness' of an unbiased estimator may be measured. This is why maximum likelihood estimators are often of interest since under certain regularity conditions, the error covariance matrix of a maximum likelihood estimator will approach the CR bound asymptotically, i.e., it is asymptotically efficient. An unbiased estimator whose error covariance matrix is asymptotically equal to the CR bound is an *asymptotically efficient* estimator.

In general the evaluation of the CR bound for an arbitrary pdf of the observation data may prove to be a formidable task. Fortunately, for the case where the pdf is gaussian, the CR bound attains relatively simple forms.

We can consider two formulations for the assumption of gaussian distributed observation data vectors, namely the stochastic where the source signals are also zero mean, gaussian distributed (temporally white) as discussed in the previous section

on the Stochastic ML estimator and the deterministic where the source signals are considered to be deterministic, as discussed in the section on the Deterministic ML estimator.

4.4.1 Stochastic CR Bound

Using the formulation as found in the Stochastic ML, the Fisher Information matrix **J** can be shown to be (see [2, 51]) comprised of the following element entries

$$J_{ik} = \frac{N}{2} Tr \left\{ \mathbf{R}^{-1} \frac{\partial \mathbf{R}}{\partial \Theta_i} \mathbf{R}^{-1} \frac{\partial \mathbf{R}}{\partial \Theta_k} \right\} \tag{4.47}$$

Here N denotes the number of snapshots available and $\mathbf{R}$ is the observation covariance matrix.

Remark: For explicit evaluations of the stochastic ML see [64, 34] etc.

4.4.2 Deterministic CR Bound

In the deterministic case with the formulation as in the Deterministic ML discussion previously, the CR bound matrix have been evaluated by Stoica and Nehorai in [62] where

$$\mathbf{J}^{-1} = \frac{\sigma^2}{2} \left\{ \sum_{k=1}^{N} Real \left[\mathbf{X}^{\dagger}(k) \mathbf{D}^{\dagger} \mathbf{P}_{\mathbf{A}}^{\perp} \mathbf{D} \mathbf{X}(k) \right] \right\}^{-1} \tag{4.48}$$

where $\mathbf{X}(k) = Diag\{\mathbf{x}(k)\}$, i.e., a diagonal matrix with its diagonal entries taken from the elements of the observation vector $\mathbf{x(k)}$ and $\mathbf{D}$ defined such that its i-th column vector is $\mathbf{d}_i = \frac{\partial \mathbf{a}(\theta)}{\partial \theta}$ evaluated at $\theta = \theta_i$.

Remark: Stoica and Nehorai derived the above expression and discussed several important special cases of interest, [62].

4.5 Information Theoretic Model Order Identification

Throughout this thesis it shall be assumed that the number of source signals is known, see assumption A4. In practice however, the number of source signals would also have to be estimated from the observed data. Two model order estimation criteria which have gained a lot of attention in the literature are the Akaike's Information Criterion (AIC), see Akaike, and the Minimum Description Length (MDL) criterion, see Rissannen, Schwartz.

Both methods attempt to find the model order that best fits the given family of parameterized model pdf $f(\mathbf{x} \mid \boldsymbol{\Theta})$. AIC is proposed as a measure (see Akaike, [1]) where it was shown that minimizing the AIC is asymptotically equivalent to minimizing the Kullback-Leibler function which is a measure of the statistical "distance" of the true model pdf and the estimated model pdf. MDL (see Rissanen, Schwartz, [46, 54]) is derived by treating the problem as that of determining the minimum code length that will describe the observation data. Thus the AIC and MDL are stated as

$$\mathbf{AIC}(k) = -2log f(\mathbf{x} \mid \hat{\boldsymbol{\Theta}}^{(k)}) + 2k \tag{4.49}$$

$$\mathbf{MDL}(k) = -log f(\mathbf{x} \mid \hat{\boldsymbol{\Theta}}^{(k)}) + \frac{1}{2}klogN \tag{4.50}$$

where $\boldsymbol{\Theta}$ is the model parameter vector and $\hat{\boldsymbol{\Theta}}^{(k)}$ is its ML estimate, k is the number of free adjusted parameters in the model and N is the number of snapshots of the observation data. The model with the minimum AIC or MDL is selected as the one that best fits the observed data.

Wax and Kailath [77] had applied AIC and MDL to the problem of determining the number of source signals in the narrowband array signal processing problem. Using the statistical assumptions in the Stochastic ML model, these criteria are shown to

be

$$\mathbf{AIC}(\hat{n}) = -2log\left(\frac{\prod_{i=\hat{n}+1}^{m}\hat{\lambda}_i^{1/(m-\hat{n})}}{\frac{1}{m-\hat{n}}\sum_{i=\hat{n}+1}^{m}\hat{\lambda}_i}\right)^{(m-\hat{n})N} + 2\hat{n}(2m-\hat{n}) \qquad (4.51)$$

$$\mathbf{MDL}(\hat{n}) = -log\left(\frac{\prod_{i=\hat{n}+1}^{m}\hat{\lambda}_i^{1/(m-\hat{n})}}{\frac{1}{m-\hat{n}}\sum_{i=\hat{n}+1}^{m}\hat{\lambda}_i}\right)^{(m-\hat{n})N} + \frac{1}{2}\hat{n}(2m-\hat{n})logN \qquad (4.52)$$

where $\hat{n}$ denotes the estimated number of source signals and $\hat{\lambda}_i$ denotes the eigen values of the estimated covariance matrix of the array observation vector $\hat{\mathbf{R}}$ arranged in order of decreasing magnitude.

Thus the estimated number of sources are picked from the value that minimizes these equations depending on which criterion is to be used.

Remark: Wax and Kailath, [77] showed that for the AIC and MDL criteria as in Eqs.(4.51), (4.52), that AIC is inconsistent, ie. asymptotically it tends to overestimate the number of sources. MDL however is asymptotically consistent. Extensions of these information theoretic model order estimation methods for wideband, coherent sources may be found in [20, 78, 75].

4.6 Spatial Averaging for Coherent Sources

In the development of the eigenstructure based approaches thus far, it has been assumed that no two source signals are fully coherent with each other, i.e., the source signal covariance matrix is positive definite (assumption A2). In the situation where two or more source signals are coherent, the application of MUSIC would only resolve the non-coherent source signals. Similarly, the ESPRIT algorithm would also fail as the signal subspace eigenvector matrix would have a rank less than the rank of the true steering matrix.

In the case of coherent sources, the technique of *spatial averaging* has been proposed in [56]. Spatial averaging assumes the use of a ULA with m identical sensors

divided into L overlapping subarrays each of size p sensors. The multiple covariance matrices of these sub-arrays are then summed and divided by L, thus getting an average covariance matrix upon which the eigenstructure based method is applied. In [56] it was shown that this pre-processing of the data would lead to the averaged source covariance matrix being of full rank, provided that the number of subarrays are greater than or equal to the number of sources, $L \geq n$. Note that the number of sensor within a subarray p must also be greater than or equal to the number of sources n. Thus the use of spatial averaging to alleviate source coherence problems lead to a tradeoff with respect to the available array aperture (i.e., it leads to a smaller aperture being used. less than the available one) since L subarray covariance matrices need to be averaged. It has been shown also that spatial averaging requires at least 50 percent more sensors for the same effective array aperture as before, see [41].

4.7 Wideband Extensions

Wideband extensions for array signal processing fall roughly into two camps or types of approaches, the so-called *incoherent* and *coherent* approaches. Both are applied in the frequency domain and may be used to extend most eigenstructure based methods to the wideband case.

4.7.1 Incoherent Approach

Intuitively, the incoherent approach for wideband array processing may be summarized as follows: take the frequency transform of the observation data which divides the data into several frequency bins. Apply the desired narrowband estimation technique then on data at various frequency bins. Finally, use the estimates found at the different frequency bins to arrive at some sort of average estimate. Thus individual

narrowband processing is done at various frequency bins with a final averaging of the results.

Consider an example of this wideband extension approach for beamforming applications. Note that first an FFT is taken of the observation data and then individual narrowband beamformers are applied to the frequency transformed data. Finally the various beamformer outputs are added and inverse FFT is performed yielding the final output estimate $y(t)$.

In the case of MUSIC, an incoherent approach was proposed in [78], where the cost function $P(\theta)$ is defined as

$$P(\theta) = \frac{1}{\sum_{k=1}^{J} \parallel \mathbf{U}_n(\omega_k)^\dagger \mathbf{a}(\omega_k, \theta) \parallel^2} \tag{4.53}$$

Here $\mathbf{U}_n(\omega_k)$ denotes the noise subspace eigenvector matrix of $\mathbf{R}(\omega_k)$, the observation covariance matrix at frequency ω_k, see Eq. (3.10).

See [65] and [78] for extensions of this type for MUSIC. Extensions for ESPRIT are found in [33].

4.7.2 Coherent Approach

The coherent approach for wideband processing is based on the idea that the observation data at the various frequeny bins should be added *coherently* in some manner before the narrowband eigenstructure based method is applied. Intuitively the addition of the information at the various frequency bins would tend to improve the SNR of the data. This approach was proposed in Wang and Kaveh, see [75] .

Define the transformation matrices $\mathbf{T}(\omega_k)$ such that:

$$\mathbf{T}(\omega_k)\mathbf{A}(\omega_k) = \mathbf{A}(\omega_0), k = 1, \cdots, J \tag{4.54}$$

where ω_0 denotes the focusing frequency to which the steering matrices of other frequencies are focused to. Note that this requires knowledge of the true DOA angles which is exactly the quantities to be estimated! This dilemma is circumvented by using a rough estimate of the DOA angles such as that found by using conventional beamforming. Then the various covariance matrices at the different frequencies are summed in the following manner.

$$\mathbf{R}_x = \sum_{k=1}^{J} \mathbf{T}(\omega_k)\mathbf{R}(\omega_k)\mathbf{T}(\omega_k)^\dagger \tag{4.55}$$

Finally the desired narrowband method is applied on the focused covariance matrix $\mathbf{R}_x$. Extensions to MUSIC for this approach can be found in [20, 8, 27]. The extensions for ESPRIT can be found in [21].

5

ANALYSIS OF ESPRIT UNDER RANDOM MODEL ERRORS

5.1 Introduction

Eigenstructure based algorithms for array signal processing has gained considerable interest in recent years. Algorithms such as MUSIC [53] and ESPRIT [50] have been proposed generally for the DOA estimation problem. Much work on performance analysis of these algorithms has been directed to studying the effects of noise and finite number of snapshots, with no errors assumed on the sensors gains/phases, locations etc. , see, e.g., [23],[35].

This chapter presents analysis results on the MSE of ESPRIT DOA angle estimates with errors in the array sensors. Such errors include random errors in the sensor gains and phases, random errors in sensor locations and random errors in sensor pair alignments. Both MUSIC and ESPRIT perform well when the sensors in the array are either calibrated (i.e., the array manifold is known) as in MUSIC or the sensors in a sensor pair are matched perfectly as in ESPRIT. In practice, however, this may not always be possible due perhaps to external environmental effects on the array, deterioration of electronic components, measurement errors, etc. As a consequence, there

has been interest in the performance analysis of these methods under model errors. Analysis of MUSIC under various model errors can be found in [82]-[68]. Analysis of ESPRIT where the steering matrix errors are modeled as uncorrelated, zero-mean Gaussian distributed can be found in [30, 68]. In [68, 69], the analysis of ESPRIT under model errors are performed using its formulation as the minimization of a certain cost function. The MSE expressions obtained therein are very complicated due to its parameterization in terms of not only the DOA angles but also other 'nuisance' parameters [35], such as the real and imaginary parts of the steering matrix, the magnitudes of the elements of a diagonal matrix, etc. In this chapter, a direct approach towards the analysis of ESPRIT under model errors is taken where the DOA angles are the sole parameters considered. This approach yields simple MSE expressions that are related explicitly to the model errors. As such, it provides interesting insight into the performance sensitivity of ESPRIT to model errors.

5.2 Problem Formulation

Throughout this chapter, the superscripts 'H', 'T', '*' and '#' denote the Hermitian, transpose, complex conjugate and the Moore-Penrose pseudo-inverse of a matrix, respectively. Also, n denotes the number of narrowband far-field sources, m denotes the number of sensors within a subarray, m_0 denotes the total number of sensors (i.e. $m_0 \leq 2m$) and $\{\mu_i, \nu_i\}$ and $\{\bar{\mu}_i, \bar{\nu}_i\}$ denote the sensor locations in the X and Y (possibly overlapping) subarrays respectively.

Here, we will be concerned with *the situation where the covariance matrix is assumed known* (i.e., the finite sample effects on data covariance matrix are not investigated here). Under nominal conditions, the sensor pairs within the X and Y subarrays are matched perfectly, with a distance spacing d between them [50]. By

appropriate choice of coordinates, one can rewrite the sensor locations within the X and Y subarrays to be $\{\mu_i, \nu_i\}$ and $\{\mu_i + d, \nu_i\}$, respectively. Then, the observation vectors from the X and Y subarrays can be written as:

$$\text{X subarray} : \mathbf{x} = \mathbf{\Gamma A s} + \eta_x \text{ and Y subarray} : \mathbf{y} = \mathbf{\Gamma A \Phi s} + \eta_y \tag{5.1}$$

Here Γ denotes the diagonal array of nominal sensor gains and phases, namely, $\Gamma = \text{Diag}\{\alpha_1 e^{j\phi_1}, .., \alpha_m e^{j\phi_m}\}$, and $\mathbf{A}$ is the steering matrix defined by the set of distinct DOA angles $\{\theta_k\}$ (the DOA angles are measured with reference to the normal of the sensor pairs),

$$\mathbf{A} = \left[\begin{array}{ccc} \mathbf{a}_1 & \cdots & \mathbf{a}_n \end{array} \right], \tag{5.2}$$

The individual steering vector at DOA angle θ_k is defined as

$$\begin{aligned} \mathbf{a}_k &= [exp\{-j\frac{2\pi}{\lambda}(\mu_1 sin\theta_k + \nu_1 cos\theta_k)\}... \\ &\quad \cdots exp\{-j\frac{2\pi}{\lambda}(\mu_m sin\theta_k + \nu_m cos\theta_k)\}]^T. \end{aligned} \tag{5.3}$$

Furthermore, $\mathbf{\Phi} = \text{Diag}\{exp(-j\frac{2\pi d}{\lambda} sin\theta_1), ..,exp(-j\frac{2\pi d}{\lambda} d sin\theta_n)\}$, λ is the wavelength of the narrowband signals, s is the source vector and η_x,η_y denote the additive noise vectors at the X and Y subarrays, respectively.

It is assumed that the matrix $\mathbf{A}$ has full column rank, the narrowband sources are incoherent and the noise vectors are uncorrelated zero mean processes with covariance $\sigma^2\mathbf{I}$, see assumptions A1-A4.

5.2.1 General Formulation of Error Models

Under small array model errors and using first order approximation, a general formulation of the array signal processing problem under model errors can be derived, namely,

$$\text{X subarray} : \mathbf{x} = (\mathbf{\Gamma A} + \partial\mathbf{A}_x)\mathbf{s} + \eta_x \text{ and Y subarray} : \mathbf{y} = (\mathbf{\Gamma A} + \partial\mathbf{A}_y)\mathbf{\Phi s} + \eta_y \tag{5.4}$$

The $\partial \mathbf{A}_x$, $\partial \mathbf{A}_y$ terms are dependent on the types of error model in question. These different error scenarios are derived as below.

Errors in Sensor Gains and Phases: $\partial \mathbf{A}_x = \Delta\mathbf{\Gamma}_x\mathbf{A}$ and $\partial \mathbf{A}_y = \Delta\mathbf{\Gamma}_y\mathbf{A}$ where

$$\Delta\mathbf{\Gamma_x} = Diag\{(\Delta\alpha_1 + j\alpha_1\Delta\phi_1)e^{j\phi_1}, \cdots, (\Delta\alpha_m + j\alpha_m\Delta\phi_m)e^{j\phi_m}\}. \tag{5.5}$$

$$\Delta\mathbf{\Gamma_y} = Diag\{(\Delta\bar{\alpha}_1 + j\alpha_1\Delta\bar{\phi}_1)e^{j\phi_1}, \cdots, (\Delta\bar{\alpha}_m + j\alpha_m\Delta\bar{\phi}_m)e^{j\phi_m}\}. \tag{5.6}$$

Here $\{(\Delta\alpha_i, \Delta\phi_i)\}$ and $\{(\Delta\bar{\alpha}_i, \Delta\bar{\phi}_i)\}$ denote errors in the sensor gains and phases of the X and Y subarrays respectively.

proof: Consider the i-th perturbed sensor gains and phases: $(\alpha_i + \Delta\alpha_i)e^{j(\phi_i+\Delta\phi_i)}$. Using first order approximation with $e^{j(\phi_i+\Delta\phi_i)} \simeq e^{j\phi_i}(1 + j\Delta\phi_i)$ and discarding all terms higher than first order, the error terms of the above is found.

Using the same approach for the other error models, we get

Errors in Sensor Locations: $\partial \mathbf{A}_x = \mathbf{\Gamma}\Delta\mathbf{A}_x$ and $\partial \mathbf{A}_y = \mathbf{\Gamma}\Delta\mathbf{A}_y$ where

$$\Delta\mathbf{A}_x = -j\frac{2\pi}{\lambda}(Diag\{\Delta\mu_1, \cdots, \Delta\mu_m\}\mathbf{A}_s + Diag\{\Delta\nu_1, \cdots, \Delta\nu_m\}\mathbf{A}_c). \tag{5.7}$$

$$\Delta\mathbf{A}_y = -j\frac{2\pi}{\lambda}(Diag\{\Delta\bar{\mu}_1, \cdots, \Delta\bar{\mu}_m\}\mathbf{A}_s + Diag\{\Delta\bar{\nu}_1, \cdots, \Delta\bar{\nu}_m\}\mathbf{A}_c). \tag{5.8}$$

Here $\{(\Delta\mu_i, \Delta\nu_i)\}$ and $\{(\Delta\bar{\mu}_i, \Delta\bar{\nu}_i)\}$ denote errors in the sensor locations of the X and Y subarrays respectively, $\mathbf{A}_s = [\mathbf{a}_1 sin\theta_1, ..., \mathbf{a}_n sin\theta_n]$ and $\mathbf{A}_c = [\mathbf{a}_1 cos\theta_1, ..., \mathbf{a}_n cos\theta_n]$.

Errors in Sensor Pair Alignments: In this case, the sensor pairs within the X and Y subarrays are perturbed by small alignment errors such that they are rotated by small angles from the nominal aligned direction. Hence, $\partial \mathbf{A}_x = \mathbf{\Gamma}\Delta\mathbf{A}_x$ and $\partial \mathbf{A}_y = \mathbf{\Gamma}\Delta\mathbf{A}_y$ where

$$\Delta\mathbf{A}_x = -j\frac{\pi d}{\lambda}Diag\{\beta_1, \cdots, \beta_m\}\mathbf{A}_c. \tag{5.9}$$

$$\Delta\mathbf{A}_y = +j\frac{\pi d}{\lambda}Diag\{\beta_1, \cdots, \beta_m\}\mathbf{A}_c. \tag{5.10}$$

Here $\{\beta_i\}$ denote the small angle rotations from the normal of the sensor pairs due to misalignment errors and $\mathbf{A}_c$ is as defined previously.

Remark: Note that the random sensor error assumptions here enter directly into the sensor parameters such as gains/phases, locations and alignments as opposed to the uncorrelated Gaussian error assumptions imposed on the steering matrix (i.e., on $\partial\mathbf{A}_x$, $\partial\mathbf{A}_y$) in [30, 68] which may not be physically justifiable.

5.3 Analysis of ESPRIT under Small Array Perturbations

Let the covariance matrix be $\mathbf{R} = E\{\mathbf{z}\mathbf{z}^H\}$, where $\mathbf{z} = \begin{bmatrix} \mathbf{x} \\ \mathbf{y} \end{bmatrix}$ and let its eigendecomposition be $\mathbf{R} = \mathbf{E}_s\mathbf{\Lambda}_s\mathbf{E}_s^H + \sigma^2\mathbf{E}_n\mathbf{E}_n^H$. The ESPRIT algorithm solves for $\mathbf{\Psi}$ from $\mathbf{E}_x\mathbf{\Psi} = \mathbf{E}_y$ and estimates the DOA angles from its eigenvalues. Here $\mathbf{E}_x$ and $\mathbf{E}_y$ are the signal subspace eigenvector matrices for the X and Y subarrays, respectively, [50], see Chapter 4.

Under the general model of Eq. (5.4), the application of the ESPRIT algorithm will result in perturbation of the eigenvalues of $\hat{\mathbf{\Psi}}$ as the next theorem shows.

Theorem 1 *Given the general formulation of the perturbed array signal processing problem of Eq. (5.4), the perturbed k-th eigenvalue of* $\hat{\mathbf{\Psi}}$ *can be written as*

$$\hat{\xi}_k = \xi_k + \Delta\xi_k \text{ where } \Delta\xi_k = \xi_k \mathbf{b}_k^T(\partial\mathbf{A}_y - \partial\mathbf{A}_x)\mathbf{e}_k. \tag{5.11}$$

Here, $\xi_k = exp\left(-j\frac{2\pi d sin\theta_k}{\lambda}\right)$, $\mathbf{b}_k^T = \mathbf{e}_k^T(\mathbf{\Gamma A})^+$ *and* $\mathbf{e}_k$ *is defined as the* $n \times 1$ *unit vector with unity value at the k-th element position and zero elsewhere.*

Proof The signal subspace eigenvector matrix $\mathbf{E}_s$ spans the perturbed steering ma-

trix $\begin{bmatrix} (\mathbf{\Gamma A} + \partial \mathbf{A}_x) \\ (\mathbf{\Gamma A} + \partial \mathbf{A}_y)\mathbf{\Phi} \end{bmatrix}$. Thus, there exists a non-singular matrix $\mathbf{T}$ such that:

$$\mathbf{E}_s = \begin{bmatrix} \mathbf{E}_x \\ \mathbf{E}_y \end{bmatrix} = \begin{bmatrix} (\mathbf{\Gamma A} + \partial \mathbf{A}_x) \\ (\mathbf{\Gamma A} + \partial \mathbf{A}_y)\mathbf{\Phi} \end{bmatrix} \mathbf{T}. \tag{5.12}$$

Solving for the least squares solution of $\hat{\mathbf{\Psi}}$ and using a first order approximation for the pseudo-inverse of $(\mathbf{\Gamma A} + \partial \mathbf{A}_x)$, [19], see also Section 3.5.2, yields

$$\hat{\mathbf{\Psi}} = \mathbf{T}^{-1} \left\{ \mathbf{I} + (\mathbf{\Gamma A})^{+} (\partial \mathbf{A}_y - \partial \mathbf{A}_x) \right\} \mathbf{\Phi} \mathbf{T}. \tag{5.13}$$

Since the eigenvalues of a matrix are invariant under a similarity transformation, the eigenvalues of $\hat{\mathbf{\Psi}}$ are the same as the eigenvalues of

$$\left\{ \mathbf{I} + (\mathbf{\Gamma A})^{+} (\partial \mathbf{A}_y - \partial \mathbf{A}_x) \right\} \mathbf{\Phi} \tag{5.14}$$

Using first order perturbation approximation, [15] and see also Section 3.5.1, for the perturbed k-th eigenvalue yields

$$\hat{\xi}_k = \xi_k + \xi_k \mathbf{e}_k^T (\mathbf{\Gamma A})^{+} (\partial \mathbf{A}_y - \partial \mathbf{A}_x) \mathbf{e}_k. \tag{5.15}$$

The proof is done.

Having found the perturbed eigenvalues of $\hat{\mathbf{\Psi}}$, the next step in ESPRIT is to solve for the estimated DOA angles. The next lemma gives a convenient form for evaluating the mean squared error of the k-th estimated DOA angle.

Lemma 1 *Given the perturbed eigenvalue $\hat{\xi}_k = \xi_k + \Delta\xi_k$, the mean squared error of the corresponding estimate of the k-th DOA is*

$$E\{ \mid \Delta\theta_k \mid^2 \} = \frac{1}{2} \left(\frac{\lambda}{2\pi d cos\theta_k} \right)^2 E \left\{ \frac{\mid \Delta\xi_k \mid^2}{\mid \xi_k \mid^2} - Re \left(\frac{\Delta\xi_k}{\xi_k} \right)^2 \right\}. \tag{5.16}$$

Proof: Note that $\xi_k = e^{-j\frac{2\pi d}{\lambda}sin\theta_k}$ and that $\hat{\xi}_k = \xi_k + \Delta\xi_k = \mid \hat{\xi}_k \mid e^{-j\frac{2\pi d}{\lambda}sin\hat{\theta}_k}$, where $\hat{\theta}_k = \theta_k + \Delta\theta_k$ Using first order approximation and $sin(\hat{\theta}_k) \simeq sin(\theta_k) + \Delta\theta_k cos(\theta_k)$ we get

$$\xi_k + \Delta\xi_k = (1 + \Delta r_k)e^{-j\frac{2\pi d}{\lambda}sin\theta_k}\left\{1 - \left(j\frac{2\pi d}{\lambda}cos\theta_k\right)\Delta\theta_k\right\} \tag{5.17}$$

where Δr_k denotes the perturbation in the magnitude of the estimated eigenvalue ξ_k. Discarding all term higher order terms except for first order, we get

$$\Delta\xi_k = \xi_k\left\{\Delta r_k - j\frac{2\pi d cos\theta_k}{\lambda}\Delta\theta_k\right\} \tag{5.18}$$

Solving for $\mid \Delta\theta_k \mid^2$ yields the desired result.

Using Lemma 1 and Theorem 1 we get the following corollary.

Corollary 1 *The mean-square-error of the ESPRIT doa estimates under model errors:*

$$E\{\mid \Delta\theta_k \mid^2\} = \frac{1}{2}\left(\frac{\lambda}{2\pi d cos\theta_k}\right)^2\left\{\mathbf{b}_k^T\mathbf{M}_{0k}\mathbf{b}_k^* - Re\left(\mathbf{b}_k^T\mathbf{M}_{1k}\mathbf{b}_k\right)\right\}. \tag{5.19}$$

Let $\mathbf{D}_k = Diag\{\mathbf{a}_k\}$, *a diagonal matrix formed from the elements of* $\mathbf{a}_k$ *and the matrix terms* $\mathbf{M}_{0k}$, $\mathbf{M}_{1k}$ *be specified as follows.*

Errors in Sensor Gains and Phases

$$\mathbf{M}_{0k} = \mathbf{D}_k E\{\mathbf{v}_k\mathbf{v}_k^H\}\mathbf{D}_k^H \text{ and } \mathbf{M}_{1k} = \mathbf{D}_k E\{\mathbf{v}_k\mathbf{v}_k^T\}\mathbf{D}_k^T. \tag{5.20}$$

where

$$\begin{aligned}\mathbf{v}_k &= [e^{j\phi_1}(\Delta\bar{\alpha}_1 - \Delta\alpha_1) + j\alpha_1 e^{j\phi_1}(\Delta\bar{\phi}_1 - \Delta\phi_1)..\\ &\quad \cdots e^{j\phi_m}(\Delta\bar{\alpha}_m - \Delta\alpha_m) + j\alpha_m e^{j\phi_m}(\Delta\bar{\phi}_m - \Delta\phi_m)]^T.\end{aligned} \tag{5.21}$$

Errors in Sensor Locations

$$\mathbf{M}_{0k} = \mathbf{\Gamma}\mathbf{D}_k E\{\mathbf{v}_k\mathbf{v}_k^H\}(\mathbf{\Gamma}\mathbf{D}_k)^H \text{ and } \mathbf{M}_{1k} = \mathbf{\Gamma}\mathbf{D}_k E\{\mathbf{v}_k\mathbf{v}_k^T\}(\mathbf{\Gamma}\mathbf{D}_k)^T. \tag{5.22}$$

where

$$\mathbf{v}_k = -j\frac{2\pi}{\lambda}\ [(\Delta\bar{\mu}_1 - \Delta\mu_1)sin\theta_k + (\Delta\bar{\nu}_1 - \Delta\nu_1)cos\theta_k ..$$
$$\cdots (\Delta\bar{\mu}_m - \Delta\mu_m)sin\theta_k + (\Delta\bar{\nu}_m - \Delta\nu_m)cos\theta_k]^T. \qquad (5.23)$$

Errors in Sensor Pair Alignments

$\mathbf{M}_{0k}$ *and* $\mathbf{M}_{1k}$ *are as defined in Eq. (5.22) where*

$$\mathbf{v}_k = +j\frac{2\pi d cos\theta_k}{\lambda}[\beta_1 \cdots \beta_m]^T. \qquad (5.24)$$

Proof: Since the proofs for the different error scenarios follow the same line of argument we shall present only the proof for the sensor gain and phase error model. Note however, that

$$\partial\mathbf{A}_x = \mathbf{\Delta\Gamma}_x\mathbf{A} \text{ and } \partial\mathbf{A}_y = \mathbf{\Delta\Gamma}_y\mathbf{A} \qquad (5.25)$$

Using Theorem 1, the perturbation in the k-th eigenvalue ξ_k is

$$\begin{aligned}\Delta\xi_k &= \xi_k\mathbf{b}_k^t(\mathbf{\Delta\Gamma}_y - \mathbf{\Delta\Gamma}_x)\mathbf{A}\mathbf{e}_k \\ &= \xi_k\mathbf{b}_k^t(\mathbf{\Delta\Gamma}_y - \mathbf{\Delta\Gamma}_x)\mathbf{a}_k \qquad (5.26)\end{aligned}$$

Note however that defining $\mathbf{v}_k$ and $\mathbf{D}_k$ as in the corollary and Eq.(5.21), we can re-write the above as

$$\Delta\xi_k = \xi_k\mathbf{b}_k^t\mathbf{D}_k\mathbf{v}_k \qquad (5.27)$$

Apply Lemma 1 and the proof is done.

Remark: In general, the matrix terms $\mathbf{M}_{0k}, \mathbf{M}_{1k}$ are not diagonal. However in the case where the X and Y subarrays do not overlap and the sensor errors (i.e., gain/phase, location or alignment errors) have zero means and are uncorrelated, these terms are found to be diagonal and more explicit expressions for $\mathbf{M}_{0k}, \mathbf{M}_{1k}$ can be

derived. The next corollary follows from Corollary 1 under the non-overlapping, uncorrelated error assumption.

Corollary 2 *Suppose that the subarrays do not overlap and that*

1. The errors in sensor gains and phases are zero mean, uncorrelated with variance σ_α^2 *and* σ_ϕ^2*, respectively. Then*

$$\mathbf{M}_{0k} = 2Diag\{\sigma_\alpha^2 + \sigma_\phi^2\alpha_1^2, \cdots, \sigma_\alpha^2 + \sigma_\phi^2\alpha_m^2\} \tag{5.28}$$

and

$$\mathbf{M}_{1k} = 2Diag\{e^{j2\phi_1}(\sigma_\alpha^2 - \sigma_\phi^2\alpha_1^2), \cdots, e^{j2\phi_m}(\sigma_\alpha^2 - \sigma_\phi^2\alpha_m^2)\} \tag{5.29}$$

2. The errors in sensor locations are zero mean, uncorrelated with variance σ_μ^2 *and* σ_ν^2 *respectively. Then*

$$\mathbf{M}_{0k} = 2\left(\frac{2\pi}{\lambda}\right)^2 \left(\sigma_\mu^2 sin^2\theta_k + \sigma_\nu^2 cos^2\theta_k\right) \mathbf{\Gamma}\mathbf{\Gamma}^H \tag{5.30}$$

and

$$\mathbf{M}_{1k} = -2\left(\frac{2\pi}{\lambda}\right)^2 \left(\sigma_\mu^2 sin^2\theta_k + \sigma_\nu^2 cos^2\theta_k\right) \mathbf{\Gamma}\mathbf{\Gamma}^T. \tag{5.31}$$

3. The angle errors in sensor pair alignments are zero mean, uncorrelated with variance σ_β^2*. Then*

$$\mathbf{M}_{0k} = \left(\frac{2\pi d cos\theta_k}{\lambda}\right)^2 \sigma_\beta^2 \mathbf{\Gamma}\mathbf{\Gamma}^H \tag{5.32}$$

and

$$\mathbf{M}_{1k} = -\left(\frac{2\pi d cos\theta_k}{\lambda}\right)^2 \sigma_\beta^2 \mathbf{\Gamma}\mathbf{\Gamma}^T \tag{5.33}$$

5.4 Discussion of Important Special Cases

In the subsequent discussion, it will be assumed that the nominal sensor gains and phases are unity and zero, respectively. The first part of the discussion deals with

the one and tow-source special cases under an arbitrary geometry array (the nominal array geometry must still fulfill the ESPRIT invariance requirement of course). The second part of the discussion is concerned with an arbitrary number of sources under the assumption of large m (number of sensors) and ULA structure for the array.

5.4.1 Arbitrary Array Geometry – One and Two Source Case

For non-overlapping subarrays, simple closed form solutions for the one source case and approximate solutions for the two source case can be found for the errors as in Eqs. (5.28)-(5.33) and Eq. (5.19). Note that for the one source case, it is easily shown that

$$\mid \mathbf{b}_1 \mid^2 = \frac{1}{m} \text{ and } Re\{\mathbf{b}_1^T \mathbf{D}_1^2 \mathbf{b}_1\} = \frac{1}{m}. \tag{5.34}$$

Proof: The pseudoinverse of the one-source steering matrix $\mathbf{a}_1$ can easily be shown to be equal to $\frac{\mathbf{a}_1^\dagger}{m}$. Thus the quantities in Eq.(5.34) are easily found.

For the two source case, the MSE is expressed approximately in a simple form when the number of sensors in a subarray m is large enough such that $\mid \mathbf{a}_1^H \mathbf{a}_2 \mid \ll m$.

$$\mid \mathbf{b}_k \mid^2 \simeq \frac{1}{m} \text{ and } Re\{\mathbf{b}_k^T \mathbf{D}_k^2 \mathbf{b}_k\} \simeq \frac{1}{m}, \; k = 1, 2. \tag{5.35}$$

proof: The evaluation of the pseudoinverse of a two-source steering matrix $\mathbf{A}$ is straightforward albeit tedious. After some manipulation it can be shown that

$$\mathbf{b}_1^t = \frac{1}{m}\left(\frac{1}{1 - \frac{|\mathbf{a}_1^\dagger \mathbf{a}_2|^2}{m^2}}\right)(\mathbf{a}_1^\dagger - \frac{\mathbf{a}_1^\dagger \mathbf{a}_2}{m}\mathbf{a}_2^\dagger) \tag{5.36}$$

$$\mathbf{b}_2^t = \frac{1}{m}\left(\frac{1}{1 - \frac{|\mathbf{a}_1^\dagger \mathbf{a}_2|^2}{m^2}}\right)(\mathbf{a}_2^\dagger - \frac{\mathbf{a}_2^\dagger \mathbf{a}_1}{m}\mathbf{a}_1^\dagger) \tag{5.37}$$

$$\tag{5.38}$$

Next assuming that $\mid \mathbf{a}_1^H \mathbf{a}_2 \mid \ll m$ the quantities of Eq.(5.35) are found.

Thus the same mean-square-error expressions is found for the one and two-source case. The following results then follow for one and two source signals.

Sensor Gain and Phase Errors

Applying Eq. (5.35) to the case of errors in sensor gains and phases of Corollary 2, we get

$$E\{|\Delta\theta_k|^2\} \simeq \frac{2}{m}\left(\frac{\lambda}{2\pi d cos\theta_k}\right)^2 \sigma_\phi^2 \tag{5.39}$$

Remark. Thus, for the one and two source case and large m, the ESPRIT DOA MSE under errors in sensor gains and phases are affected only by the sensor phase errors.

Sensor Location Errors

For uncorrelated errors in sensor locations

$$E\{|\Delta\theta_k|^2\} \simeq \frac{2}{m}\left(\frac{1}{d cos\theta_k}\right)^2 (\sigma_\mu^2 sin^2\theta_k + \sigma_\nu^2 cos^2\theta_k) \tag{5.40}$$

Sensor Pair Alignment Errors

For uncorrelated errors in sensor pair alignments

$$E\{|\Delta\theta_k|^2\} \simeq \frac{1}{m}\sigma_\beta^2 \tag{5.41}$$

5.4.2 Uniform Linear Array (ULA) – n sources

We now turn to the special case of a uniform linear array (ULA) and where *the total number of sensors m_0 is assumed to be large.* There are two cases for the selection of the ESPRIT subarrays discussed here. The subarrays are chosen from the ULA to be either non-overlapping (i.e. , $m = m_0/2$, the so-called interleaved array, [35]) or to have maximum overlapping (i.e. , $m = m_0 - 1$), with the distance spacing between sensors in a sensor pair kept at d.

Before continuing on with the evaluation of the various MSE expressions, we first recall from Appendix G of [62] that for a ULA with m sensors that

$$\lim_{m\to\infty} \frac{1}{m}\mathbf{A}^\dagger\mathbf{A} = \mathbf{I} \tag{5.42}$$

Thus this implies that

$$\mathbf{b}_k^\dagger = \mathbf{e}_k^\dagger(\mathbf{A}^\dagger\mathbf{A})^{-1}\mathbf{A}^\dagger \simeq \frac{1}{m}\mathbf{a}_k^\dagger \tag{5.43}$$

for large m. Also note that

$$\mathbf{a}_k^\dagger\mathbf{D}_k = [1\ 1\ \cdots 1] \tag{5.44}$$

Having found these useful quantities the examination of the MSE for the non-overlapping and maximally overlapping subarrays begins.

Non-Overlapping Subarrays

The non-overlapping case involves the evaluation of the expressions in Corollary 2 and the use of Eqs. (5.43), (5.44).

For the case of zero mean, uncorrelated errors in sensor gains and phases it can be shown that

$$\mathbf{b}_k^T\mathbf{M}_{0k}\mathbf{b}_k^* \simeq \frac{2}{m_0/2}(\sigma_\alpha^2 + \sigma_\phi^2) \text{ and } Re\{\mathbf{b}_k^T\mathbf{M}_{1k}\mathbf{b}_k\} \simeq \frac{2}{m_0/2}(\sigma_\alpha^2 - \sigma_\phi^2), \ . \tag{5.45}$$

Hence, applying Theorem 1, we find

$$E\{|\ \Delta\theta_k\ |^2\} \simeq \frac{4}{m_0}\left(\frac{\lambda}{2\pi d cos\theta_k}\right)^2 \sigma_\phi^2,\ k = 1,..,n. \tag{5.46}$$

Proof: The $\mathbf{M}_{0k}, \mathbf{M}_{1k}$ terms are found from Corollary 2 and yields

$$\mathbf{M}_{0k} = 2(\sigma_\alpha^2 + \sigma_\phi^2)\mathbf{I} \text{ and } \mathbf{M}_{1k} = 2(\sigma_\alpha^2 - \sigma_\phi^2)\mathbf{I} \tag{5.47}$$

Using Eqs.(5.43) and (5.44) yields Eq.(5.45).

Similarly, for the other two error scenarios we get

Sensor Location Errors

For the case of zero mean uncorrelated errors in sensor locations

$$E\{|\Delta\theta_k|^2\} \simeq \frac{4}{m_0}\left(\frac{1}{dcos\theta_k}\right)^2(\sigma_\mu^2 sin^2\theta_k + \sigma_\nu^2 cos^2\theta_k) \tag{5.48}$$

Sensor Pair Alignment Errors

For the case of zero mean uncorrelated errors in sensor pair alignments

$$E\{|\Delta\theta_k|^2\} \simeq \frac{2}{m_0}\sigma_\beta^2 \tag{5.49}$$

Subarrays with Maximum-Overlapping

The case with maximum overlapping of subarrays is handled in a similar manner. Note however that the evaluation of the matrix terms $\mathbf{M}_{0k}, \mathbf{M}_{1k}$ is different from the Non-overlapping case.

Sensor gain and phase errors

For zero mean, uncorrelated errors in sensor gains and phases, it can be shown, when the subarrays are selected such that they have maximum overlapping (i.e. , $m = m_0 - 1$), that

$$\mathbf{b}_k^T\mathbf{M}_{0k}\mathbf{b}_k^* \simeq \frac{2}{m_0^2}(\sigma_\alpha^2 + \sigma_\phi^2) \text{ and } Re\{\mathbf{b}_k^T\mathbf{M}_{1k}\mathbf{b}_k\} \simeq \frac{2}{m_0^2}(\sigma_\alpha^2 - \sigma_\phi^2), \; . \tag{5.50}$$

Hence,

$$E\{|\Delta\theta_k|^2\} \simeq \frac{2}{m_0^2}\left(\frac{\lambda}{2\pi dcos\theta_k}\right)^2\sigma_\phi^2, \; k = 1, .., n. \tag{5.51}$$

Proof: Consider the evaluation of $\mathbf{M}_{0k}$. It requires the evaluation of $E\{\mathbf{v}_k\mathbf{v}_k^\dagger\}$ with $\mathbf{v}_k$ as defined in Eqs.(5.20),(5.21). With maximally overlapping subarrays we get

$$E\{\mathbf{v}_k\mathbf{v}_k^\dagger\} = \begin{bmatrix} 2 & -1 & & \bigcirc \\ -1 & 2 & -1 & \\ & \ddots & \ddots & -1 \\ \bigcirc & & -1 & 2 \end{bmatrix}(\sigma_\alpha^2 + \sigma_\phi^2) \tag{5.52}$$

Also,

$$E\{\mathbf{v}_k\mathbf{v}_k^t\} = \begin{bmatrix} 2 & -1 & & \bigcirc \\ -1 & 2 & -1 & \\ & \ddots & \ddots & -1 \\ \bigcirc & & -1 & 2 \end{bmatrix} (\sigma_\alpha^2 - \sigma_\phi^2) \tag{5.53}$$

Thus, from Eqs.(5.20) and (5.43) we have

$$\mathbf{b}_k^t\mathbf{M}_{0k}\mathbf{b}_k^* \simeq \frac{1}{m_0^2}[1\cdots 1] \begin{bmatrix} 2 & -1 & & \bigcirc \\ -1 & 2 & -1 & \\ & \ddots & \ddots & -1 \\ \bigcirc & & -1 & 2 \end{bmatrix} (\sigma_\alpha^2 - \sigma_\phi^2)[1\cdots 1]^t \tag{5.54}$$

This is equal to the expression for $\mathbf{b}_k^t\mathbf{M}_{0k}\mathbf{b}_k^*$ found in Eq.(5.50). $\mathbf{b}_k^t\mathbf{M}_{1k}\mathbf{b}_k$ is determined in the same manner. The proof is done.

Remarks: Thus, when the subarrays are chosen with maximum overlappping, the MSE of ESPRIT estimates are smaller by a factor of $2m_0$ than when the subarrays are non-overlapping. This is intuitively satisfying as in this case, the subarrays have a larger aperture than in the non-overlapping subarrays case. Again, the MSE are affected only by the phase errors.

The expressions for the other error scenario is analogously

Se nsor location errors

For uncorrelated errors in sensor locations and with maximum overlapping subarrays

$$E\{|\Delta\theta_k|^2\} \simeq \frac{2}{m_0^2}\left(\frac{1}{dcos\theta_k}\right)^2(\sigma_\mu^2 sin^2\theta_k + \sigma_\nu^2 cos^2\theta_k) \tag{5.55}$$

Comparison with MUSIC under sensor gain and phase errors

The MSE expressions for MUSIC under random model errors can be found in [67]. As before, by arguments similar to those found in [62], for the case of zero mean, uncorrelated errors in the sensor gains and phases, the MUSIC MSE is

$$E\{|\Delta\theta_k|^2\} \simeq \frac{6}{m_0^3}\left(\frac{\lambda}{2\pi dcos\theta_k}\right)^2(\sigma_\alpha^2 + \sigma_\phi^2),\ ,k = 1,..n. \tag{5.56}$$

Remarks: It can be seen that the MUSIC MSE is affected by both errors in gains and phases. In contrast ESPRIT is affected only by phase errors. Furthermore, from Eqs. (5.46), (5.51) and (5.56) it is clear that the MUSIC MSE is smaller when the number of sensors m_0 is large. The fact that the MSE of MUSIC is less than that for ESPRIT for large m_0 is also consistent with the results in [63]. Similar observations for ESPRIT and MUSIC can be made for the other model error scenarios.

5.5 Extension of Results to DOA-dependent Sensor Gain and Phase Errors

In the previous discussions, it has been assumed that the sensor gain and phases errors are independent of the DOA angles of the source signals. Surprisingly all the previous results concerning the MSE errors for this error model still holds when this model is generalized to the case where the errors are dependent on the DOA angles (i.e., the errors are different for different angles). Specifically, consider the case where the errors in gains and phases are different for different DOAs. Then for the perturbed model in the general model of Eq. (5.4), we write

$$\partial \mathbf{A}_x = [\Delta\mathbf{\Gamma}_1\mathbf{a}_1 \mid \cdots \Delta\mathbf{\Gamma}_n\mathbf{a}_n] \tag{5.57}$$

and

$$\partial \mathbf{A}_y = [\Delta\bar{\mathbf{\Gamma}}_1\mathbf{a}_1 \mid \cdots \Delta\bar{\mathbf{\Gamma}}_n\mathbf{a}_n] \tag{5.58}$$

where the terms $\Delta\mathbf{\Gamma}_k, \Delta\bar{\mathbf{\Gamma}}_k$ are the first order perturbation terms for the k-th DOA angle of the X and Y sub-arrays respectively.

Thus Theorem 1 can still be applied using these generalisations for the sensor gain and phase errors thereby giving the k-th perturbed eigenvalue from Theorem 1 to be

$$\Delta\xi_k = \xi_k \mathbf{b}_k^t(\Delta\mathbf{\Gamma}_k - \Delta\bar{\mathbf{\Gamma}}_k)\mathbf{a}_k \tag{5.59}$$

From this equation we can see that it is in the same form as the DOA independent error model and hence all the previous discussions regarding the sensor gain and phase error model would still hold.

5.6 Simulations

Two uncorrelated sources are given at DOA angles -20^o and -10^o both with unit power. The X and Y subarrays are taken from a uniform linear array with distance spacing between the sensors in sensor-pairs taken to be $d = \frac{\lambda}{2}$. The nominal sensor gains and phases are unity and zero respectively. Zero mean, uncorrelated errors in the sensor gains and phases are introduced with standard deviations of 10^{-2} and 4 degrees, respectively. The total number of sensors m_0 is varied from 6 to 20 and a hundred trial runs are used to average the MSE of the TLS-ESPRIT (see [50]) DOA estimate for both the non-overlapping and maximum overlapping case. Their respective Root-MSE are plotted in Figs.5.1, 5.2 where the solid line depicts the approximate Root-MSE for the non-overlapping case as computed from Eq. (5.46), the dashed line gives the approximate Root-MSE for the maximum-overlapping case as computed from Eq. (5.51) while the symbols '*' and '+' denote the simulation Root-MSE of ESPRIT for the non-overlapping and maximum-overlapping cases, respectively. The approximate Root-MSE for MUSIC as computed from Eq. (5.56) shown by a dotted-line and the simulation Root-MSE for MUSIC denoted by the symbol 'o' are plotted in these figures.

5.7 Conclusions

The MSE expressions of the ESPRIT DOA estimates under three random model error scenarios are derived assuming that the covariance matrix is known. Solutions for the

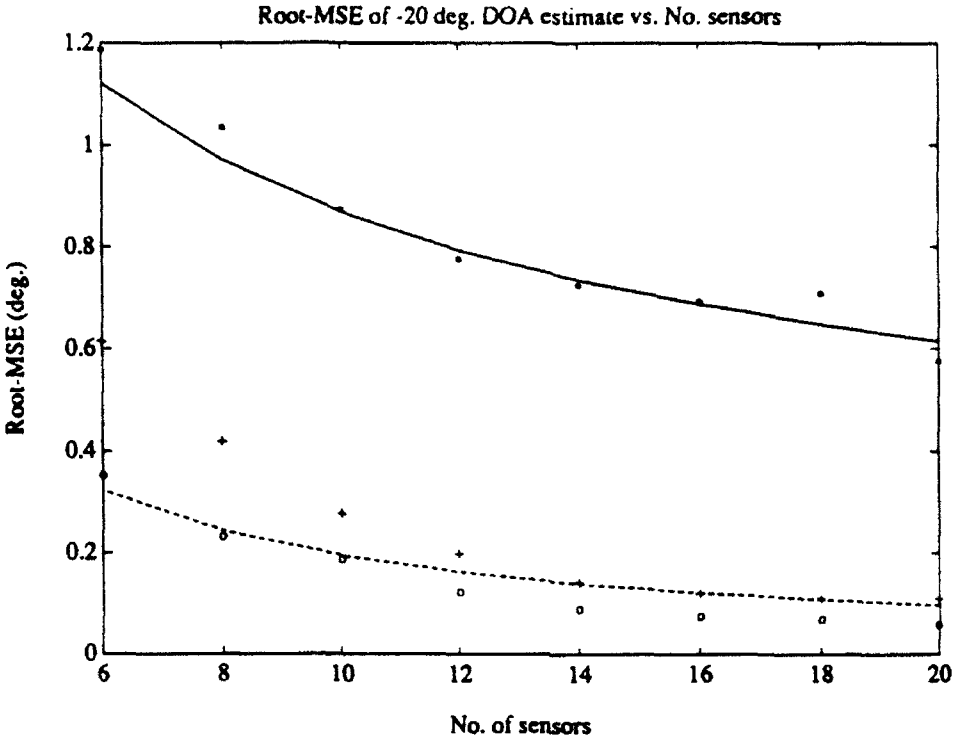

Figure 5.1: Estimate of DOA at -20 deg.

ESPRIT MSE with an arbitrary ESPRIT array geometry and one and two sources are given. Approximate solutions for a uniform linear array (ULA) and arbitrary number of sources with a large number of sensors are also given. Solutions for both cases suggest that ESPRIT is affected only by phase errors. Furthermore, it is shown that ESPRIT with maximum-overlapping subarrays will exhibit lower MSE (which decreases at the rate $\frac{1}{m_0^2}$) than ESPRIT with non-overlapping subarrays (which decreases at the rate $\frac{1}{m_0}$). When compared to MUSIC estimates (whose MSE decreases at the rate $\frac{1}{m_0^3}$), it is found that MUSIC estimates will generally give a lower MSE than ESPRIT. The simulation MSE are well in accordance with the analytical results.

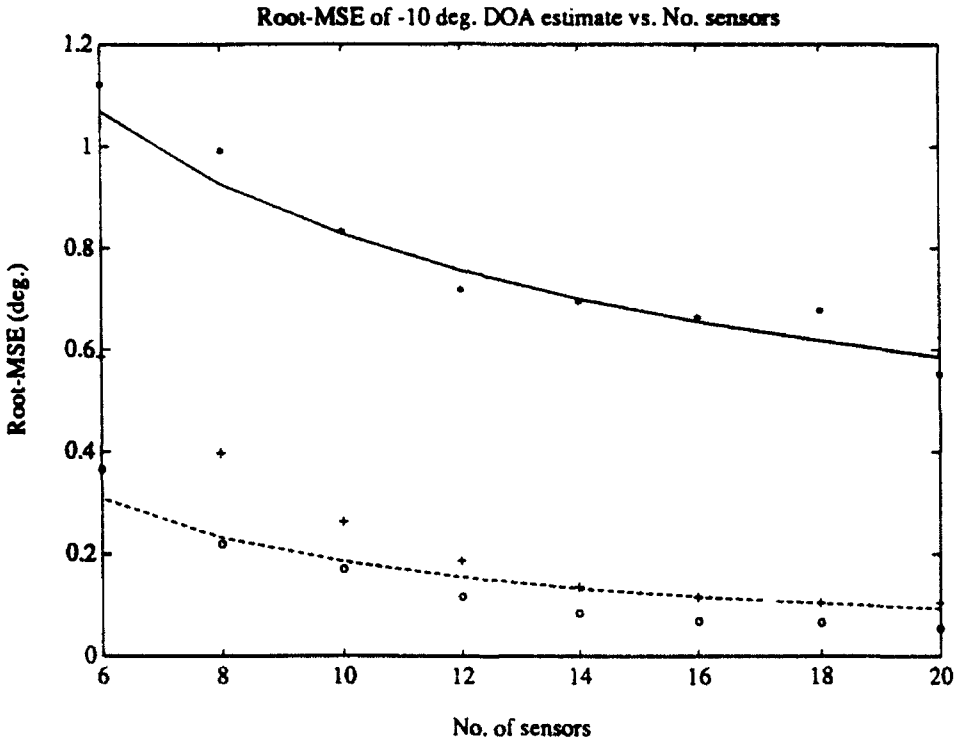

Figure 5.2: Estimate of DOA at -10 deg.

6

A SIGNAL SUBSPACE APPROACH TO MODEL ERRORS

6.1 Introduction

Eigenstructure methods such as MUSIC [53] and ESPRIT [50] have gained considerable interest in recent years due to their superresolution capabilities in resolving closely spaced sources. These methods are hampered however by the requirement of a known array manifold (i.e. , the collection of array signal vector for all possible direction of arrival (DOA) angles) as in MUSIC or that the sensor subarrays as in ESPRIT be matched.

It has been observed that in practice, even after hardware calibration, sensor arrays still suffer from gain and phase errors, location errors, etc. , [40]. The effects of random array model errors on the DOA estimates, in terms of their mean-square-error (MSE) and sensitivity, of algorithms such as ESPRIT and MUSIC have been a subject of many recent studies (see e.g. [13]-[60]). These studies have shown that the mean-square-error (MSE) of their DOA estimates will increase due to these errors. As a result, several methods have been proposed for DOA estimation under various

array model errors. For the case of DOA estimation with unknown sensor gains and phases, a method applicable only to uniform linear arrays is proposed in [38]. In [79, 39] methods based on the orthogonality of the noise subspace to the steering vector are proposed. This algorithm involves the computation of the inverse of a matrix that is close to being singular when the SNR (Signal-to-Noise Ratio) is high and when the estimates of the DOA angles are close to the true ones, as will be shown in Section III of this paper. Calibration methods using known DOA angles and experimental results on an ultrasonic sensor array testbed is presented in [40]. An approach requiring uncorrelated sources is found in [6] while a maximum-likelihood based algorithm which requires known field covariance (i.e. , the covariance matrix with no sensor gain and phase errors) is proposed in [14].

Studies of the Cramer-Rao lower bounds of the DOA estimates in the presence of random sensor locations errors and an algorithm for DOA estimation under these errors can be found in [47], [48]. The algorithm in [48] requires that sources do not overlap either in time or in frequency. An algorithm for estimating unknown sensor locations is proposed in [31] but requires that the DOA angles be known. An iterative maximum-likelihood algorithm was proposed in [80].

In this paper, a constraint on the set of sensor gains and phases and DOA angles consistent with the signal subspace is studied. This constraint is shown to yield a simple way of computing the sensor gains and phases for a given set of DOA angles. The issue of uniqueness of the set of sensor gains and phases and DOA angles is examined. It is shown that when the DOA angles are known, the estimates of the sensor gains and phases computed using the constraint are asymptotically unbiased. When the DOA angles are unknown, an iterative procedure incorporating the constraint is proposed. The iterative procedure is shown to be able to handle other array error models, notably, errors in sensor locations and errors in sensor-pair

alignments of ESPRIT-type subarrays. Simulation results are presented to show that the iterative procedure outperforms conventional ESPRIT under array model errors.

6.2 Definitions and Model Formulation

The following notational convention is used in this paper. All matrix quantities will be denoted by bold faced capital letters while vector quantities will be denoted by bold faced small letters. $(.)^T$, $(.)^\dagger$, $(.)^{-1}$ denote matrix transpose, matrix conjugate transpose and matrix inverse respectively. The determinant of a matrix is denoted as $Det(.)$.

The vector norm used here is the Euclidean vector norm denoted as $\| \, . \, \|$ and the matrix 2-norm will be denoted as $\| \, . \, \|_2$. The 2-norm of a matrix $\mathbf{M}$ is defined as that induced by the Euclidean vector norm, [15]:

$$\| \mathbf{M} \|_2 = \max_{\|\mathbf{u}\|=1.0} \| \mathbf{Mu} \| \tag{6.1}$$

The notation $\mathbf{Diag\{v\}}$ is taken to denote a diagonal matrix formed from the elements in the column vector $\mathbf{v}$.

We now define the nominal model of the DOA estimation problem.

Let m be the number of sensors in the array, n be the number of narrowband far-field sources and $\{x_i, y_i\}$ be the location of the $i-th$ sensor in the array. The nominal sensor gains and phases are assumed to be equal to unity and zero, respectively. Then the nominal model for the narrowband array signal processing problem can be stated as follows:

$$\mathbf{z} = \mathbf{As} + \eta \tag{6.2}$$

where $\mathbf{z}$ denotes the observation vector from the sensor array, $\mathbf{A}$ is the steering matrix defined by the set of distinct DOA angles $\{\theta_k\}$ (the DOA angles are measured with

reference to the y-axis of the sensor array).

$$\mathbf{A} = \left[\begin{array}{ccc} \mathbf{a}(\theta_1) & \cdots & \mathbf{a}(\theta_n) \end{array} \right]. \tag{6.3}$$

Here, the nominal steering vector at DOA angle θ as

$$\begin{aligned} \mathbf{a}(\theta) &= [1\ exp\{-j\frac{2\pi}{\lambda}(x_1 sin\theta + y_1 cos\theta)\}... \\ &\quad \cdots exp\{-j\frac{2\pi}{\lambda}(x_{m-1} sin\theta + y_{m-1} cos\theta)\}]^T \end{aligned} \tag{6.4}$$

where λ is the wavelength of the narrowband signals, s is the source vector and η denotes the additive noise at the sensor array.

The following assumptions are made throughout this paper.

(A.1) The array of m sensors is **unambiguous**, [34], i.e. , it satisfies the property that for any collection of $k \leq m$ distinct DOA angles, $\{\theta_i\}_{i=1,\ldots,k}$, the matrix $[\mathbf{a}(\theta_1), \cdots, \mathbf{a}(\theta_k)]$ has full column rank, where $m > n$, and n is known.

(A.2) The source covariance matrix $\mathbf{Q} = E\{\mathbf{s}\mathbf{s}^\dagger\}$ is positive definite.

(A.3) s and η are mutually uncorrelated and are stationary processes.

(A.4) η is additive white Gaussian with covariance $E\{\eta\eta^\dagger\} = \sigma^2\mathbf{I}$.

From the observation vector $\mathbf{z}$ the nominal covariance matrix can be expressed as :

$$\mathbf{R}_o = E\{\mathbf{z}\mathbf{z}^\dagger\} = \mathbf{A}\mathbf{Q}\mathbf{A}^\dagger + \sigma^2\mathbf{I}. \tag{6.5}$$

6.3 Array Processing Under Unknown Sensor Gains and Phases

III.1 Computation of Sensor Gains and Phases

For unknown sensor gains and phases the array model would be written as:

$$\mathbf{z} = \Gamma\mathbf{A}\mathbf{s} + \eta \tag{6.6}$$

with Γ being the diagonal matrix of unknown (DOA angle independent) sensor gains and phases where

$$\Gamma = \text{Diag}\{1, \alpha_1 e^{j\phi_1}, \cdots, \alpha_{m-1} e^{j\phi_{m-1}}\}$$

with α_i and ϕ_i denoting the i-th sensor gain and phase, respectively. We assume that all sensor gains are non-zero. Without loss of generality, the first diagonal element in Γ is assumed to be unity.

Computing the covariance matrix of $\mathbf{z}$ yields

$$\mathbf{R} = E\{\mathbf{z}\mathbf{z}^\dagger\} = (\Gamma\mathbf{A})\,\mathbf{Q}\,(\Gamma\mathbf{A})^\dagger + \sigma^2\mathbf{I}. \tag{6.7}$$

Taking the eigenvector-eigenvalue decomposition of $\mathbf{R}$ gives

$$\mathbf{R} = \mathbf{E}_s\mathbf{\Lambda}_s\mathbf{E}_s^\dagger + \sigma^2\mathbf{E}_n\mathbf{E}_n^\dagger. \tag{6.8}$$

where $\mathbf{E}_s$ denotes the eigenvector matrix of $\mathbf{R}$ associated with the signal subspace spanned by $\Gamma\mathbf{A}$, $\mathbf{\Lambda}_s$ is the eigenvalue matrix associated with it and $\mathbf{E}_n$ denotes the eigenvector matrix associated with the noise or null subspace with eigenvalue σ^2. Thus, the solution set of sensor gains and phases and DOA angles are constrained such that

$$\mathbf{E}_s\mathbf{E}_s^\dagger\Gamma\mathbf{A} = \Gamma\mathbf{A}, \tag{6.9}$$

The constraint of Eq.(6.9) is equivalent to

$$\mathbf{E}_s\mathbf{E}_s^\dagger\Gamma\mathbf{a}(\theta_i) = \Gamma\mathbf{a}(\theta_i), i = 1, 2, \cdots, n. \tag{6.10}$$

By defining $\mathbf{D}_i = \text{Diag}\{\mathbf{a}(\theta_i)\}$, a diagonal matrix composed of the components of the steering vector $\mathbf{a}(\theta_i)$, and $\mathbf{v}$ as the $m \times 1$ column vector formed from the diagonal components of Γ, i.e. , $\mathbf{v} = [1\ \alpha_1 e^{j\phi_1}\ \cdots\ \alpha_{m-1} e^{j\phi_{m-1}}\ ]^T$, we can rewrite Eq.(6.10) as

$$\mathbf{E}_s\mathbf{E}_s^\dagger\mathbf{D}_i\mathbf{v} = \mathbf{D}_i\mathbf{v}, i = 1, 2, \cdots, n. \tag{6.11}$$

Since $\mathbf{D}_i$ is a diagonal matrix composed entirely of the steering vector $\mathbf{a}(\theta_i)$ (see Eq.(6.4)), it is also unitary, i.e. $\mathbf{D}_i^\dagger \mathbf{D}_i = \mathbf{D}_i \mathbf{D}_i^\dagger = \mathbf{I}$ and therefore

$$\mathbf{D}_i^\dagger \mathbf{E}_s \mathbf{E}_s^\dagger \mathbf{D}_i \mathbf{v} = \mathbf{v}, i = 1, 2, \cdots, n. \tag{6.12}$$

In other words, from Eq.(6.12), the vector of the sensor gains and phases must be an eigenvector with unit eigenvalue of the matrices $\mathbf{W}_i$ as defined by

$$\mathbf{W}_i = \mathbf{D}_i^\dagger \mathbf{E}_s \mathbf{E}_s^\dagger \mathbf{D}_i. \tag{6.13}$$

We note that $\mathbf{W}_i$ has n unity eigenvalues and $m - n$ zero eigenvalues. Observe that the constraint of Eq.(6.9) can now be re-stated as the set of n eigenvector constraints of Eq.(6.12). This set of constraints will be used in computing the sensor gain and phase vector $\mathbf{v}$. The following theorem shows how these n eigenvector constraints can be combined into a single eigenvector constraint.

Theorem 2 *Let $\mathbf{D}_i$ and $\mathbf{W}_i$ be defined by Eqs. (6.11) and (6.13), respectively. Then ($\mathbf{v}$, 1) is an eigen-pair (eigenvector-eigenvalue pair) for $\mathbf{W}_i = \mathbf{D}_i^\dagger \mathbf{E}_s \mathbf{E}_s^\dagger \mathbf{D}_i$, $i = 1, 2, \cdots, n$ if and only if ($\mathbf{v}$, n) is an eigen-pair for*

$$\mathbf{W} = \sum_{i=1}^{n} \mathbf{W}_i = \sum_{i=1}^{n} \mathbf{D}_i^\dagger \mathbf{E}_s \mathbf{E}_s^\dagger \mathbf{D}_i. \tag{6.14}$$

where $\mathbf{v}$ is the vector defined in Eq. (6.11). Furthermore, the eigenvalue n is the largest eigenvalue of $\mathbf{W}$.

Proof: It is easy to see that if $\mathbf{v}$ is an eigenvector with unit eigenvalue for the matrices $\mathbf{W}_i$ for $i = 1, 2, \cdots, n$, then it will also be an eigenvector with eigenvalue equal to n for $\mathbf{W}$.

So, we need only show that if $\mathbf{v}$ is an eigenvector of W with eigenvalue n, then it is also an eigenvector of $\mathbf{W}_i$ with unit eigenvalue.

Suppose that $\mathbf{W}\mathbf{v} = n\mathbf{v}$. We write $\mathbf{v} = \| \mathbf{v} \| \bar{\mathbf{v}}$, where $\mathbf{v}$ has unit norm. Then,

$$\| \mathbf{W}\bar{\mathbf{v}} \| = n \leq \sum_{i=1}^{n} \| \mathbf{W}_i \bar{\mathbf{v}} \| \tag{6.15}$$

Since the 2-norm of a Hermitian, semi-positive definite matrix is equal to its largest eigenvalue, we get $\| \mathbf{W}_i \|_2 = 1.0$. From Eq.(6.15) and the definition of the matrix norm as in Eq.(6.1), we conclude that

$$\| \mathbf{W}_i \bar{\mathbf{v}} \| = 1.0, i = 1, 2, \cdots, n. \tag{6.16}$$

Eq. (6.16) is sufficient to ensure that $\bar{\mathbf{v}}$ and consequently $\mathbf{v}$ is an eigenvector of $\mathbf{W}_i$ with unit eigenvalue.

To show that n is the largest eigenvalue of $\mathbf{W}$, we need to show that $\| \mathbf{W} \|_2 = n$. Suppose that $\mathbf{W}\bar{\mathbf{v}} = n\bar{\mathbf{v}}$. Then, from the definition of the 2-norm of a matrix as in Eq.(6.1), we get

$$\| \mathbf{W} \|_2 \geq n. \tag{6.17}$$

However, we also have

$$\| \mathbf{W} \|_2 \leq \sum_{i=1}^{n} \| \mathbf{W}_i \|_2 = n. \tag{6.18}$$

Therefore, $\| \mathbf{W} \|_2 = n$.

Remark: Theorem 2 provides a way to compute the sensor gains and phases given the DOA angles, utilizing the signal subspace constraint of Eq. (6.9). As such, calibration of the array for sensor gains and phases can be done for known DOA angles.

The following corollary is an immediate consequence of the previous result.

Corollary 3 *The eigenvector* $\mathbf{v}$ *found in Theorem 2 is also an eigenvector associated with the zero eigenvalue of* $\mathbf{M}$, *where*

$$\mathbf{M} = \sum_{i=1}^{n} \mathbf{D}_i^{\dagger} \mathbf{E}_n \mathbf{E}_n^{\dagger} \mathbf{D}_i. \tag{6.19}$$

Remarks: In [79], an alternative approach was taken to arrive at related results. The approach of [79] is based on the orthogonality of $\mathbf{\Gamma A}$ to the noise subspace and a solution for $\mathbf{v}$ was proposed as :

$$\mathbf{v} = \frac{\mathbf{M}^{-1}\mathbf{e}_0}{\mathbf{e}_0^T\mathbf{M}^{-1}\mathbf{e}_0}. \tag{6.20}$$

where, $\mathbf{e}_0 = [1\ 0\cdots\ 0]^T$. It is seen from the previous corollary that, at the true DOA angles, the matrix $\mathbf{M}$ is singular. In simulations, it has been observed that the estimate of this matrix tends to have a large condition number, although it is usually still invertible (due to noise, errors in DOA estimates, etc.). In [39] the orthogonality of $\mathbf{\Gamma A}$ to the noise subspace is also exploited. From the requirement that $\mathbf{E}_n^\dagger\mathbf{\Gamma a}(\theta_k) = \mathbf{0}, k = 1, 2, .., n$, the minimum singular vector of the matrix $\mathbf{G}$ is proposed as the the gain/phase vector estimate, where

$$\mathbf{G} = \begin{bmatrix} \mathbf{E}_n^\dagger\mathbf{D}_1 \\ \mathbf{E}_n^\dagger\mathbf{D}_2 \\ \vdots \\ \mathbf{E}_n^\dagger\mathbf{D}_n \end{bmatrix} \tag{6.21}$$

Note that the evaluation of the large matrix $\mathbf{G}$ as in [39] is not neccessary. Note that the right singular vectors of $\mathbf{G}$ are the eigenvectors of $\mathbf{G}^\dagger\mathbf{G}$ and therefore,

$$\mathbf{G}^\dagger\mathbf{G} = \sum_{i=1}^{n} \mathbf{D}_i^\dagger\mathbf{E}_n\mathbf{E}_n^\dagger\mathbf{D}_i = \mathbf{M} \tag{6.22}$$

Thus from Corollary 3, the proposed estimate of the gain/phase vector of [39] and the method suggested by Theorem 1 are equivalent.

At this point however, it is not immediately apparent that the computed eigenvector $\mathbf{v}$ is unique. This issue is investigated in the sequel.

III.2 Uniqueness Issues

Given the signal subspace constraint of Eq. (6.9), there are three questions that should be addressed.

First, given $\mathbf{A}$, is the corresponding sensor gain and phase matrix $\mathbf{\Gamma}$ as constrained by Eq. (6.9) unique? Second, given the sensor gain and phase matrix $\mathbf{\Gamma}$, is the corresponding steering matrix $\mathbf{A}$ unique? Third, is there only one pair of sensor gain and phase matrix $\mathbf{\Gamma}$ and steering matrix $\mathbf{A}$ which are consistent with the constraint of Eq. (6.9)?

We examine the first question in the folowing result which gives a sufficient condition for the affirmative.

Theorem 3 *If $m \geq 2n-1$ and if all size n subarrays of the array are unambiguous, then for a given $\mathbf{A}$ (as defined by the given set of DOA angles), the set of sensor gains and phases as constrained by Eq.(6.9) is unique.*

Proof Appendix.

Remarks

1. If the condition in Theorem 3 are fulfilled, the matrix $\mathbf{W}$ of Theorem 2 would yield only one eigenvector associated with the eigenvalue n.

2. The condition in Theorem 3 that all size n sub-arrays be unambiguous imposes certain constraints on the geometry of the array. It is also equivalent to requiring that all $n \times n$ sub-matrices of $\mathbf{A}$ be non-singular. For the *case of two sources*, this condition is readily met. The determinant of any sub-matrix of $\mathbf{A}$ can then be written as:

$$Det \begin{pmatrix} a_{i1} & a_{i2} \\ a_{k1} & a_{k2} \end{pmatrix} = (a_{i1}a_{k2} - a_{i2}a_{k1}), i \neq k. \tag{6.23}$$

The quantity in Eq.(6.23) will be zero if and only if: $a_{i1}a_{k2} = a_{i2}a_{k1}$. After some algebraic manipulation, this implies that $\theta_1 = \theta_2$, and hence would violate the assumption

that $\mathbf{A}$ has full column rank.

The second question is: given the sensor gain and phase matrix $\mathbf{\Gamma}$, is the corresponding set of DOA angles (i.e. $\mathbf{A}$) as constrained by the signal subspace constraint unique? The answer is also affirmative with the condition of (A.1) proving to be sufficient in this case. This follows directly from the proof for Theorem 1 in [76].

The two questions addressed so far only guarantee that there is a one-to-one correspondence between the set of sensor gains/phases and the set of DOA angles such that the constraint is fulfilled. It leaves open the question of how many distinct pairs of sensor gains/phases and DOA angles there are. This leads to the final question, i.e. , is the set of sensor gains/phases and DOA angles consistent with the constraint Eq. (6.9) unique? This question is still an open one. We can however, state a neccessary condition which must be fulfilled.

Neccessary condition: For uniqueness of the pair $(\mathbf{\Gamma}.\mathbf{A})$ as constrained by Eq. (6.9), it is neccessary that for all diagonal matrices $\mathbf{\Lambda}$ and all steering matrices $\mathbf{A}_1 \neq \mathbf{A}_2$, we have $\mathbf{A}_1 \neq \mathbf{\Lambda}\mathbf{A}_2$.

Proof Suppose there exists a diagonal matrix $\mathbf{\Lambda}$ such that $\mathbf{A}_1 = \mathbf{\Lambda}\mathbf{A}_2$. Thus, if the pair $(\mathbf{\Gamma}, \mathbf{A}_1)$ satisfies the signal subspace constraint Eq. (6.9), then the pair $(\mathbf{\Gamma}\mathbf{\Lambda}, \mathbf{A}_2)$ which is distinct from the previous pair would also satisfy the constraint.

Remarks:

1. It can be easily shown that a linear array would violate the above neccessary condition. In [38] and in [79] it has been shown that a linear array would not yield unique solutions for the set of sensor gains and phases and DOA angles.

III.3 Calibration of Sensor Array

Known DOA angles

If the DOA angles are known *a-priori*, then Theorem 1 can be applied directly. Theorem 2 provides sufficient conditions for uniqueness of the estimate of the sensor gain and phase vector. Therefore, the eigenvector associated with the largest eigenvalue of the matrix $\mathbf{W}$ (as defined in Theorem 1) is taken to be the estimated sensor gains and phase vector. Suppose that N snapshots of the observation vector $\mathbf{z}$ are taken and the covariance matrix is estimated as:

$$\hat{\mathbf{R}} = \frac{1}{N}\sum_{i=1}^{N} \mathbf{z}(i)\mathbf{z}(i)^{\dagger} \tag{6.24}$$

The estimate of the sensor gain and phase vector in Theorem 1 can be shown to be asymptotically unbiased. Using first order perturbation analysis, the estimated signal subspace eigenvector matrix can be written as $\hat{\mathbf{E}}_s = \mathbf{E}_s + \Delta\mathbf{E}_s$, where $\Delta\mathbf{E}_s$ is the perturbation in the signal subspace due to the finite number of snapshots and noise effects. Thus, we get the estimated matrix $\hat{\mathbf{W}} = \mathbf{W} + \Delta\mathbf{W}$, where

$$\Delta\mathbf{W} = \sum_{i=1}^{N} \mathbf{D}_i^{\dagger}(\Delta\mathbf{E}_s\mathbf{E}_s^{\dagger} + \mathbf{E}_s\Delta\mathbf{E}_s^{\dagger} + \Delta\mathbf{E}_s\Delta\mathbf{E}_s^{\dagger})\mathbf{D}_i \tag{6.25}$$

Let the eigenvalues of $\mathbf{W}$ be denoted by $\{g_k\}$ where $g_1 = n > g_2 \geq \cdots \geq g_m$ and their associated unit norm eigenvectors by $\{\mathbf{v}_k\}$. Thus, we have $\mathbf{v}_1 = \frac{\mathbf{v}}{\|\mathbf{v}\|}$ where $\mathbf{v} = [1\ \alpha_1 e^{j\phi_1} \cdots \alpha_{m-1} e^{j\phi_{m-1}}]^T$. Then the estimate of the sensor gains and phases vector is written as

$$\hat{\mathbf{v}} = \frac{\mathbf{v}_1 + \Delta\mathbf{v}_1}{e_0^T(\mathbf{v}_1 + \Delta\mathbf{v}_1)e_0} \tag{6.26}$$

where $\hat{\mathbf{v}} = [1\ \hat{\alpha}_1 e^{j\hat{\phi}_1} \cdots \hat{\alpha}_{m-1} e^{j\hat{\phi}_{m-1}}]^T$, $\mathbf{e}_0 = [1\ 0 \cdots 0]^T$ and

$$\Delta\mathbf{v}_1 = \sum_{k=2}^{m} \frac{\left\{\mathbf{v}_k^{\dagger}\Delta\mathbf{W}\mathbf{v}_1\right\}}{(n - g_k)}\mathbf{v}_k \tag{6.27}$$

Approximation to first order yields

$$\hat{\mathbf{v}} = \mathbf{v} + \|\mathbf{v}\|\Delta\mathbf{v}_1 - \|\mathbf{v}\|\mathbf{v}(e_0^T\Delta\mathbf{v}_1 e_0) \tag{6.28}$$

Thus, see [23] for evaluation of $E\{\Delta\mathbf{E}_s\Delta\mathbf{E}_s^\dagger\}$ and $E\{\Delta\mathbf{E}_s\}$, we obtain

$$E\{\hat{\mathbf{v}}\} = \mathbf{v} + O(N^{-1}) \tag{6.29}$$

Hence, when the DOA angles are known, the estimates of the sensor gains and phases as computed from Theorem 1 are asymptotically unbiased.

Unknown DOA angles

In the case where both the set of sensor gains and phases and the DOA angles are not known, an iterative procedure which utilizes the constraint Eq. (6.9) is proposed. The algorithm starts with the initial DOA estimates found by assuming nominal sensor gains and phases and applying the eigenstructure algorithm. This algorithm can be either MUSIC or ESPRIT or any other eigenstructure-based algorithm. The iterative procedure is summarized in the following:

Step I. Given the previous DOA angle estimates, compute the matrix $\mathbf{W}$ where $\mathbf{W} = \sum_{i=1}^{n} \mathbf{D}_i^\dagger \mathbf{E}_s \mathbf{E}_s^\dagger \mathbf{D}_i$. Here, $\mathbf{D}_i = \mathrm{Diag}\{\mathbf{a}(\theta_i)\}$. Evaluate the eigenvector $\mathbf{v}$ associated with its largest eigenvalue and use it as the updated estimate of the sensor gains and phases.

Step II. Apply an eigenstructure method to estimate the DOA angles, using the updated sensor gains and phases to modify the method appropriately where $\hat{\mathbf{\Gamma}} = \mathrm{Diag}\{\mathbf{v}\}$.

Step III. Check for convergence of the estimates of the sensor gains and phases and DOA angles according to some convergence criterion. If converged, stop. If not, go to Step I.

In the above procedure, Step II specified for the use of ESPRIT can be stated as follows. The matrix $\mathbf{\Gamma A}$ is defined as

$$\mathbf{\Gamma A} \equiv \begin{bmatrix} \mathbf{\Gamma}_X \mathbf{B} \\ \mathbf{\Gamma}_Y \mathbf{B} \mathbf{\Phi} \end{bmatrix}.$$

Here $\mathbf{\Gamma} \equiv \begin{bmatrix} \mathbf{\Gamma}_X & \mathbf{O} \\ \mathbf{O} & \mathbf{\Gamma}_Y \end{bmatrix}$, $\mathbf{B}$ is the nominal steering matrix of the X-subarray and $\mathbf{\Phi}$

is the rotational invariance diagonal matrix. We partition the matrix $\mathbf{E}_s \equiv \begin{bmatrix} \mathbf{E}_X \\ \mathbf{E}_Y \end{bmatrix}$. Then solve for the matrix $\mathbf{\Psi}$ from the equation:

$$\mathbf{E}_X \mathbf{\Psi} = \mathbf{\Gamma}_X \mathbf{\Gamma}_Y^{-1} \mathbf{E}_Y. \tag{6.30}$$

The DOA angle estimates are then computed from the eigenvalues of $\mathbf{\Psi}$, [50]. In Section V, the use of ESPRIT in the iterative procedure will be called M-ESPRIT (Modified-ESPRIT).

6.4 Array Processing Under Other Error Models

Under appropriate assumptions, other model error scenarios can be cast in the same form as Eq. (6.6). One assumption that is needed is that:

(B.1) The magnitudes of the DOA angles lie within a "narrow" enough angular region such that their cosine values are approximately equal to each other, i.e. , $cos\theta_k \simeq cos\theta_i = const$, for $k \neq i$.

Errors in Sensor Locations (see [60]): Under small errors in sensor locations, denoting the perturbed location of the k-th sensor as $(x_k + \Delta x_k, y_k + \Delta y_k)$, we write the model as:

$$\mathbf{z} = \tilde{\mathbf{A}}\mathbf{s} + \eta \tag{6.31}$$

where $\tilde{\mathbf{A}} = [\tilde{\mathbf{a}}(\theta_1), \cdots, \tilde{\mathbf{a}}(\theta_n)]$ with $\tilde{\mathbf{a}}(\theta_k) = \tilde{\Gamma}_k \mathbf{a}(\theta_k)$ and

$$\begin{aligned} \tilde{\mathbf{\Gamma}}_k &= \mathbf{I} - j\frac{2\pi sin\theta_k}{\lambda} Diag\{\Delta x_1, \cdots, \Delta x_m\} \\ &\quad -j\frac{2\pi cos\theta_k}{\lambda} Diag\{\Delta y_1, \cdots, \Delta y_m\}. \end{aligned} \tag{6.32}$$

If the sensor location errors are such that $\Delta x_k \ll \Delta y_k$, i.e. the error is much less along the x-axis than the y-axis (which is likely to be the situation in an underwater

towed array, [67]) and using assumption (B.1), we can approximate the matrix $\tilde{\Gamma}_k$ by a constant matrix Γ where

$$\Gamma \simeq \mathbf{I} - j\frac{2\pi}{\lambda}\text{Diag}\{\Delta y_1, \cdots, \Delta y_m\} \times const.$$

Thus the model can be written as in Eq. (6.6).

Errors in Sensor-Pair Alignments (see [60]): In ESPRIT, two subarrays, denoted here as X- and Y-subarrays are configured in such a way that their observation vectors are related by a rotational invariance diagonal matrix. Each sensor in the X-subarray is paired with a sensor in the Y-subarray and all of these sensor pairs are aligned such that their normal face the same direction, (see Fig. 1). A source of error would then be the misalignments of these sensor-pairs such that they are rotated about their mid-points by small angles $\{\beta_k\}_{k=1,\ldots,m}$. Here m is the number of sensors in a subarray. We write the model as:

$$\mathbf{z} = \tilde{\mathbf{A}}\mathbf{s} + \eta \tag{6.33}$$

where

$$\tilde{\mathbf{A}} \equiv \begin{bmatrix} \tilde{\mathbf{B}}_X \\ \tilde{\mathbf{B}}_Y \Phi \end{bmatrix}.$$

Where Φ is the rotational invariance matrix defined by

$$\Phi = \text{Diag}\{exp(-j\frac{2d\pi}{\lambda}sin\theta_1), \ldots, exp(-j\frac{2d\pi}{\lambda}sin\theta_n)\}$$

and

$$\tilde{\mathbf{B}}_X = [\Gamma_{X1}\mathbf{b}(\theta_1), \cdots, \Gamma_{Xn}\mathbf{b}(\theta_n)] \tag{6.34}$$

$$\tilde{\mathbf{B}}_Y = [\Gamma_{Y1}\mathbf{b}(\theta_1), \cdots, \Gamma_{Yn}\mathbf{b}(\theta_n)] \tag{6.35}$$

Here

$$\tilde{\Gamma}_{Xk} = \mathbf{I} - j\frac{2\pi d\cos\theta_k}{\lambda}\mathrm{Diag}\{\beta_1, \cdots, \beta_m\}$$

and

$$\tilde{\Gamma}_{Yk} = \mathbf{I} + j\frac{2\pi d\cos\theta_k}{\lambda}\mathrm{Diag}\{\beta_1, \cdots, \beta_m\}.$$

Here, d is the spacing between the sensors in a sensor-pair and $\mathbf{b}(\theta_k)$ is the nominal steering vector of the X-subarray at angle θ_k.

Under assumption (B.1), we can write the error model in the same form as Eq. (6.6) with

$$\mathbf{\Gamma}_X \simeq \mathbf{I} - j\frac{2\pi d}{\lambda}\mathrm{Diag}\{\beta_1, \cdots, \beta_m\} \times const.$$

$$\mathbf{\Gamma}_Y \simeq \mathbf{I} + j\frac{2\pi d}{\lambda}\mathrm{Diag}\{\beta_1, \cdots, \beta_m\} \times const.$$

Thus, the problem of estimating DOA angles under the scenarios of errors in sensor locations (where errors in the y-axis dominates) and where the sensor-pairs in ESPRIT type of subarrays are mis-aligned can also be handled by the proposed iterative algorithm also.

Remark: The situation where more than one type of errors are present can still be handled by the iterative procedure as their combined error model would still be of the same form as that of the single error model.

6.5 Simulation Examples

Example 1 (Errors in sensor gains and phases)

The ESPRIT subarrays used in the simulation experiments are configured as in Fig. 4.3. The total number of sensors in the array is eight, i.e. $m = 8$, and the spacing

between sensor pairs is taken to be $d = \frac{\lambda}{2}$. Nominal sensor gains and phases are unity and zero respectively.

There are three uncorrelated sources at DOA angles of -30, +5, and +20 degrees. all at the same SNR level. The means and MSEs are averaged over two hundred trials. ESPRIT and M-ESPRIT are applied with fifty iterations of M-ESPRIT per trial.

Fig. 2 shows a typical plot of the MSE vs. SNR for the estimate of the DOA at +20 degrees. The solid and dashed-lines denote M-ESPRIT and ESPRIT, respectively. Four hundred snapshots are taken per trial and errors are introduced such that the gains are perturbed by up to 8 percent of their nominal values while the phases are perturbed by up to 9 degrees.

Next, the SNR is fixed at 20 dB and the snapshot size (N) is varied. The sensor phases are perturbed by up to ± 17 degrees (with zero nominal phase) and the sensor gains by up to 8 percent of the nominal gain of unity. Fig. 3 shows a typical plot of the MSE for the estimate of the DOA angle at +20 degrees. As before, the solid and dashed-lines denote M-ESPRIT and ESPRIT, respectively.

M-ESPRIT is able to provide better DOA angle estimates than conventional ESPRIT as can be seen from Figs. 2 and 3. Our experiments also suggests that the DOA angle estimates of M-ESPRIT show smaller bias as opposed to ESPRIT estimates which demonstrate significant bias.

Example 2 (Errors in sensor gains, phases and locations)

There are three uncorrelated sources at DOA angles of -20, +5 and +20 degrees all at SNR of 30dB. Five hundred snapshots are taken per trial and the means and MSEs of the DOA estimates averaged over two hundred Monte Carlo trials are evaluated. The sensor locations are perturbed in the y-axis by up to 0.1λ while no error is

induced in the x-axis, and the sensor gains and phases are perturbed by up to 10 percent and $\pm$ 90 degrees respectively.

The M-ESPRIT algorithm (two hundred iterations per trial) and the conventional ESPRIT algorithm are applied and the estimated means and root-MSE of the DOA estimates are tabulated in Table 1. As can be seen from Table 1, the iterative algorithm is able to give better DOA estimates under these combined errors than the conventional ESPRIT algorithm.

6.6 Conclusions

The problem of array signal processing under unknown sensor gains and phases is studied. A signal subspace constraint is used to yield a simple way of computing the sensor gains and phases from a given set of DOA angles. The question of uniqueness of the set of sensor gains and phases and DOA angles is discussed. When the DOA angles are known *a-priori*, the estimates of the sensor gains and phases are shown to be asymptotically unbiased. For the case where the DOA angles are also unknown, an iterative procedure is proposed. The approach in the paper is shown to be applicable to two other model error scenarios under appropriate assumptions. These scenarios are: unknown sensor locations and unknown rotation of sensor pairs in ESPRIT type subarrays. Simulation experiments show that the iterative algorithm provides better DOA estimates than does the conventional ESPRIT.

Appendix

Proof of Theorem 3 We argue by contradiction. Suppose, for a given $\mathbf{A}$, that there exists two sets of sensor gains and phases as defined by the matrices $\mathbf{\Gamma_1}$ and $\mathbf{\Gamma_2}$ such that $\mathbf{\Gamma_1} \neq \mathbf{\Gamma_2}$ and they both fulfill Eq.(6.9).

Then $\mathbf{E_s E_s^\dagger \Gamma_1 A} = \mathbf{\Gamma_1 A}$ and $\mathbf{E_s E_s^\dagger \Gamma_2 A} = \mathbf{\Gamma_2 A}$ This implies that rank$[\mathbf{A}|\mathbf{\Lambda A}] = n$, where $\mathbf{\Lambda} = \mathbf{\Gamma_1^{-1}\Gamma_2} = \text{Diag}\{\ 1, \lambda_1, \cdots, \lambda_{m-1}\ \}$. Thus,

$$rank[\mathbf{A} - \mathbf{\Lambda A}|\mathbf{\Lambda A}] = n \tag{6.36}$$

Writing out this matrix explicitly, with $\mathbf{A} \equiv [a_{ik}]$, we have

$$[\mathbf{A}-\mathbf{\Lambda A}|\mathbf{\Lambda A}] = \left[\begin{array}{ccc|ccc} 0 & \cdots & 0 & 1 & \cdots & 1 \\ (1-\lambda_1)a_{11} & \cdots & (1-\lambda_1)a_{1,n} & \lambda_1 a_{11} & \cdots & \lambda_1 a_{1,n} \\ \vdots & \cdots & \vdots & \vdots & \cdots & \vdots \\ (1-\lambda_{m-1})a_{m-1,1} & \cdots & (1-\lambda_{m-1})a_{m-1,n} & \lambda_{m-1}a_{m-1,1} & \cdots & \lambda_{m-1}a_{m-1,n} \end{array}\right] \tag{6.37}$$

Consider the $(n+1) \times (n+1)$ sub-matrix of Eq.(6.37) found by taking the block from the first row to the $(n+1)$-th row and the first column to the $(n+1)$-th column. We can write this as:

$$submatrix[\mathbf{A} - \mathbf{\Lambda A}|\mathbf{\Lambda A}] = \left[\begin{array}{ccc|c} 0 & \cdots & 0 & 1 \\ (1-\lambda_1)a_{11} & \cdots & (1-\lambda_1)a_{1,n} & \lambda_1 a_{11} \\ \vdots & \cdots & \vdots & \vdots \\ (1-\lambda_n)a_{n,1} & \cdots & (1-\lambda_n)a_{n,n} & \lambda_n a_{n,1} \end{array}\right] \tag{6.38}$$

This sub-matrix is singular from Eq.(6.36). Taking the determinant and using the fact that every $n \times n$ sub-matrix of A is non-singular, we conclude that

$$\prod_{i=1}^{n}(1-\lambda_i) = 0 \tag{6.39}$$

Hence, from Eq.(6.39), for at least one i, it must be that $\lambda_i = 1.0$. Using the same reasoning repeatedly as in eqs.(6.37)-(6.39), we can show that at least $(m-n)$ of the λ_i terms are equal to 1.0.

We next show that the remaining $(n-1)$ λ_i terms are also equal to 1.0. Without loss of generality we can assume that the first $(m-n)$ λ_i terms have been shown to equal 1.0. We now consider the matrix $[\mathbf{A}|\mathbf{\Lambda A}]$ with these $(m-n)$ unit values of λ_i plugged into the matrix.

Consider the $(n+1) \times (n+1)$ sub-matrix of $[\mathbf{A}|\mathbf{\Lambda A}]$ found by taking the block from the first to the $(n+1)th$ column and the $(m-2n+1)th$ row to the $(m-n+1)th$ row. Note that the assumption that $m \geq 2n-1$ ensures that there are enough rows such that this is possible. Then

$$submatrix[\mathbf{A}|\mathbf{\Lambda A}] = \left[\begin{array}{ccc|c} a_{m-2n+1,1} & \cdots & a_{m-2n+1,n} & a_{m-2n+1,1} \\ \vdots & \cdots & \vdots & \vdots \\ a_{m-n,1} & \cdots & a_{m-n,n} & a_{m-n,1} \\ a_{m-n+1,1} & \cdots & a_{m-n+1,n} & \lambda_{m-n+1}a_{m-n+1,1} \end{array}\right] \tag{6.40}$$

Subtracting the last column vector from the first column vector in Eq.(6.40) we get the matrix:

$$\left[\begin{array}{ccc|c} 0 & a_{m-2n+1,2} & \cdots & a_{m-2n+1,n} & a_{m-2n+1,1} \\ \vdots & \vdots & \cdots & \vdots & \vdots \\ 0 & a_{m-n,2} & \cdots & a_{m-n,n} & a_{m-n,1} \\ (1-\lambda_{m-n+1})a_{m-n+1,1} & a_{m-n+1,2} & \cdots & a_{m-n+1,n} & \lambda_{m-n+1}a_{m-n+1,1} \end{array}\right] \tag{6.41}$$

Taking the determinant of Eq.(6.41) which is equal to zero, and using the fact that any $n \times n$ sub-matrix of $\mathbf{A}$ has to be non-singular, we get the result that either $a_{m-n+1,1} = 0$ or $\lambda_{m-n+1} = 1.0$. Since all the elements of A have unit magnitude as can be seen from Eq. (6.4) implying $a_{m-n+1,1} \neq 0$, we conclude that $\lambda_{m-n+1} = 1.0$.

Using similar reasoning, we can show that

$$\lambda_i = 1.0, i = m-n+1, ..., m-1. \tag{6.42}$$

Hence, we can write $\Lambda = \mathbf{I}$ or equivalently $\mathbf{\Gamma_1} = \mathbf{\Gamma_2}$. This contradicts our initial assumption that $\mathbf{\Gamma_1} \neq \mathbf{\Gamma_2}$. □

TABLE 1

True DOA	Mean (deg.)		
	-20	+5	+20
ESPRIT	-14.279	11.690	43.372
M-ESPRIT	-18.949	2.052	21.290

True DOA	Root-MSE (deg.)		
	-20	+5	+20
ESPRIT	5.721	6.690	23.372
M-ESPRIT	1.060	2.976	1.311

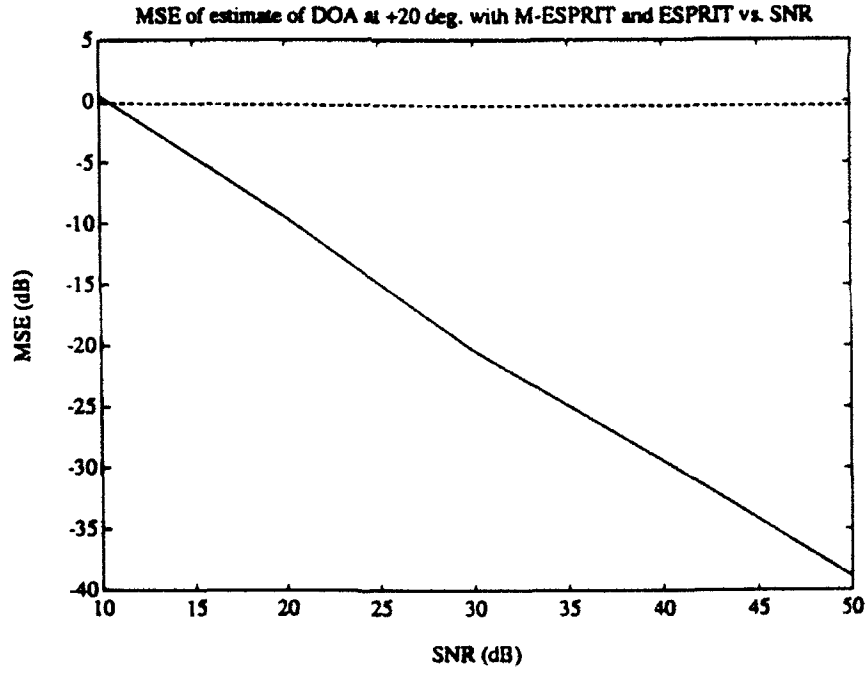

Figure 6.1: Plots of MSE DOA estimate at +20 degrees vs. SNR

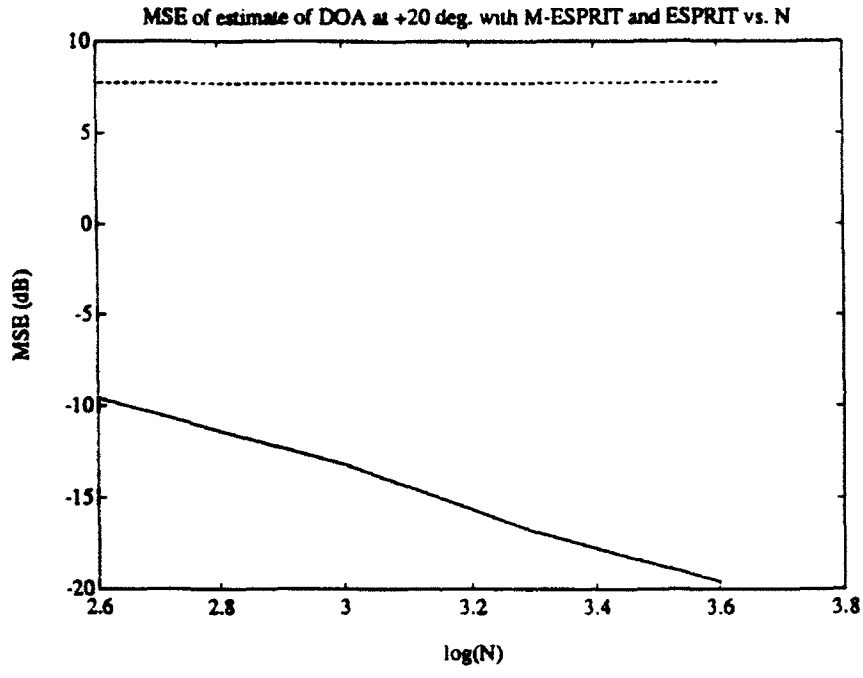

Figure 6.2: Plots of MSE DOA estimate at +20 degrees vs. N

7

A BLIND IDENTIFICATION APPROACH TO SIGNAL SEPARATION

7.1 Introduction

In recent years, there has been interest in wideband array signal processing - i.e., the processing of wideband signals obtained from arrays of sensors. This is of interest in such diverse areas as in radar and sonar processing, where parameters of interest include the direction-of-arrival (DOA) of multiple signal sources, their respective power, signal copy, time delay estimation, or as in speech processing where the desired speech source signals are extracted from corrupted or mixed recordings from microphone arrays (the so-called 'cocktail party problem'); or as in biomedical signal processing where EMG recordings from multiple sensors are processed.

In practical applications, robustness is often a major problem for many modern array signal processing techniques. Most algorithms assume certain array structure with known or accurately calibrated characteristics such as sensor gains/phases and locations. In reality, errors always present in actual physical systems and as a result these algorithms may not perform as well or even fail completely [60],[68, 69].

Consider the teleconference scenario where an array of microphone is set before an audience. The speakers may be distributed near or far away from the array and there may be interference sources such as fan hum, music, etc. In this situation it is not realistic to assume that the speaker locations are known *a-priori*. Note also that the relative powers of the speakers would be stronger when they are directly facing the array and not as strong otherwise. This scenario shows that the source locations and sensor gains cannot be assumed to be known. Thus there is a need for new algorithms or approaches that is robust to these types of uncertainties.

7.1.1 A New Approach and Its Features

In this chapter, a new method based on the so called blind identification is proposed for the source estimation (signal copy) problem. By exploiting signal characteristics such as statistical independencies, the proposed approach allows maximum uncertainties associated with sensor array and signal propagation environment. The key feature of the proposed algorithm is its robustness against the following model uncertainties:

- *Unknown Sensor Gains*: Complete calibration of sensors may be costly. Sensors may have different gain patterns in different directions. While most methods assume known sensor gains, the proposed method is not only insensitive to gain uncertainties, it also provides estimates of array sensor gains.

- *Unknown Combinations of Near-Field and Far-Field Sources*: The proposed method can deal with near-field and far-field sources *simultaneously*. It offers source location estimates for near-field sources and direction of arrival estimates for the far-field sources. Such capability is potentially important in applications such as robotic vision.

- *Unknown Combinations of Narrowband and Wideband Sources*: The sources may be a combination of wideband signals such as voices and narrow-band signals such as humming noise with *unknown* frequency locations. The proposed approach is able to estimate each source and in fact identify their frequency characteristics (narrow-band or wideband).

- *Unknown Source Spectral Characteristics*: The sources can be overlapping or non-overlapping in their *unknown* power spectra. The proposed approach fully utilizes the entire freqency band to obtain joint estimates of the signal location and channel parameters.

- *Unknown number of signals*: The proposed method does not assume that the number of signals is known. A new clustering-based technique is proposed to determine the number of sources. Such a method is crucial when the number of sources can not be determined at a particular frequency. As an example, consider the case where there are four sources, two of which have overlapping spectra disjoint from the other two. Then any estimation of the number of sources at any particular frequency would yield less than four sources.

The proposed method will be demonstrated both for wideband scenarios such as separate multiple voice sources and for narrowband plus wideband scenarios, involving near-field and far-field sources and different array uncertainties.

7.1.2 Related Works

In radar and sonar applications, the directions-of-arrivals of multiple sources are of much interest. A variety of eigenstructure-based methods have been developed for estimating DOAs of these sources and when the model assumptions of these methods are satisfied, they are capable of giving good estimation performance, see eg., [53, 50].

However, in the presence of sensor errors or model uncertainties, these methods would deteriorate or fail altogether.

Sensor errors in the actual physical array system can arise from changes in the environment in which the sensor array is placed, the degradation of electronic components, calibration errors which result in uncertainties in the sensor gains and phases. As a result of this, several eigenstructure-based approaches have been proposed for the DOA estimation problem under sensor errors for narrowband sources, see [81, 80, 6]. These methods are usually iterative in nature and involve some sort of multi-dimensional search over the space of the unknown sensor parameters and DOA angles. Consequently, these methods are computationally intensive and may suffer from convergence to local minimum solutions.

Microphone array processing have been proposed for speech de-reverberation, enhancement and noise reduction, co-channel interference rejection and extraction of desired speech sources from noise or jammer contaminated observations, see [25, 36, 32, 12, 16, 57, 22]. The use of microphone arrays has a host of intriguing and exciting applications such as a front end for automatic speech recognition, teleconferences and hands-free cellular telephony in cars. Most of these approaches are based on the beamformer concept in array signal processing, where the individual outputs of the array are delayed and summed in such a way as to produce a narrow beam of sensitivity towards the direction of the desired signal. These approaches however require model assumptions that are not easily satisfied such as identical microphones, ideal point sources for the source signals, calibration of the microphone array, known source locations or in the far field, etc.

This chapter is organized as follows. After presenting the problem models and assumptions in Section 2, we summarize certain results in blind identification and estimation of independent sources in Section 3. In Section 4, we outline the proposed

approach and give detailed discussions. We present simulations separating multiple voice sources to demonstrate our approach. We conclude with some comments on some variations and future work.

Throughout this chapter, we assume the following notational convention: All matrix quantities will be denoted by upper case bold faced symbols while vector quantites will be denoted by lower case bold faced symbols. Also, the symbols $(.)^t$, $(.)^\dagger$, $(.)^{-1}$ and $(.)^\#$ will denote the transpose of (.), the complex conjugate transpose of (.), the inverse of (.) and the pseudo-inverse of (.) respectively.

7.2 Models and Assumptions

The problem of estimating multiple sources is illustrated in Figure 7.1. From the

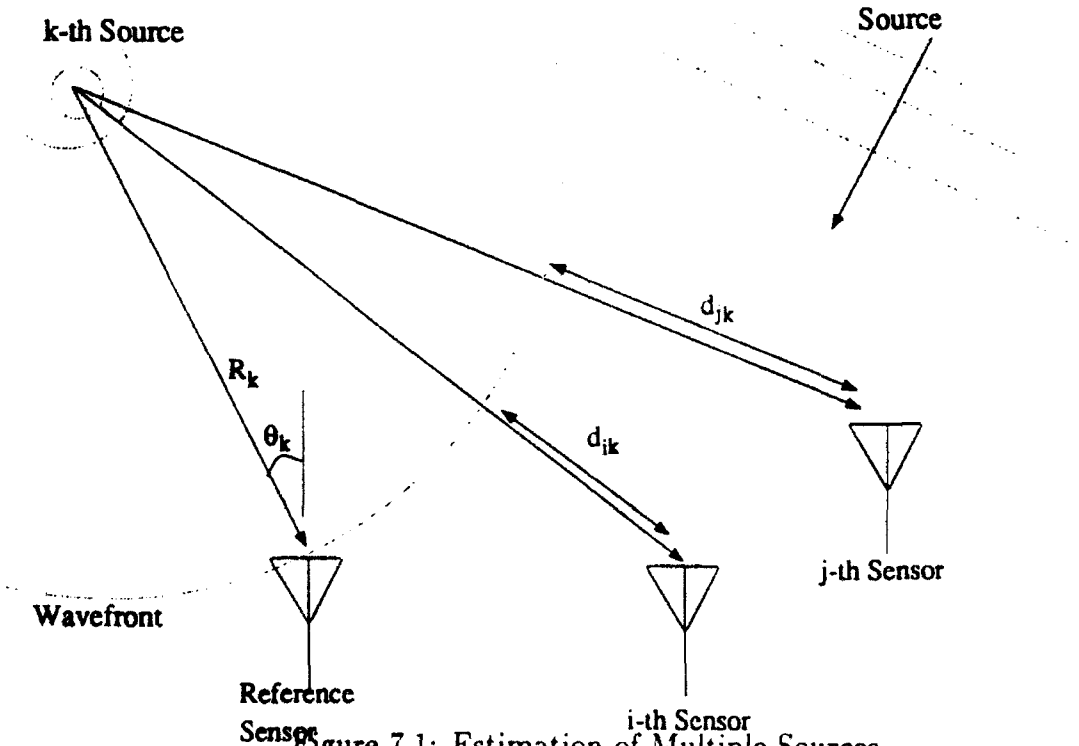

Figure 7.1: Estimation of Multiple Sources

signals collected by m sensors $\{x_i(t)\}$, our objective is to estimate the n sources

$\{s_i(t)\}$. A wideband model is given in time domain by

$$x_i(t) = \sum_{k=1}^{n} a_{ik} s_k(t - \tau_{ik}) + \eta_i(t), \; i = 1, 2, \cdots, m. \tag{7.1}$$

where

$x_i(t)$: received signal at the ith sensor.

m: the number of sensors (known).

a_{ik}: (unknown) channel coefficient that characterizes attenuation of the kth source at the ith sensor as the results the sensors and sources directionality, sensitivity, gains, geometrical spreading, etc. Without loss of generality, the first sensor is taken as a reference and $a_{1k} = 1$.

s_k: the k-th (unknown) source signal.

τ_{ik}: (unknown) time delay at the i-th sensor of the k-th source. Again, the delays are taken as the relative delays with respective to the reference sensor and $\tau_{1k} = 0$. The delays are related to the path difference given by $\tau_{ik} = \frac{d_{ik}}{c}$, where d_{ik} is the path difference of the k-th source to the i-th sensor (relative to the reference sensor) and c is the speed of propagation. See Figure (7.1). The time delays are due to the spatial distribution of the sensors and source locations (i.e., the DOA angles θ_k and ranges R_k). Propagation of the signals through the channel can be far-field or near field or any combination thereof.

n: the number of sources (unknown).

The corresponding frequency domain description of the above model is obtained by taking Fourier transform of the time domain model

$$\mathbf{x}(\omega) = \mathbf{A}(\omega)\mathbf{s}(\omega) + \eta(\omega) \tag{7.2}$$

where, $\mathbf{x}(\omega)$, $\mathbf{s}(\omega)$, and $\eta(\omega)$ are the Fourier transform of $\mathbf{x}(t)$,$\mathbf{s}(t)$ and $\eta(t)$, respectively, and

$$\mathbf{A}(\omega) = \begin{bmatrix} 1.0 & \cdots & 1.0 \\ a_{21}e^{-j\omega\tau_{21}} & \cdots & a_{2n}e^{-j\omega\tau_{2n}} \\ \vdots & \cdots & \vdots \\ a_{m1}e^{-j\omega\tau_{m1}} & \cdots & a_{mn}e^{-j\omega\tau_{mn}} \end{bmatrix} \tag{7.3}$$

The problem then is to estimate the gains a_{ik} (the channel coefficients), delays τ_{ik} (or DOA angles θ_k and ranges R_k) and the individual signals, $s_k(t)$.

Remarks: Considerable simplification of the problem can be achieved if the sources are all narrowband. However, most signals of interest (such as acoustic ones) are not narrowband signals. Consider the following case for a speech signal. For a speech signal with a bandwidth of 4kHz, the time delays would have to be much less than .25 milliseconds to meet the narrowband assumption. At a sound velocity (in air) of 340 m/s, this implies that the path lenghts of the signal to any two sensors cannot differ by more than .085m. Thus, in order for the narrowband assumption to be valid, *all* the sensors within the array must lie within a distance of 8.5cm or less from each other! It is therefore essential to consider the wideband case.

The key assumption used in the proposed approach is signal (statistical) independency. Although such an assumption appears rather restrictive, it holds approximately among signals from different sources. It is also important to note that, from our simulations of using different speech and music signals, our algorithm performs well even if there is no proof that the signals involved are statistically independent. Specifically, the assumptions adopted in this chapter is given as follows.

Basic Model Assumption

A1: $s_i(t)$'s are zero-mean and mutually independent.

A2: $\eta_i(t)$'s are zero-mean Gaussian noise independent of $s_i(t)$'s.

7.3 Proposed Approach

The central idea of the proposed approach stems from the idea of applying blind identification techniques to the frequency domain model

$$\mathbf{x}(\omega) = \mathbf{A}(\omega)\mathbf{s}(\omega) + \eta(\omega) \tag{7.4}$$

where matrix $\mathbf{A}(\omega)$ contains the information of source location and channel characteristics as specified by (7.3). The source can then be extracted from the observation by applying least-square methods to (7.4). A schematic diagram of the proposed approach is shown in Figure (7.2).

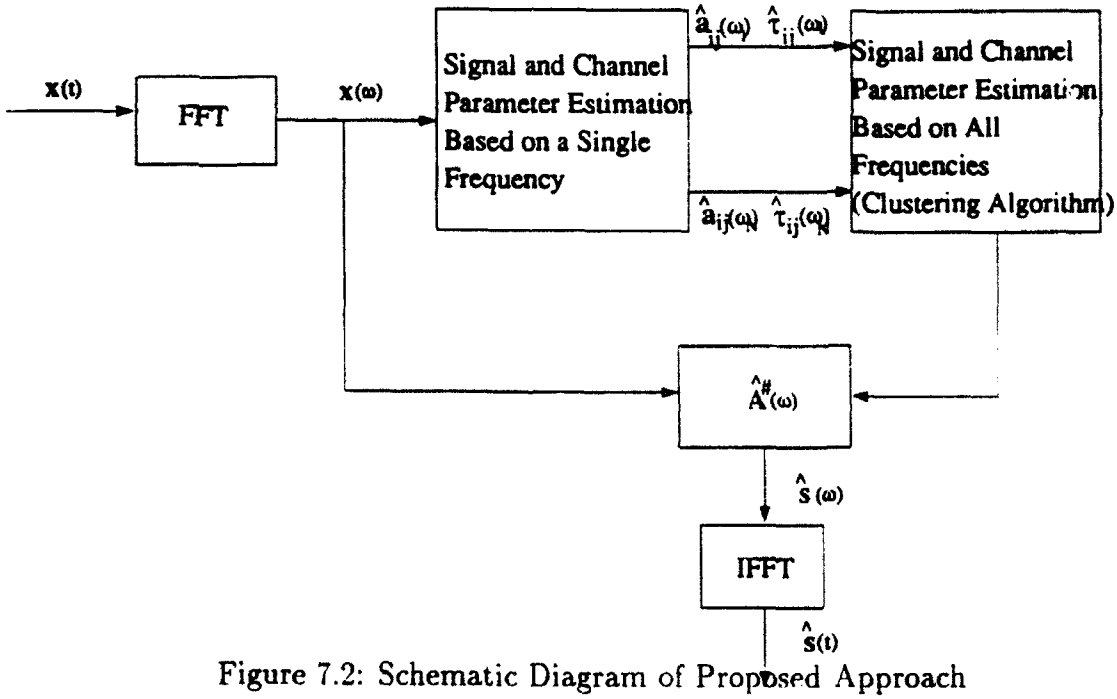

Figure 7.2: Schematic Diagram of Proposed Approach

We must, however, pay special attention to certain subtleties due to the fact that the spectra of the source signals are unknown. Because each source may or may not have energy at a particular frequency, not all the source locations and channel

parameters can be estimated. The challenge is to obtain estimates at each frequency and combine them to form joint estimates. We shall next discuss the functions of blocks in the schematic diagram.

7.3.1 Blind Identification and Estimation of Independent Sources

The so-called blind identification and estimation deals with the problem of estimating source signals when the transmission channel is unknown [10, 70]. This seemingly ill-posed problem is approached by exploiting the statistical properties of the source signals. In the context of signal estimation problem considered in this chapter, the statistical independency of different sources enables us to allow various model uncertainties as outlined in the Introduction.

The basic identification and estimation (blind) problem considered in this chapter involves a linear model

$$\mathbf{x}(t) = \mathbf{A}\mathbf{s}(t) + \mathbf{n}(t) \tag{7.5}$$

where $\mathbf{x}$ is the observation random vector, matrix $\mathbf{A}$ corresponds to the channel characteristics, $\mathbf{s}(t)$ is the source random vector, and $\mathbf{n}(t)$ is the measurement noise. The objective of blind identification and estimation is to identify and estimate both $\mathbf{A}$ and $\mathbf{s}(t)$ from $\mathbf{x}(t)$. In particular, we deal with the folowing questions:

Given $\mathbf{x}(t)$ *generated from independent source* $\mathbf{s}(t)$, *nonsingular channel parameter matrix* $\mathbf{A}$, *and additive Gaussian noise* $\mathbf{n}(t)$,
Q1: to what extend $\mathbf{A}$ *and* $\mathbf{s}(t)$ *can be determined?*
Q2: how to estimate $\mathbf{A}$ *and* $\mathbf{s}(t)$.

These questions have been resolved recently [73], [74], and their answers are summarized in the following.

Theorem 4 *The channel parameter matrix* $\mathbf{A}$ *is uniquely determined by the observation statistics up to post multiplications of a diagonal matrix and a permutation matrix if and only if all except perhaps one source are non-Gaussian.*

An important implication of the above theorem is that the waveforms of the independent sources can be recovered from the observation without knowing the channel as long as they are non-Gaussian. Although scales and orders of these signals can not be determined without further information, it is hardly a problem in practice since the waveforms of these signals are obtained. Such kind of identification is referred to as waveform-preserving blind identification.

There are different methods of determining the channel parameter matrix from the statistics of the observation. Using the fourth-order moments, Cardoso proposed the fourth-order blind identification algorithm (FOBI) [10]. The FOBI algorithm has the restriction that the source signals must have distinct kurtoses and be noise-free. A slight extension can be obtained when the noise is spatially white or the noise statistics are known [70], [61]. Algorithms using cumulants of arbitrary-orders was presented in [74]. These algorithms eliminates the restrictions on the source and applies to arbitrary unknown Gaussian source.

7.3.2 Source Location Estimation using a Single Frequency

At a fixed frequency ω_0, we can estimate, by a applying blind identification method, K columns of matrix $\mathbf{A}(\omega)$ that correspond the K signals having energy at ω_0,. Consequently, we obtain the estimates of the gain factors $\{a_{ij}\}$ and the phases $\{e^{-j\omega\tau_{ij}}\}$ corresponding to these K signals. The key question addressed here is how to infer the locations of the K sources from the estimates $\{e^{-j\omega\tau_{ij}}\}$.

There are two ways to go about estimating the source locations from the estimates

of $\{e^{-j\omega\tau_{ij}}\}$, found by using blind identification. The first approach applies when a certain uniqueness condition imposed on the sensor and source holds. In [59], several closed form solutions for the source locations given the relative path differences is proposed that may be readily applied to the present problem. Note however, that the relative path differences are determined from the estimates of $\{e^{-j\omega\frac{d_{ij}}{c}}\}$ which limit the path difference values (to avoid phase wrapping) such that

$$|\frac{\omega}{c}|\, max\{|\, d_{ik}\,|\} \leq \pi. \tag{7.6}$$

Unfortunately, it is impossible to verify the above condition since d_{ik}'s are unknown. A more useful (sufficient) condition can be obtained easily as

$$|\frac{\omega}{c}|\, r \leq \pi, \tag{7.7}$$

where r is the maximum radial distance of the sensor array. The above constraint can of course always be satisfied if only the low frequencies are used. The advantage of this method is its simplicity while the disadvantage is that the entire frequency range is not fully utilized. Note also that the sources may themselves not contain much energy at low frequencies. Thus, a method that is able to exploit the full range of available frequencies is more attractive, and the next subsection presents one such method.

Source Location Estimation Method

Instead of obtaining source location estimates from the relative path differences, this method obtains the source location estimates from $\{e^{-j\omega\frac{d_{ij}}{c}}\}$ directly, and hence avoid the problem of phase wrapping.

Consider the sensor pair $(i,\bar{i})$ located at the same radial distance and separated by an angle of 180 degrees, see for example Fig. 7.3. This type of sensor pair can be

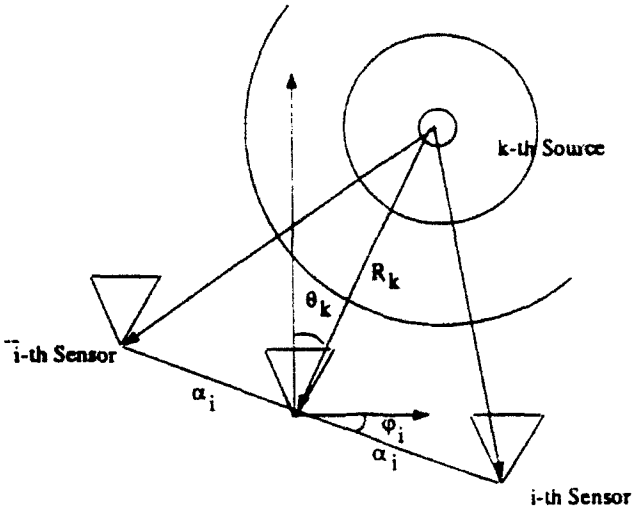

Figure 7.3: Sensor Pair

found in common array configurations such as ULAs (uniform linear arrays), circular arrays and cross arrays. Then their path differences (relative to the reference sensor at the origin) are

$$d_{ik} = \alpha_i sin(\theta_k + \phi_i) - \frac{\alpha_i^2}{2R_k} cos^2(\theta_k + \phi_i). \tag{7.8}$$

$$d_{\bar{i}k} = -\alpha_i sin(\theta_k + \phi_i) - \frac{\alpha_i^2}{2R_k} cos^2(\theta_k + \phi_i). \tag{7.9}$$

where R_k denotes the range of the k-th source relative to the reference sensor, θ_k is the DOA angle of the k-th source relative to the reference sensor (measured from the vertical axis), α_i is the radial distance of the i-th sensor from the reference sensor and ϕ_i is the angle position of the i-th sensor relative to the reference sensor (measured from the horizontal axis).

Both the path differences in the $(i, \bar{i})$ sensor pair have the same curvature term $\frac{\alpha_i^2}{2R_k} cos^2(\theta_k + \phi_i)$. This fact is used in decoupling the search for the DOA angles from

the search for the source range.

Suppose that the application of blind identification at a frequency of ω yields the following for the steering elements of the $(i,\bar{i})$ sensor pair.

$$\mathbf{a}_i(\theta_k, R_k) = \begin{bmatrix} exp\{-j\frac{\omega}{c}\alpha_i sin(\theta_k+\phi_i)\} \\ exp\{j\frac{\omega}{c}\alpha_i sin(\theta_k+\phi_i)\} \end{bmatrix} exp\{j\frac{\omega}{c}\frac{\alpha_i^2}{2R_k}cos^2(\theta_k+\phi_i)\} \tag{7.10}$$

We ignore the gain terms since they appear in the magnitudes of the steering elements and can be normalized to unity once estimated. Then consider the problem of fitting the steering vector for the $(i,\bar{i})$ sensor pair, say $\mathbf{c}_i(\theta, R)$, with the estimated blind id. estimate, using

$$f_i(\theta, R) = \| \mathbf{c}_i^{\dagger}(\theta, R)\mathbf{a}_i(\theta_k, R_k) \|^2 \tag{7.11}$$

where

$$\mathbf{c}_i(\theta, R) = \begin{bmatrix} exp\{-j\frac{\omega}{c}\alpha_i sin(\theta+\phi_i)\} \\ exp\{j\frac{\omega}{c}\alpha_i sin(\theta+\phi_i)\} \end{bmatrix} exp\{j\frac{\omega}{c}\frac{\alpha_i^2}{2R}cos^2(\theta+\phi_i)\} \tag{7.12}$$

Note however that the terms involving R and R_k are eliminated in the above fitting function since they appear as scaling phases and have unit magnitude. The function is thus dependent only on the angle θ and attains a maximum value at the angle $\theta = \theta_k$. For L sensor pairs we define the fitting function as

$$f(\theta) = \sum_{i=1}^{L} \| \mathbf{c}_i^{\dagger}(\theta)\hat{\mathbf{a}}_i \|^2 \tag{7.13}$$

where

$$\mathbf{c}_i(\theta) = \begin{bmatrix} exp\{-j\frac{\omega}{c}\alpha_i sin(\theta+\phi_i)\} \\ exp\{j\frac{\omega}{c}\alpha_i sin(\theta+\phi_i)\} \end{bmatrix} \tag{7.14}$$

and $\hat{\mathbf{a}}_i$ denotes the blind identification estimate of $\mathbf{a}_i(\theta_k, R_k)$. The DOA estimate for the k-th source is then found by

$$\hat{\theta}_k = arg\left\{\max_{\theta} f(\theta)\right\} \tag{7.15}$$

Remark: The k-th source range can be estimated once the k-th DOA is estimated by defining a fitting function similar to the one above.

The k-th source range can also be estimated independently of the DOA angle estimate through the use of a cross-array structure, see Fig. 7.4 for an example of a cross-array. In this case the search for the range can be conducted in parallel

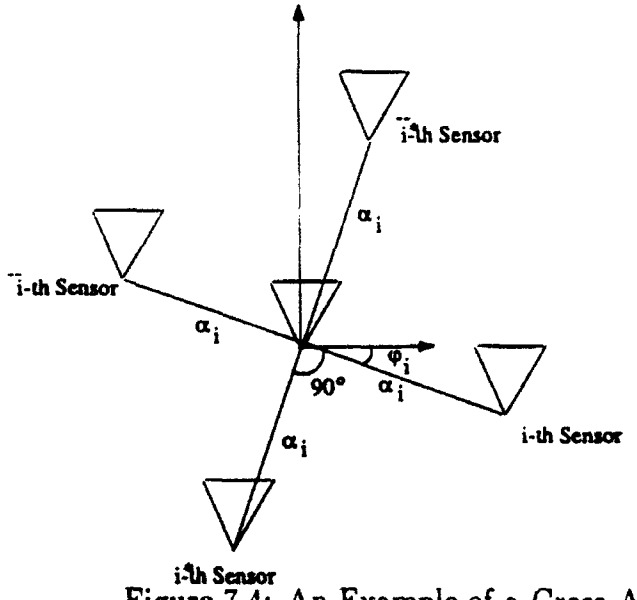

Figure 7.4: An Example of a Cross Array

to the search for the DOA angle. Note that the cross-array can be viewed as consisting of two sensor pairs, which we shall denote as $(i, \bar{i})$ and $(i^*, \bar{i}^*)$ with locations $(\{\alpha_i, \phi_i\}, \{\alpha_i, \phi_i - \pi\})$ and $(\{\alpha_i, \phi_i + \pi/2\}, \{\alpha_i, \phi_i - \pi/2\})$ (in polar form), respectively. Thus the path differences for the $(i, \bar{i})$ sensor pair is as found in Eqs. (7.8), (7.9) while the path differences for the $(i^*, \bar{i}^*)$ sensor pair are found to be

$$d_{i^*k} = \alpha_i cos(\theta_k + \phi_i) - \frac{\alpha_i^2}{2R_k} sin^2(\theta_k + \phi_i). \tag{7.16}$$

$$d_{\bar{i}^*k} = -\alpha_i cos(\theta_k + \phi_i) - \frac{\alpha_i^2}{2R_k} sin^2(\theta_k + \phi_i). \tag{7.17}$$

Writing the steering elements of the sensors within the cross-array

$$\mathbf{a}_i(\theta_k, R_k) = \begin{bmatrix} exp\{-j\frac{\omega}{c}\alpha_i sin(\theta_k+\phi_i)\}exp\{j\frac{\omega}{c}\frac{\alpha_i^2}{2R_k}cos^2(\theta_k+\phi_i)\} \\ exp\{j\frac{\omega}{c}\alpha_i sin(\theta_k+\phi_i)\}exp\{j\frac{\omega}{c}\frac{\alpha_i^2}{2R_k}cos^2(\theta_k+\phi_i)\} \\ exp\{-j\frac{\omega}{c}\alpha_i cos(\theta_k+\phi_i)\}exp\{j\frac{\omega}{c}\frac{\alpha_i^2}{2R_k}sin^2(\theta_k+\phi_i)\} \\ exp\{j\frac{\omega}{c}\alpha_i cos(\theta_k+\phi_i)\}exp\{j\frac{\omega}{c}\frac{\alpha_i^2}{2R_k}sin^2(\theta_k+\phi_i)\} \end{bmatrix} \tag{7.18}$$

Define a 2-by-1 vector $\mathbf{b}_i(\theta_k, R_k)$ from $\mathbf{a}_i(\theta_k, R_k)$ by the following procedure: The first element in $\mathbf{b}_i(\theta_k, R_k)$ is set equal to the product of the first and third elements of $\mathbf{a}_i(\theta_k, R_k)$ and the second element in $\mathbf{b}_i(\theta_k, R_k)$ is set equal to the product of the conjugates of the second and fourth elements of $\mathbf{a}_i(\theta_k, R_k)$. Writing out this vector explicitly,

$$\mathbf{b}_i(\theta_k, R_k) = \begin{bmatrix} exp\{j\frac{\omega}{c}\frac{\alpha_i^2}{2R_k}\} \\ exp\{-j\frac{\omega}{c}\frac{\alpha_i^2}{2R_k}\} \end{bmatrix} exp\{-j\frac{\omega}{c}\alpha_i(sin(\theta_k+\phi_i)+cos(\theta_k+\phi_i))\} \tag{7.19}$$

Thus the range has been decoupled from the DOA angle and using a similar fitting function as previously, we estimate the range for the k-th source as

$$\hat{R}_k = arg\left\{\max_R g(R)\right\} \tag{7.20}$$

where

$$g(R) = \| \mathbf{d}_i^{\dagger}(R)\hat{\mathbf{b}}_i \|^2 \tag{7.21}$$

and $\hat{\mathbf{b}}_i$ denotes the blind identified estimate of $\mathbf{b}_i(\theta_k, R_k)$ while

$$\mathbf{d}_i(R) = \begin{bmatrix} exp\{j\frac{\omega}{c}\frac{\alpha_i^2}{2R}\} \\ exp\{-j\frac{\omega}{c}\frac{\alpha_i^2}{2R}\} \end{bmatrix} \tag{7.22}$$

Thus the estimation for the DOA angle and range of the k-th source can be performed in parallel since they are decoupled from each other.

7.3.3 Source Location Estimation using a Range of Frequencies

At this stage of the proposed approach, a clustering technique is applied to the multiple estimates of source locations and gains found for a given range of frequencies.

The final source locations and gains estimates are computed as the averages of the estimates found within the clusters.

There is a question of why processing over a range of frequencies would be advantageous compared to that of just using a single bin. The obvious answer would be the fact that more information is available through the use of multiple frequency bins as opposed to using just a single bin. Furthermore, clustering of the multiple source estimates found over a range of frequencies is a natural way to consolidate the information contained in the given range of frequencies. The reasons for this are twofold.

First, at any particular frequency, the sources may not be all present. Thus, in order to estimate *all* the source locations and gains, it necessary to consider more than just a single frequency bin. Suppose that at a particular frequency bin, K sources are present. Then only the source locations of the K sources present can be estimated. At the next frequency bin, say M sources are present and their source locations estimated. The sources at this frequency may or may not be found in the previous frequency. Note however that the sources that are present at both frequencies would give source location estimates that are close to each other (ideally, the same source locations), while the location estimates of the sources that are absent at the previous frequency would be further away (disjoint from the other sources). By sweeping through a range of frequencies and clustering the resulting source location estimates, then all the source locations may be found from the clusters.

The second reason for clustering has to do with the effect of observation noise on the estimates and the varying relative source signal powers over a frequency range. The quality of data at different frequencies may vary significantly over the range of frequencies on which the blind identification algorithm is applied. This is because that the source signals may have different power spectral characteristics, thus varying the

relative energies of the source signals at different frequencies. Note however that at the frequencies where the signal powers are strong (i.e., high SNRs), the corresponding source location estimates found through blind identification should be near to the true parameter values. The frequencies where the signal energies are small or almost non-existent would yield parameter estimates that are erratically distributed (the "outlier estimates") since the information contained within those frequencies are strongly dominated by the spurious observation noise power. Note that the noise components at different frequencies are mutually uncorrelated and therefore it is not likely that the "outlier estimates" would map to the same locations for different frequencies. Thus the application of blind identification over a range of frequencies would yield clusters of estimates which are near the true parameter values and other 'outlier' estimates which are erratically distributed. It is clear then that any post processing of the multiple source location estimates would neccessitate the omission of the "outlier" estimates which fall outside these clusters.

We present one clustering technique in the following which is simple and have found to work well in simulations. Note however, that there are various other clustering techniques found in pattern recognition, see [37], which may be used at this point.

One clustering method is by the use of a 2-D histogram of the multiple estimates of the source locations. The modes (i.e., the bins within the histogram where the highest count of source location estimates fall into) of the histogram is selected as the center of the clusters. This method is summarized below.

Clustering via 2D Histogram

- Collect all the source location estimates into a 2-D histogram. The number of source signals can be found by determining the number of clusters present in

the 2-D histogram of the source location estimates. Find their modes.

- For a specified cluster size ($\Delta\theta$ and ΔR) of the modes, pick up all the source location estimates falling within such a cluster size and their corresponding gains. Compute the averages of these estimates.

This averaging of the estimates falling within a cluster may be viewed as a weighted averaging of all the parameter estimates found in the range of frequencies of interest. That is,

for the k-th source location

$$\hat{\theta}_k = \frac{1}{N_k} \sum_l I_{kl} \hat{\theta}(\omega_l) \tag{7.23}$$

$$\hat{R}_k = \frac{1}{N_k} \sum_l I_{kl} \hat{R}(\omega_l) \tag{7.24}$$

for the k-th source gains

$$\hat{\mathbf{g}}_k = \frac{1}{N_k} \sum_l I_{kl} \hat{\mathbf{g}}(\omega_l) \tag{7.25}$$

where

$(\hat{\theta}(\omega_l), \hat{R}(\omega_l))$: Source location estimate found at frequency ω_l.

$\hat{\mathbf{g}}(\omega_l)$: Vector of gain estimates found at frequency ω_l.

$\mathcal{N}_k$: k-th source location cluster.

I_{lk}: Indicator function defined as follows

$$I_{lk} = \left\{ \begin{array}{ll} 1, & \text{if } (\hat{\theta}(\omega_l), \hat{R}(\omega_l)) \in \mathcal{N}_k \\ 0 & \text{otherwise.} \end{array} \right\} \tag{7.26}$$

Here $N_k = \sum_l I_{lk}$.

Remark: Other weighting strategies may be employed instead of the indicator function weights given above, such as one employing variable weights which give greater

weight to the estimates closer to the cluster centers and less weight to estimates further away.

Note that the post-processing of the estimates through clustering as proposed above is fundamentally different from the coherent approach as in [75] and the incoherent approach as in [78]. Both the approaches in [75, 78] applies pre-processing of the *observation data* and not post-processing of the parameter estimates. In [75], the observation data at different frequencies is focused onto a single frequency while in [78], the observation data is averaged across different frequencies.

7.3.4 Source Separation

This is the stage where the final source location and channel gains estimates is used to extract the source signals from the observation.

The source signal vector $\mathbf{s}(t)$ can be estimated in a number of ways. The most straightforward way is to use the estimates of the gains and source locations, $\{a_{ik}, \theta_k, R_k\}$, to solve for $\mathbf{S}(\omega)$, i.e.,

$$\hat{\mathbf{S}}(\omega) = \hat{\mathbf{A}}(\omega)^{\#}\mathbf{X}(\omega) \tag{7.27}$$

An alternative approach to extract the different source signals using the estimated source locations and gains would be to use spatial filters (beamforming approach) to extract the individual signals, see [83] for the various beamforming approaches that may be applied.

7.3.5 Summary of Proposed Approach

In summary, the proposed approach proceeds in the following manner.

Proposed Approach

1. Apply FFT to data $\mathbf{x}(t)$.

2. At the current frequency, estimate the number of sources present in the observation. This can be accomplished by examining the singular values of the covarince matrix or through such criteria as found in [77, 26].

3. Apply Blind Identification to $\mathbf{X}(\omega)$. The locations of the signal sources are estimated from the estimated matrix $\mathbf{A}(\omega)$ and the channel gains are estimated from the magnitudes of the same matrix. Collect these estimates of gains and source locations.

4. Go to the next frequency and return to Step 2, unless the maximum desired frequency has been exceeded. If so, go to Step 5.

5. Apply a 2-D clustering technique onto the collection of source locations. Such clustering methods can be a simple histogram or the methods as found in pattern recognition, [37]. The number of sources is estimated from the number of clusters. Using these clusters, estimate the averages of the various source locations and associated gains.

6. Using estimates of $\{a_{ik}, \theta_k, R_k\}$, extract $\{S_i(\omega)\}$ from $\mathbf{X}(\omega)$, i.e. $\hat{\mathbf{S}}(\omega) = \hat{\mathbf{A}}(\omega)^{\#}\mathbf{X}(\omega)$.

7. Inverse FFT to obtain s(t).

Discussions

Unknown Sensor Gains: As is clear from the previous section, the proposed approach is able to estimate the unknown sensor gains.

Unknown number of signals: The number of sources is estimated after clustering is performed on the source location estimates. Thus the total number of sources present over the whole range of frequency bins is determined. This is as opposed to the estimation of number of sources at any particular frequency bin which may be

less than the total number of sources. As an example, consider the case where there are four sources, two of which have overlapping spectra disjoint from the other two. Then any estimation of the number of sources at any particular frequency would yield less than four sources.

Unknown Source Spectral Characteristics: The proposed approach is not dependent on the spectral characteristics of the sources. Thus, the sources can be overlapping or non-overlapping in their power spectra.

Unknown Combinations of Narrowband and Wideband Sources: The sources may be a combination of narrowband and wideband signals. Our approach is able to still cluster the narrowband sources even though the number of points within the narrowband source cluster is relatively less than the number of points within the wideband sources. This is achieved through the use of time segmentation of the observation data, i.e., by exploiting the fact that the number of points within the narrowband cluster may be increased by using multiple observation intervals. Note that the 'outlier' estimates would tend to distribute themselves erratically with different observation intervals while the 'good' estimates would tend to stay near the true estimates.

Unknown Combinations of Near-Field and Far-Field Sources: Source location estimation is performed for all sources, regardless of whether they are far-field or near-field. Thus the fact that the sources may consists of both far-field and near-field sources is immaterial to the proposed approach.

7.4 Simulations

7.4.1 Simulation 1: Three Near Field Sources

The array is a cross array consisting of five sensors located at (0,0) (reference sensor), (.5,0), (-.5,0), (0,.5), (0,-.5) meters. Three source signals, one of interfering white noise with power equal to 2.0, while the others are a male speech sequence and a female speech sequence, both of unit power. The interfering white noise signal is located at a range of 5 meters and angle 20 degrees, the male speech signal is located at a distance of 1.5 meters and angle -5 degrees while the female speech sequence is located at a distance of 1.5 meters and angle 20 degrees. Additive observation noise is taken to be AWGN (additive white gaussian noise) with variance equal to $(.1)^2$. Speed of propagation is taken to be 340 m/s.

The channel attenuations in the model is assumed to be due only to geometrical attenuation of the signal sources (from the spherical spreading of the wavefront) and thus the gains a_{ik} are inversely proportional to the distances R_{ik}, i.e., the distance between the i-th sensor and the k-th source. The gains are computed to be $a_{ik} = R_{1k}/R_{ik}$, where the gains for the first sensor are normalized to unity. Then the gains are

$$\begin{bmatrix} 1.0 & 1.0 & 1.0 \\ 1.1 & 1.5 & 1.44 \\ 1.03 & .92 & 1.06 \\ .91 & .75 & .76 \\ .96 & .97 & .86 \end{bmatrix} \tag{7.28}$$

16000 samples of observations from the array is taken at a sampling rate of 8000 Hz.

These samples are then chopped into 30 blocks of non-overlapping intervals of 512 samples each and 512 point FFT is applied to these intervals. Wideband blind identification is then applied on the data for frequency bins ranging from 50 Hz to 1.6 kHz.

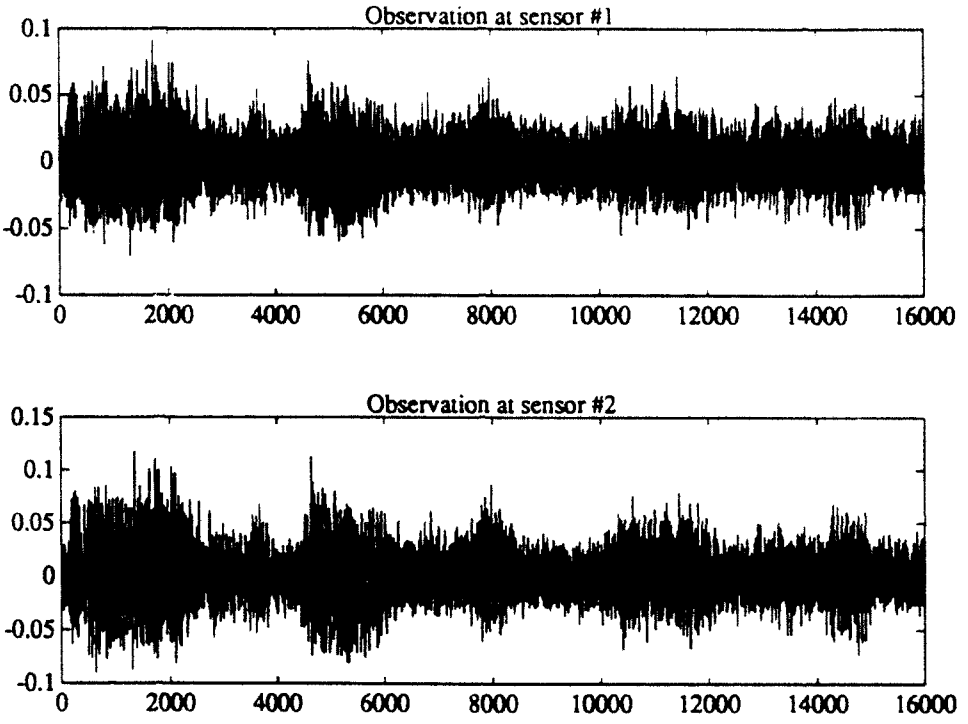

Figure 7.5: Simulation 1: Typical observations from sensors no. 1 and 2.

Note that this selection of frequency bins does not satify the constraint for avoiding phase wrapping and therefore the closed form least squares based methods cannot be applied. The source locations are estimated using the Approximate Method. Figs. 7.6 show the 2-D histogram plots of the source location estimates.

It is clear from the 2-D histogram that there are three definite clusters and therefore there are three souce signals present.

Picking the size of the clusters to be $\Delta\Theta = 5$ deg and $\Delta R = 2$ meters, i.e., all source location estimates falling within this distance from the modes of the clusters are collected and averaged, we find that the final estimated DOA angles, ranges and gains are: (19.79 deg, 4.21 meters), (-4.48 deg, 1.65 meters) and (19.15 deg., 1.83

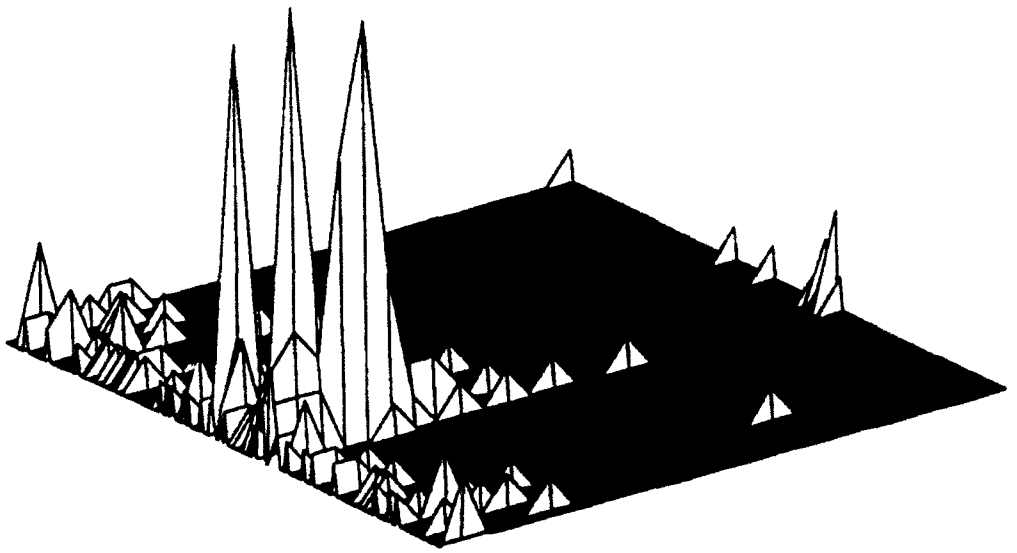

Figure 7.6: Simulation 1: 2-D Histogram of the Source Location Estimates.

meters), respectively, and their corresponding gains are

$$\begin{bmatrix} 1.0 & 1.0 & 1.0 \\ 1.12 & 1.5 & 1.36 \\ 1.06 & .95 & 1.06 \\ .9 & .75 & .8 \\ .98 & 1.05 & .88 \end{bmatrix} \tag{7.29}$$

Using these averaged gains and source location estimates, the source signals are extracted from the observation data. The true and separated speech sequences is shown in Figs. 7.7-7.8. Computation of the correlation between the estimated and the true speech sequences shows the correlation to be 99 percent and 95 percent respectively.

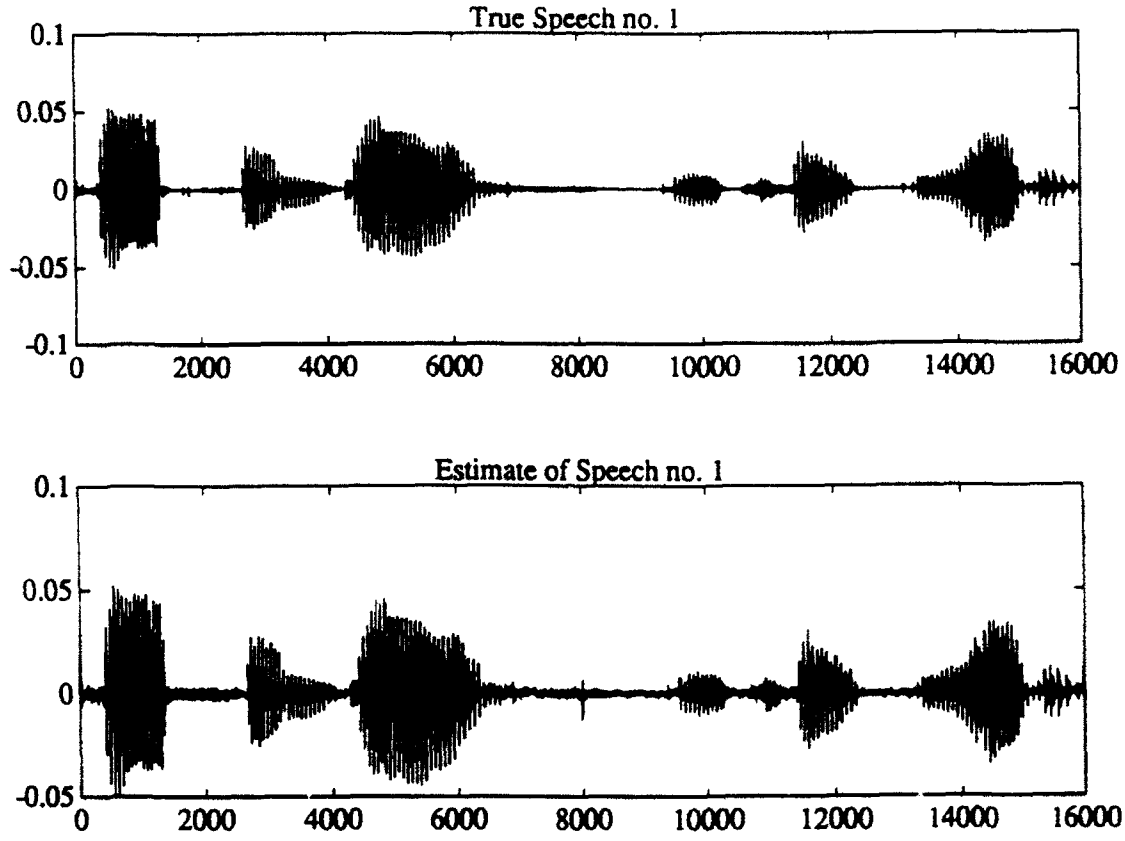

Figure 7.7: Simulation 1: Plots of Estimate of Speech no. 1.

7.4.2 Simulation 2: Near-Field (Wideband) Source and Far-Field (Narrowband) Source

The shape of the array is the same as in Simulation 1, except that the radial distances of the sensors from the reference is set to 0.25 meters. The wideband source is a speech source located at range of 1.5 meters and angle –45 degrees. The narrowband source is synthetically generated to contain sinusoidal lines at the frequencies of 55, 60 and 65 Hz. It is situated at a range of 20 meters and angle of 5 degrees. Thus we have a combination of wideband near-field source and narrowband far-field source in the observations. Both sources are at unity power. Additive observation noise is taken to be AWGN with variance equal to $(.1)^2$. Speed of propagation is taken to be 340

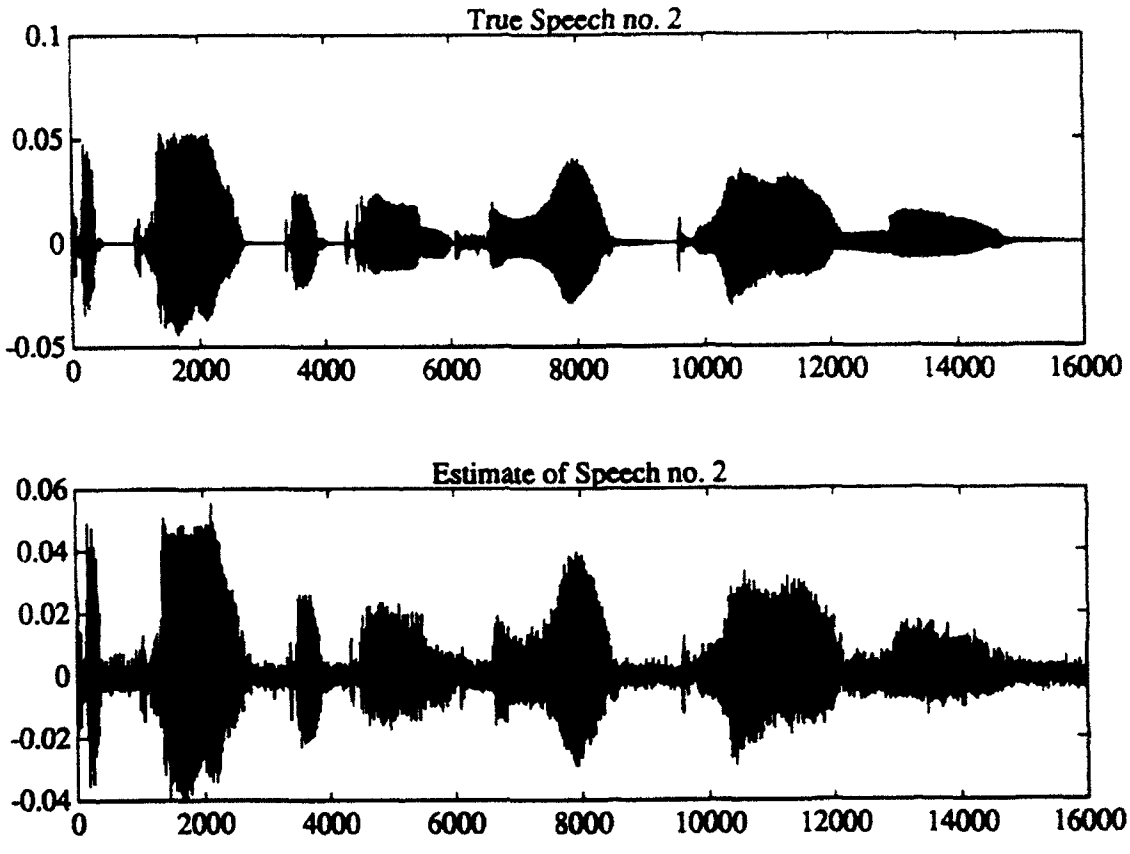

Figure 7.8: Simulation 1: Plots of Estimate of Speech no. 2.

m/s.

The channel attenuations in the model is assumed to be due only to geometrical attenuation of the signal sources (from the spherical spreading of the wavefront) and thus

$$\begin{bmatrix} 1.0 & 1.0 \\ 1.12 & 1.01 \\ .89 & 1.0 \\ .89 & .99 \\ 1.12 & 1.0 \end{bmatrix} \tag{7.30}$$

As done previously, 16000 samples are collected and 30 sub-intervals of 512 points each are obtained. The range of frequencies over which the proposed approach is applied is from 15 Hz to 234 Hz, giving a total of 15 frequency bins. The proposed

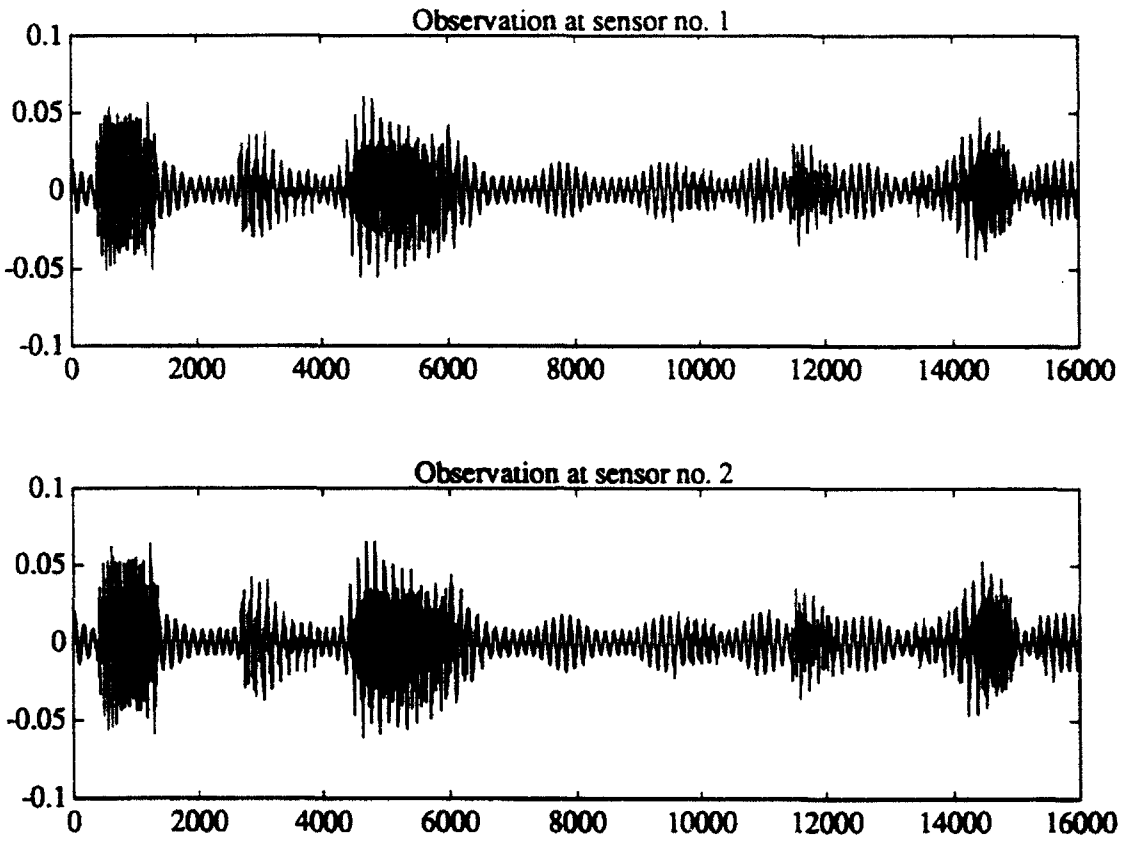

Figure 7.9: Simulation 2: Typical observations from sensors no. 1 and 2.

algorithm is applied to the FFT of the data. Then, another 30 sub-intervals of 512 points each is obtained from the same observation set by shifting the sub-intervals window by 200 points and the proposed approach is again applied. Next, the same procedure is done for a sub-interval window shift of 400 points, and also for a shift of 600 points. Finally, the collection of source location estimates is clustered using a 2D histogram, shown in Fig. 7.10. Two clusters are evident from the histogram.

Picking the size of the clusters to be $\Delta\Theta$ = 5 deg and ΔR =2 meters, i.e., all source location estimates falling within this distance from the modes of the clusters are collected and averaged, we find that the final estimated DOA angles, ranges and gains are: (-44.6 deg, 1.43 meters) and (5.23 deg., 25 mete.), respectively, and their

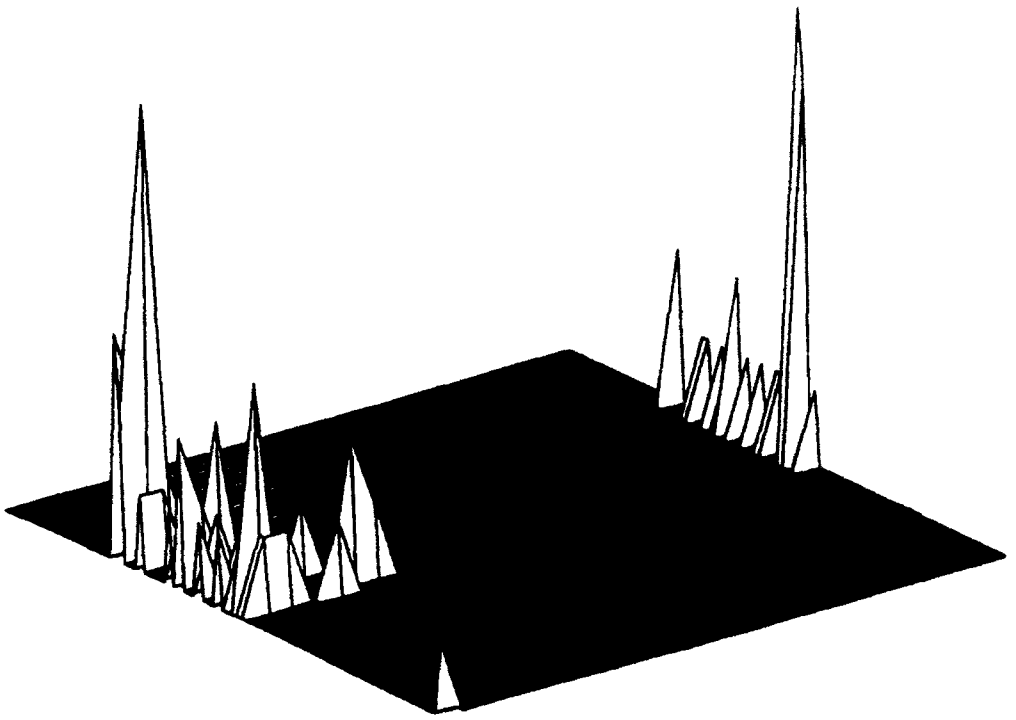

Figure 7.10: Simulation 2: 2-D Histogram of the Source Location Estimates.

corresponding gains are

$$\begin{bmatrix} 1.0 & 1.0 \\ 1.17 & .99 \\ .88 & 1.0 \\ .89 & 1.0 \\ 1.16 & 1.0 \end{bmatrix} \tag{7.31}$$

Using these averaged gains and source location estimates, the source signals are extracted from the observation data. The true and separated speech and narrowband sources are shown in Figs. 7.11-7.12.

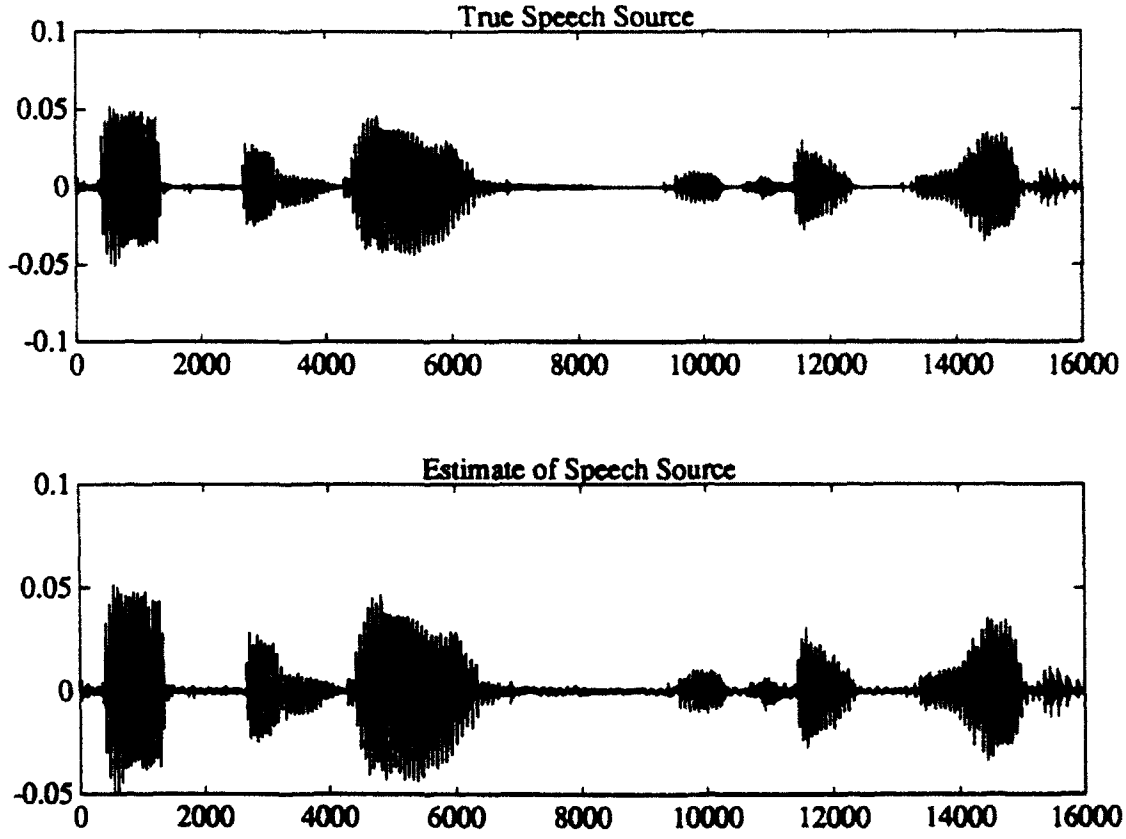

Figure 7.11: Simulation 2: Plots of Estimate of Speech Source.

7.4.3 Simulation 3: Far-Field Sources

It is assumed that the number of sources is three and the number of sensors (i.e., microphones) is four. The sources are two male speech signals and a female speech signal, respectively with no multipaths. The sources are located in the far field with DOA angles of –40, +10 and +50 degrees respectively. The four sensors are located at $(0,0),(1,0),(1,1),(0,1)$ meters respectively. The speed of propagation is taken as 340 meters-per-second.

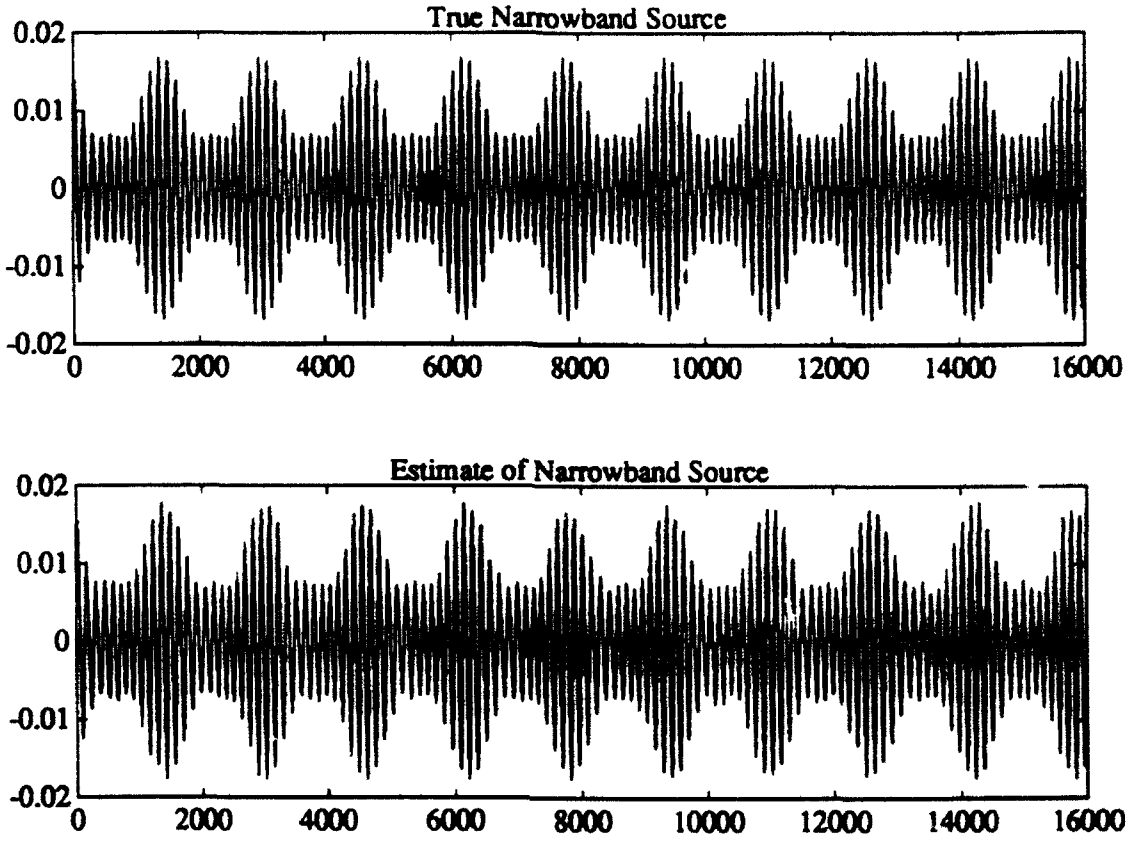

Figure 7.12: Simulation 2: Plots of Estimate of Narrowband Source.

The gains are arbitrarily selected as follows:

$$\begin{bmatrix} 1.0 & 1.0 & 1.0 \\ 1.2 & 1.5 & 0.5 \\ 0.7 & 0.9 & 1.5 \\ 1.7 & 0.9 & 2.0 \end{bmatrix} \tag{7.32}$$

16,000 time samples of the microphone array are taken at a sampling rate of 8000 samples/s. The signal sources are all of equal power, with the total energy of a signal source summed over the 16,000 samples set to unity. The separation of the speech signals from the array observations is desired. The time samples are divided into 30 sub-intervals of 512 samples each and 512-pt FFT taken over the 30 sub-intervals. Wideband blind identification is then applied across the frequency spectrum ranging

from 93.75 Hz to 703.125 Hz, giving a total of 40 frequency bins. DOA estimates are found. The incoherent clustering algorithm is applied to obtain the final DOA and gain estimates. Using these estimates, individual estimates of the speech sources are made, using (7.27).

Modes of DOAs are found to be at: –41 deg., +10 deg., and +50 deg. A plot of the histogram of the DOA estimates is shown in Fig. 7.13.

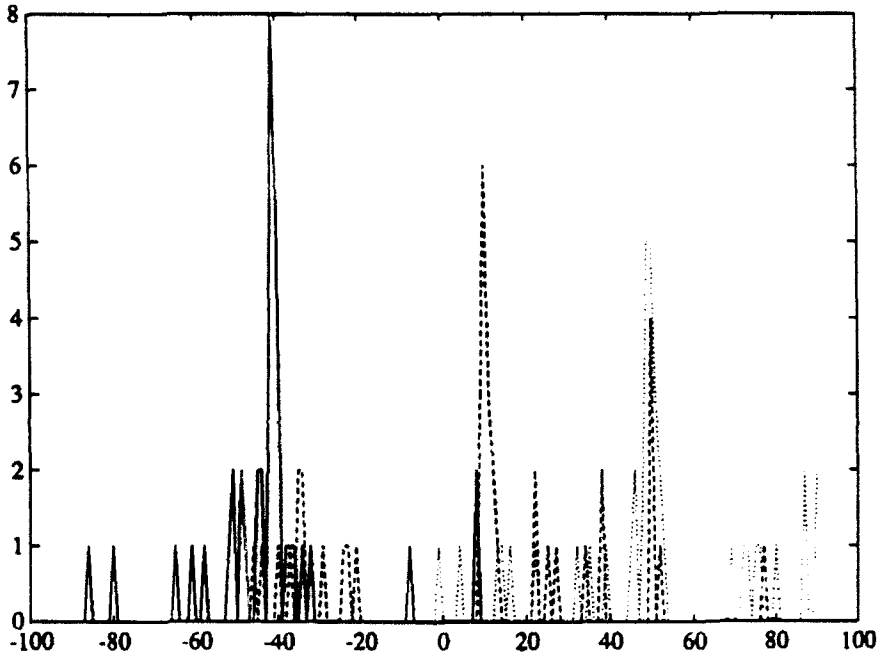

Figure 7.13: Simulation 3: Histogram of DOA estimates

Picking the size of the clusters to be $\Delta\Theta = 5$ deg, i.e., all , we find that the final (incoherent) estimated DOA angles are:

Est. DOAs:–40.667 deg., +10.417 deg., +50.0 deg.

Also, using the sensor gains correponding to the collected DOA estimates, we find

that the final gain estimates are:

$$\begin{bmatrix} 1.0 & 1.0 & 1.0 \\ 1.196 & 1.709 & 0.504 \\ 0.702 & 1.06 & 1.14 \\ 1.794 & 1.23 & 1.572 \end{bmatrix} \tag{7.33}$$

Figs. 1 (a,b) show two typical observations from the array. It can be seen from Figs. 2(a,b), Fig. 3(a,b), Fig. 4(a,b) that the speech signals are succesfully separated from the array observations.

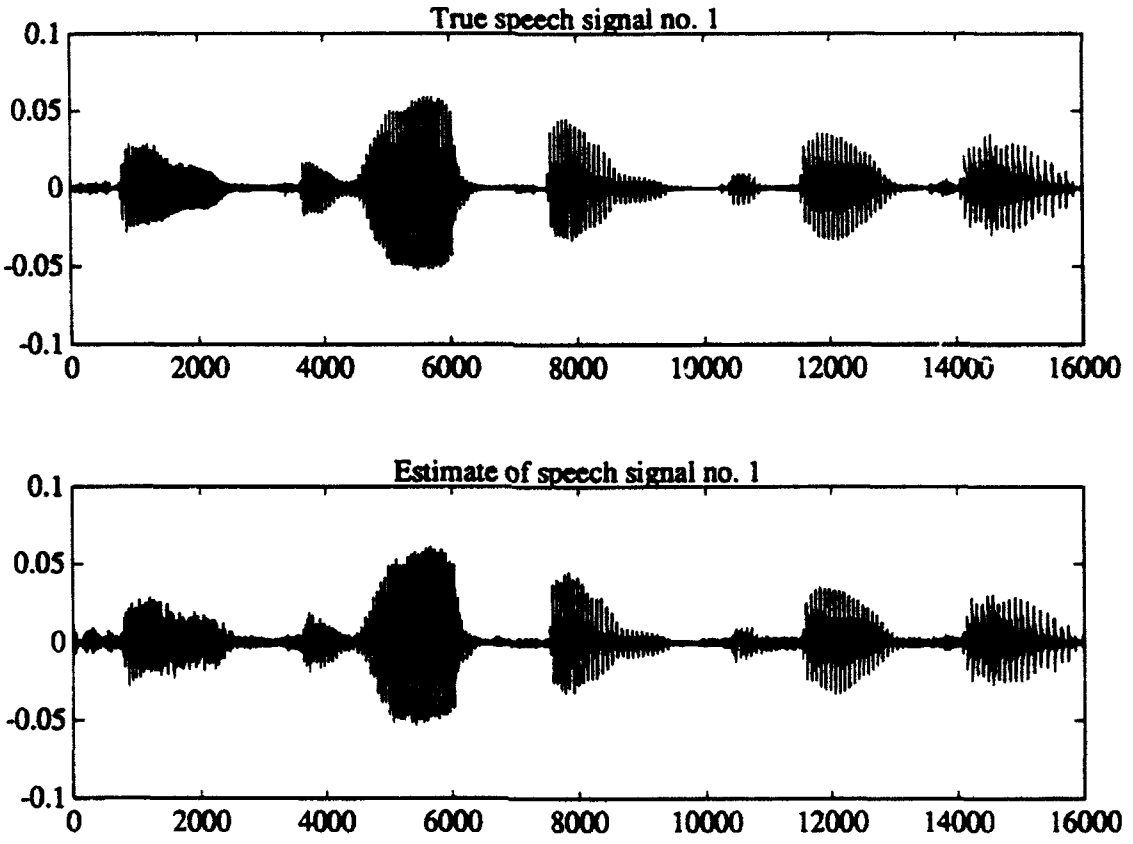

Figure 7.14: Simulation 3: Estimate of Speech no. 1

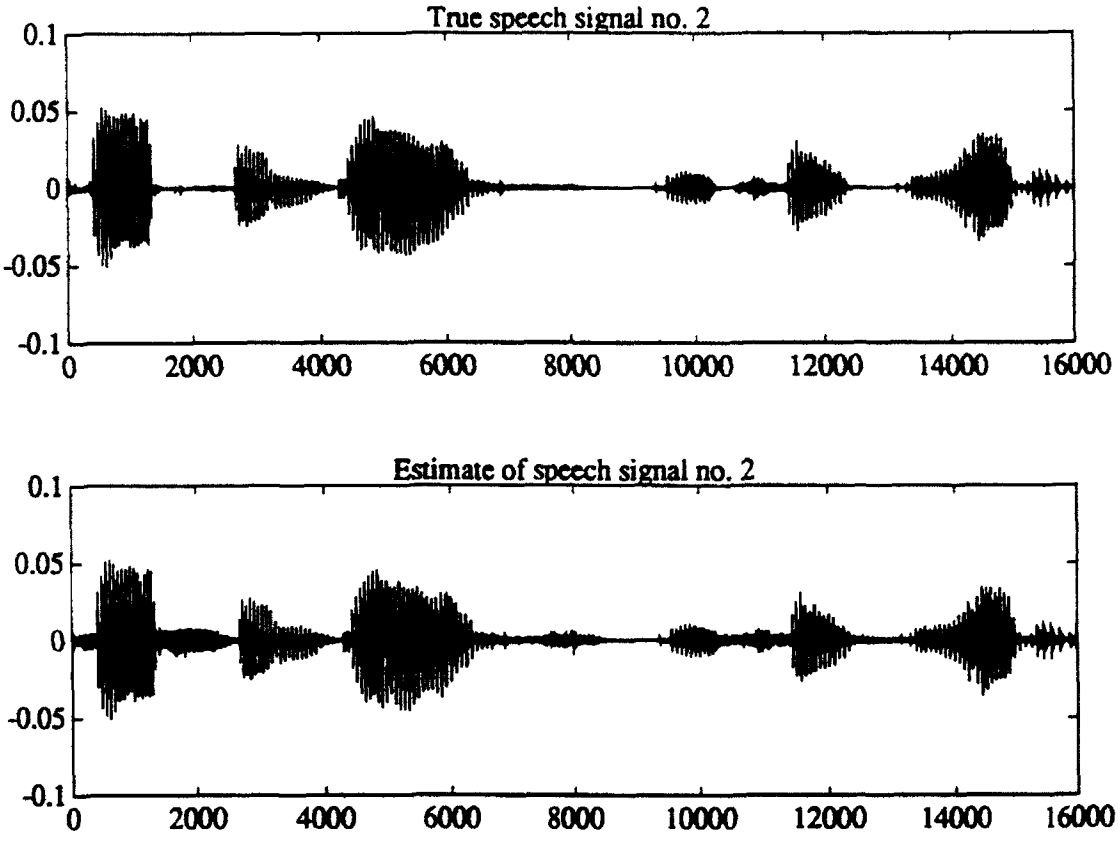

Figure 7.15: Simulation 3: Estimate of Speech no. 2

7.4.4 Simulation 4: Non-stationary Source and Speech Source

The scenario is the same as is in Simulation 2, except that the narrowband source is now replaced by a non-stationary source. The non-stationary source is generated by scaling a gaussian distributed source differently at each time instant, thus making the source have different ensemble variances at different times.

The proposed approach is applied over a frequency range of 50 Hz. to 1.6 kHz.

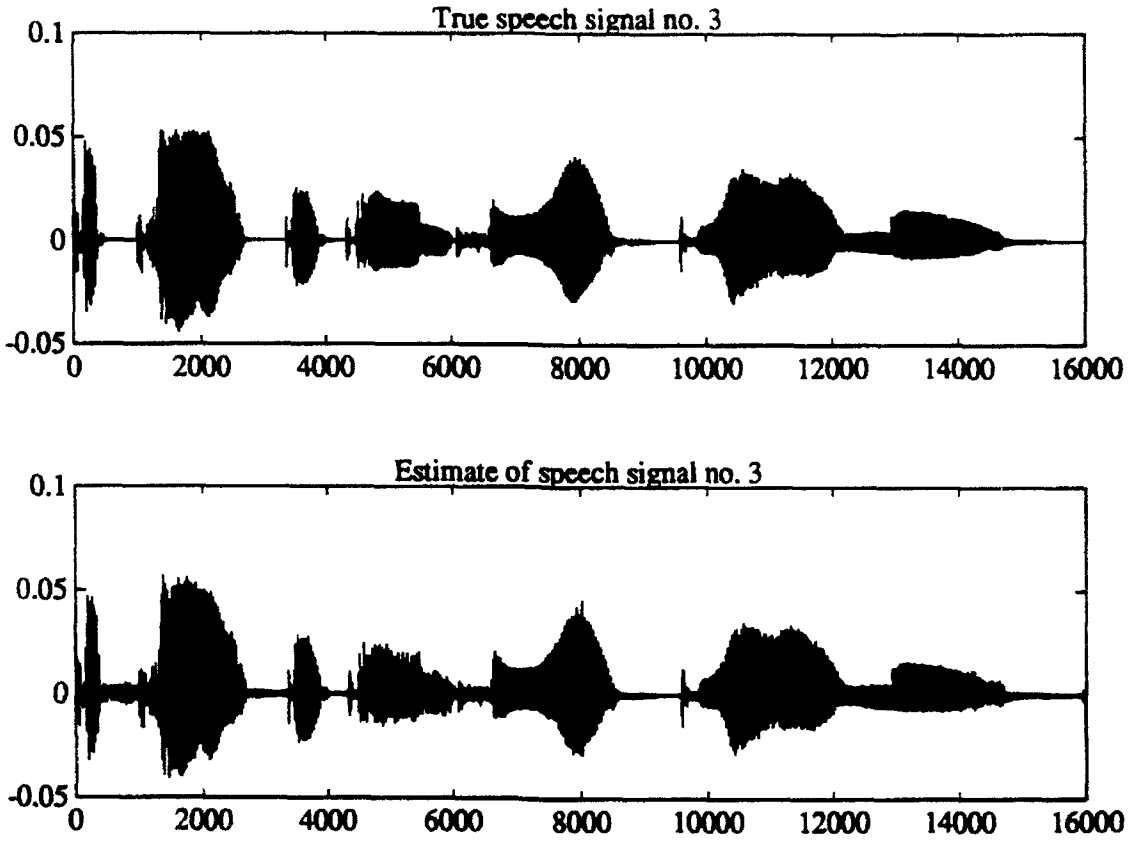

Figure 7.16: Simulation 3: Estimate of speech no. 3

$$\text{True Gains} \begin{bmatrix} 1.0 & 1.0 \\ 1.12 & 1.01 \\ .89 & 1.0 \\ .89 & .99 \\ 1.12 & 1.0 \end{bmatrix} \quad \text{Estimated Gains} \begin{bmatrix} 1.0 & 1.0 \\ 1.07 & .927 \\ .89 & .984 \\ .943 & 1.03 \\ 1.11 & .992 \end{bmatrix} \tag{7.34}$$

The true source locations are: (1.5 m, –45 deg.) and (20 m, 5 deg.)

The estimated source locations are: (1.31 m, –45.08 deg.) and (25 m, 4.393 deg.).

From fig. 7.17, it is clear that the speech signal is succesfuly separated from the non-stationary signal.

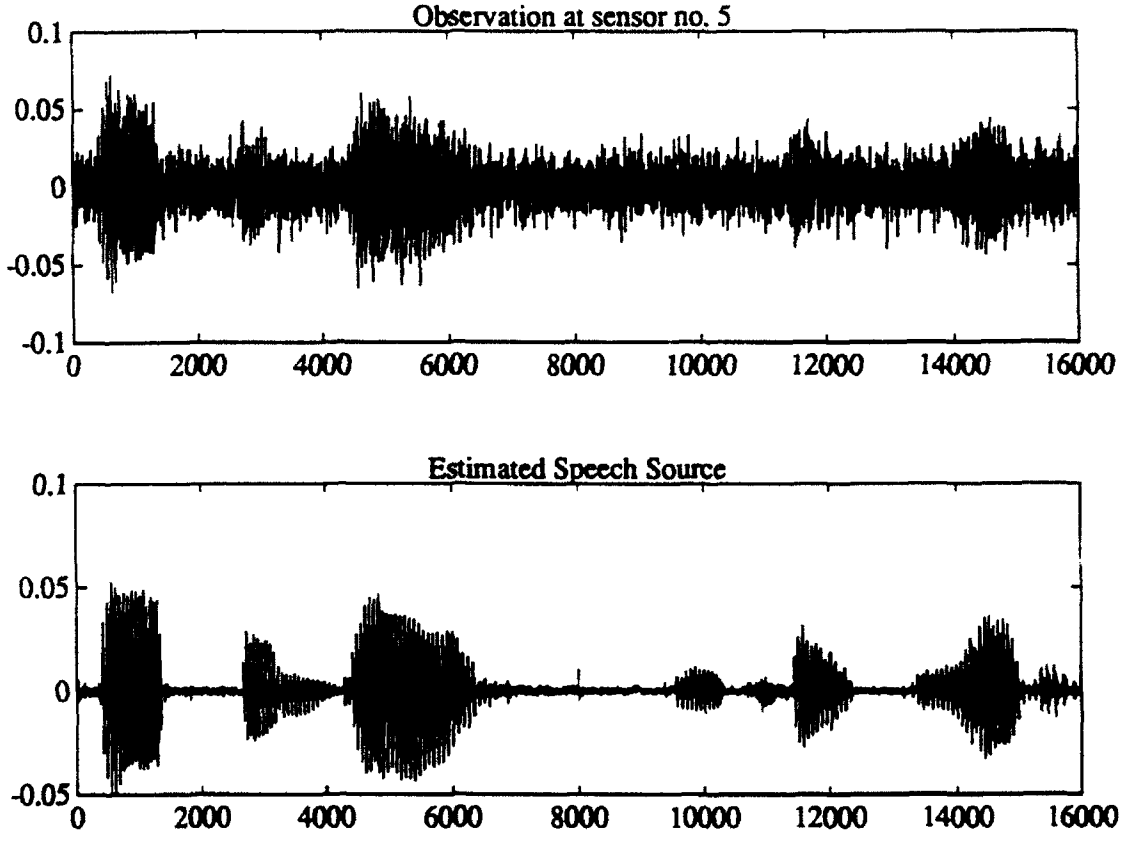

Figure 7.17: Simulation 4: Typical observation and estimated speech source.

7.4.5 Simulation 5: Non-stationary Source and Two Speech Sources

The scenario is the same as is in Simulation 1, except that the white noise interference source is now replaced by a non-stationary source. The non-stationary source is generated by switching between uniform and gaussian distributions every 250 time samples where their variances are different.

The proposed approach is applied over a frequency range of 50 Hz. to 1.6 kHz.

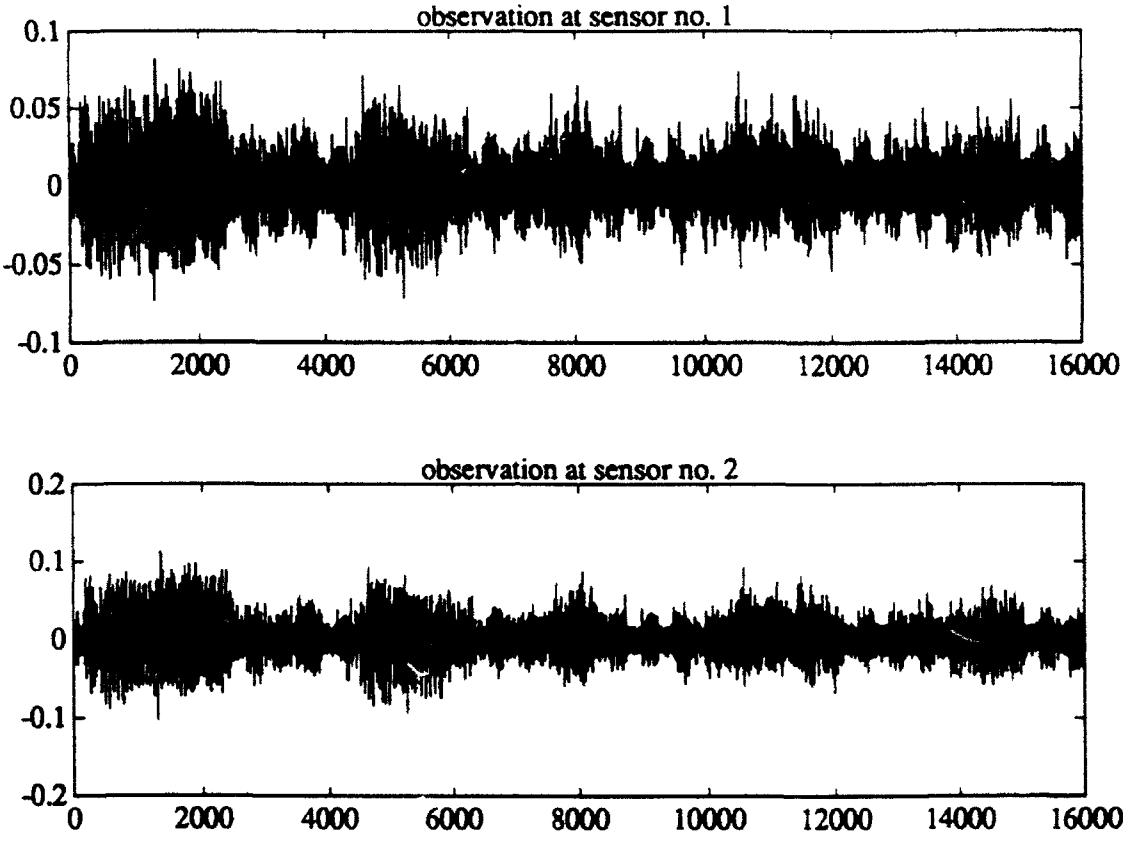

Figure 7.18: Simulation 5: Typical observations from sensors no. 1 and 2.

$$\text{True Gains: } \begin{bmatrix} 1.0 & 1.0 & 1.0 \\ 1.1 & 1.5 & 1.44 \\ 1.03 & .92 & 1.06 \\ .91 & .75 & .76 \\ .96 & .97 & .86 \end{bmatrix} \quad \text{Estimated Gains: } \begin{bmatrix} 1.0 & 1.0 & 1.0 \\ 1.1 & 1.4 & 1.31 \\ 1.04 & .87 & 1.07 \\ .894 & .77 & .81 \\ .99 & .905 & .89 \end{bmatrix} \tag{7.35}$$

Using these averaged gains and source location estimates, the source signals are extracted from the observation data.

Computation of the correlation between the estimated and the true speech sequences shows the correlation to be 99 percent and 94 percent respectively.

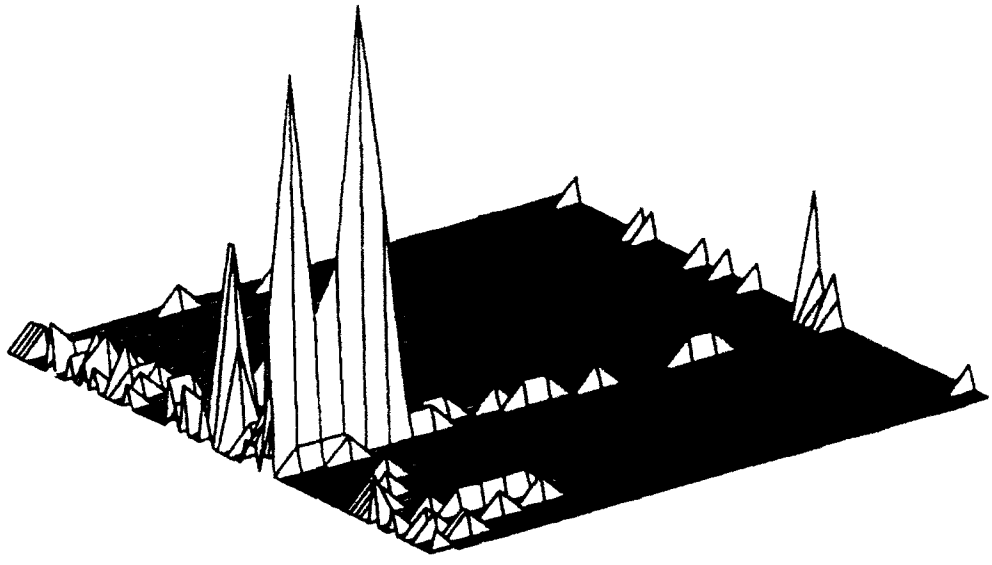

Figure 7.19: Simulation 5: 2-D Histogram of source location estimates.

7.5 Extension of Approach to Multipath Cases

The proposed approach is also applicable to the multipath case, specifically the **specular multipath scenario**, i.e., perfectly coherent multipaths are present. In this subsection, we will discuss the application of wideband blind identification to this problem.

For ease of discussion, assume 1 multipath signal and n other signals.

The observation at the i-th sensor is written as

$$x_i(t) = \sum_{k=1}^{n} a_{ik} s_k(t - \tau_{ik}) + \beta_i s_1(t - \xi_i) + \eta_i.$$

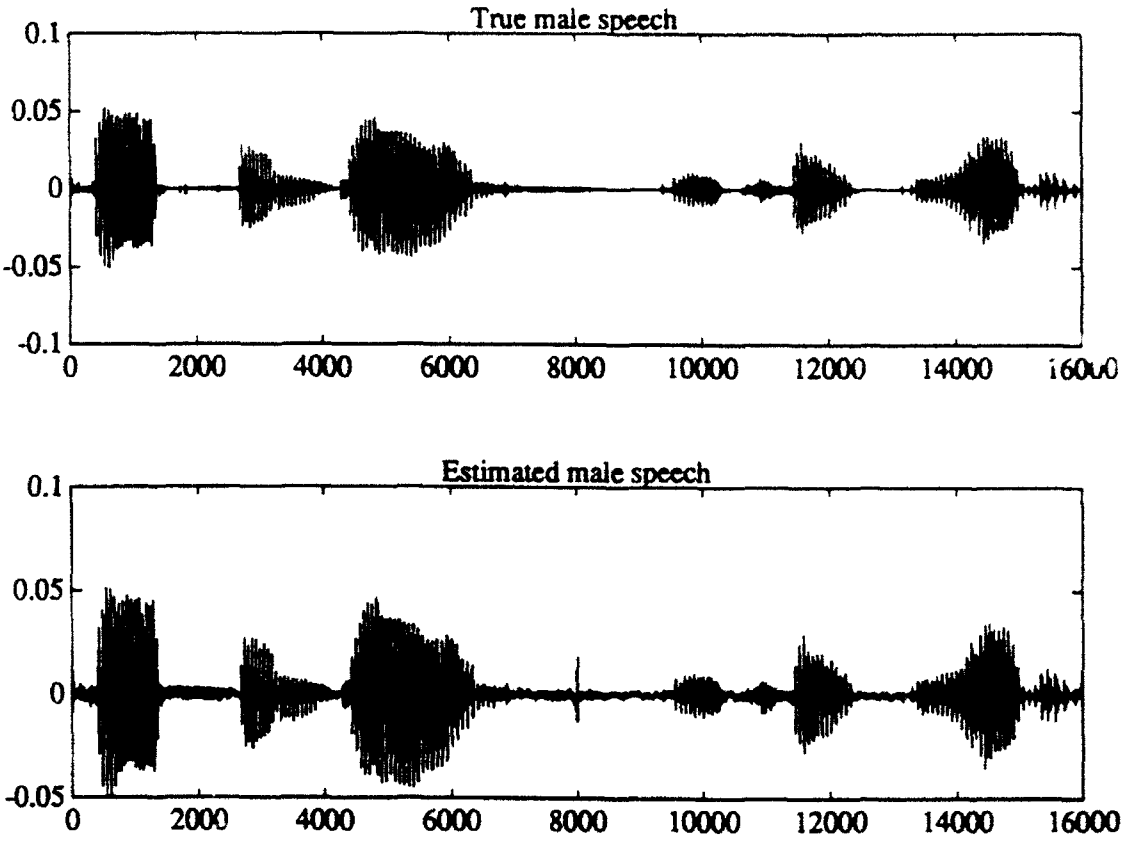

Figure 7.20: Simulation 5: Plots of Estimate of Speech no. 1.

(β_i, ξ_i) denotes the multipath gains and delays. Thus the signal $s_1(t)$ has a direct and a multipath component.

In the frequency domain,

$$\mathbf{X}(\omega) = \tilde{\mathbf{A}}(\omega)\mathbf{S}(\omega) + \eta(\omega)$$

where

$$\tilde{\mathbf{A}}(\omega) = \begin{bmatrix} (1.0 + \beta_1 e^{-j\omega\xi_1}) & \cdots & 1.0 \\ (a_{21}e^{-j\omega\tau_{21}} + \beta_2 e^{-j\omega\xi_2}) & \cdots & a_{2n}e^{-j\omega\tau_{2n}} \\ \vdots & \cdots & \vdots \\ (a_{m1}e^{-j\omega\tau_{m1}} + \beta_m e^{-j\omega\xi_m}) & \cdots & a_{mn}e^{-j\omega\tau_{mn}} \end{bmatrix} \tag{7.36}$$

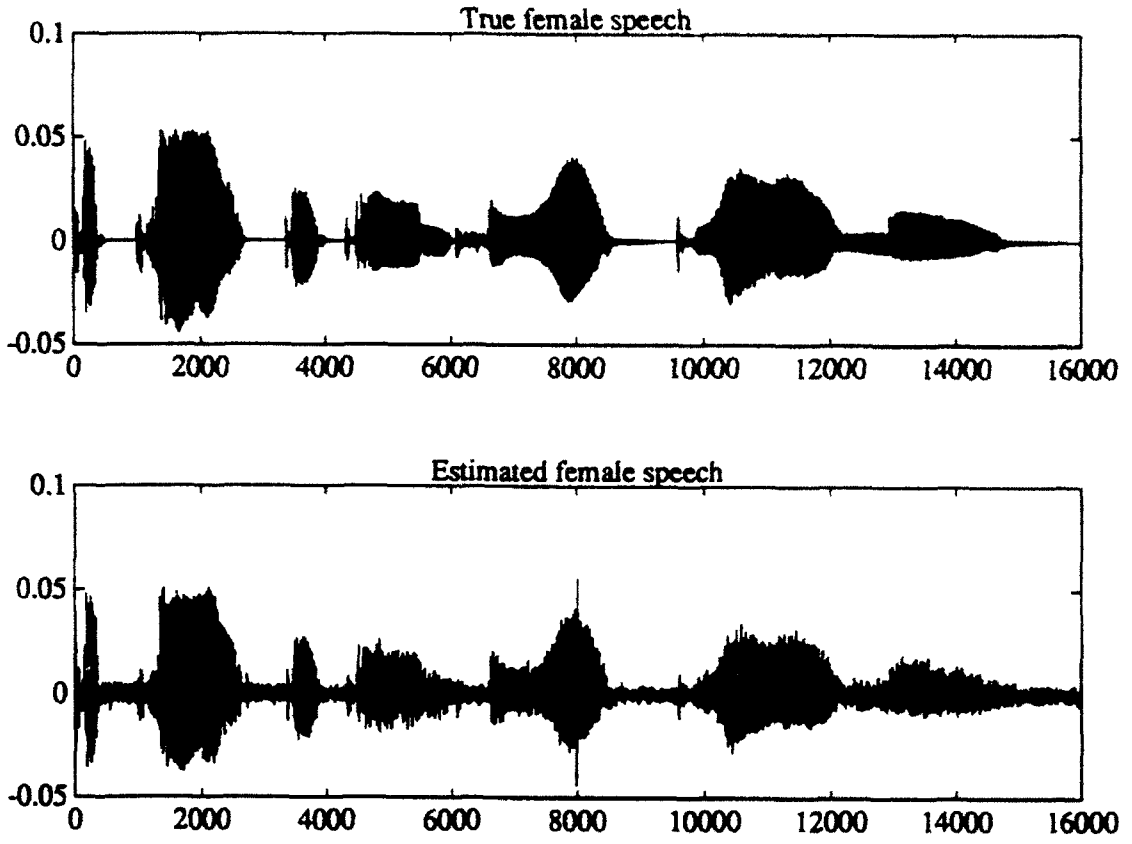

Figure 7.21: Simulation 5: Plots of Estimate of Speech no. 2.

Blind identification is then performed. The signal with multipath can be distinguished from the other signals (with no multipaths) by examining the column vectors of the matrix $\tilde{\mathbf{A}}(\omega)$. The magnitudes of elements within the column vector associated with the signal $s_1(t)$ would vary with different ω's while those with no multipaths would have constant magnitudes. Therefore, the estimates of $\{a_{ik}, \tau_{ik}\}$, for $i = 2, ..., m$, $k = 2, ..., n$ can be found directly from $\tilde{\mathbf{A}}$. Estimates of $\{a_{i1}, \tau_{i1}\}$ and $\{\beta_i, \xi_i\}$ may be found from the estimates of $\tilde{\mathbf{A}}(\omega)$ at several different frequencies.

In general however, the use of blind identification raises the problem of scaling and ordering indeterminacy of the signals, see [70]. When there are several signals with multipaths this indeterminacy is undesirable because in order to solve for the

direct and multipath parameters, estimates of $\tilde{\mathbf{A}}$ must be made at several frequencies. However with several signals with multipaths, their corresponding column vectors in $\tilde{\mathbf{A}}$ may be scaled and ordered differently at different frequencies. Since signals with no multipath can be easily distinguished from signals with multipath (as noted previously) it is assumed that $\tilde{\mathbf{A}}$ contains only those column vectors corresponding to signals with multipaths. Without loss of generality, we consider the case where there are two signals each with a multipath. Thus,

$$\tilde{\mathbf{A}} = \begin{bmatrix} (1.0 + \beta_{11}e^{-j\omega\xi_{11}}) & (1.0 + \beta_{12}e^{-j\omega\xi_{12}}) \\ (a_{21}e^{-j\omega\tau_{21}} + \beta_{21}e^{-j\omega\xi_{21}}) & (a_{22}e^{-j\omega\tau_{22}} + \beta_{22}e^{-j\omega\xi_{22}}) \\ \vdots & \vdots \\ etc & etc \end{bmatrix} \tag{7.37}$$

To eliminate the unknown scaling of the column vectors in the blind identified value of (7.37), a 'normalized' matrix $\bar{\mathbf{A}}(\omega)$ is defined by dividing the column vectors of the estimate of the matrix with their first elements, i.e.,

$$\bar{\mathbf{A}} = \begin{bmatrix} 1.0 & 1.0 \\ \frac{(a_{21}e^{-j\omega\tau_{21}} + \beta_{21}e^{-j\omega\xi_{21}})}{1+\beta_{11}e^{-j\omega\xi_{11}}} & \frac{(a_{22}e^{-j\omega\tau_{22}} + \beta_{22}e^{-j\omega\xi_{22}})}{1+\beta_{12}e^{-j\omega\xi_{12}}} \\ \vdots & \vdots \\ etc & etc \end{bmatrix} \tag{7.38}$$

Thus the unknown scaling of the column vectors in $\tilde{\mathbf{A}}$ at different frequencies have been eliminated. Next the problem of ordering of the column vectors is examined. Define

$$f_i(\omega) = \frac{(a_{2i}e^{-j\omega\tau_{2i}} + \beta_{2i}e^{-j\omega\xi_{2i}})}{1 + \beta_{1i}e^{-j\omega\xi_{1i}}} \tag{7.39}$$

When the separation between adjacent bin frequencies ($\Delta\omega$) are small enough such that $|\Delta\omega\tau_{ik}| << 1.0$, $|\Delta\omega\xi_{ik}| << 1.0$, then

$$f_i(\omega_0 + \Delta\omega) = f_i(\omega_0) - j\Delta\omega g_i(\omega_0) \tag{7.40}$$

where,

$$g_i(\omega) = \frac{(a_{2i}\tau_{2i}e^{-j\omega\tau_{2i}} + \beta_{2i}\xi_{2i}e^{-j\omega\xi_{2i}} - f_i(\omega)\beta_{1i}\xi_{1i})}{1 + \beta_{1i}e^{-j\omega\xi_{1i}}} \tag{7.41}$$

Similarly at the bin frequency $\omega_0 + \Delta\omega$, we have

$$f_i(\omega_0 - \Delta\omega) = f_i(\omega_0) + j\Delta\omega g_i(\omega_0) \tag{7.42}$$

Now consider the ratio of differences:

$$\rho_{ikl} = \frac{f_i(\omega_0 + \Delta\omega) - f_k(\omega_0)}{f_l(\omega_0 + \Delta\omega) - f_k(\omega_0)} \tag{7.43}$$

It can be seen from (7.40) and (7.42) that generally, ρ_{ikl} is **equal** to -1.0 for $i = k = l$ and **not equal** to -1.0, otherwise. Thus, given the matrices $\mathbf{A}(\omega_0)$, $\mathbf{A}(\omega_0 + \Delta\omega)$, $\mathbf{A}(\omega_0 - \Delta\omega)$ (with possibly different and unknown permutations of their column vectors), the ratio in (7.43) can be used to determine their correct ordering.

Thus the re-scaling and re-ordering of the column vectors may be accomplished as follows:

Scaling: Define the 'normalized' matrix $\bar{\mathbf{A}}(\omega)$ as in (7.38).

Ordering: Given the matrices $\bar{\mathbf{A}}(\omega_0)$, $\bar{\mathbf{A}}(\omega_0 + \Delta\omega)$, $\bar{\mathbf{A}}(\omega_0 - \Delta\omega)$.

1. Suppose the correct column vectors in $\bar{\mathbf{A}}(\omega_0 + \Delta\omega)$, $\bar{\mathbf{A}}(\omega_0 - \Delta\omega)$ are to be associated with the i-th column vector in $\bar{\mathbf{A}}(\omega_0)$. Denote the second element in the i-th column vector of $\bar{\mathbf{A}}(\omega_0)$ as α.

2. Denote the elements in the second row of $\bar{\mathbf{A}}(\omega_0+\Delta\omega)$, $\bar{\mathbf{A}}(\omega_0-\Delta\omega)$ as $\{\mu_1, \mu_2, ...\}$ and $\{\nu_1, \nu_2, ...\}$ respectively. Here the term μ_k denotes the second element of the k-th column vector in $\bar{\mathbf{A}}(\omega_0+\Delta\omega)$ and similarly for ν_k. Define the differences $\delta\mu_k = \mu_k - \alpha$, and $\delta\nu_k = \nu_k - \alpha$.

3. Compute the ratios: $\frac{\delta\mu_j}{\delta\nu_k}$. The ratio closest to the value of -1.0 would signify the correct ordering of the column vectors, i.e., the (j, k) index of the ratio denotes that the j-th column vector of $\bar{\mathbf{A}}(\omega_0+\Delta\omega)$ and the k-th column vector of $\bar{\mathbf{A}}(\omega_0-\Delta\omega)$ are associated with the i-th column vector of $\bar{\mathbf{A}}(\omega_0)$.

7.6 Extension of Approach to 3-D Scenario

The proposed approach may also be extended to the case where 3 parameters determine the source location (eg., range, azimuth angle and elevation angle). Conside fig. 7.22. The path differences (relative to the reference sensor which is assumed to be at

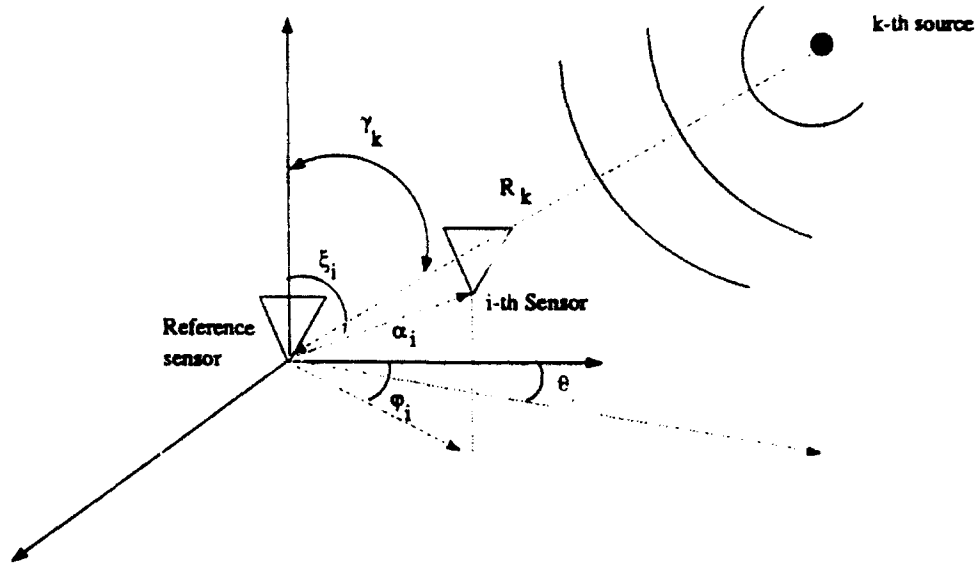

Figure 7.22: 3-Dimensional Scenario for Sources and Sensors

the origin) can then be shown to be

$$d_{ik} = d_{ik}^f - \frac{1}{2R_k}\{\alpha_i^2 - (d_{ik}^f)^2\} \tag{7.44}$$

where $d_{ik}^f = \alpha_i\{\sin\gamma_k \sin\xi_i \sin(\theta_k + \phi_i)\}$, is the far-field component of the time delay.

Similarly, to the previous discussion on the sensor pairs in the 2-D case, the estimation of the azimuth and elevation angles may be decoupled from the estimation of the range through the use of a specific sensor pair configuration. Specifically, suppose that

the i^*-th sensor associated with the i-th is located at the location $(\alpha_i, -\pi + \varphi_i, \pi - \xi_i)$. Then its path difference for the k-th source is written as

$$d_{i^*k} = -d_{ik}^f - \frac{1}{2R_k}\{\alpha_i^2 - (d_{ik}^f)^2\} \tag{7.45}$$

where d_{ik}^f is as defined previously for the i-th sensor. Thus, by defining a fitting function similar to the one in the 2-D case, the search for the azimuth and elevation angles (θ_k, γ_k) is decoupled from the range search.

Remarks:

(i) The search for the source range may be performed once the azimuth and elevation angles are estimated.

(ii) On the other hand, it may be possible to configure the sensor array structure analogously to the cross-array strucutre of the 2-D case, such that the source range can be estimated independently of the azimuth and elevation angle estimation.

8

CONCLUSIONS

We conclude the with the following summary of the results of this investigation.

- An analysis of ESPRIT under random model errors is conducted which provides insight into its performance and robustness against such random model errors as unknown sensor gains and phases, unknown sensor locations and unknown rotations of sub-arrays within the ESPRIT array. In particular, it is shown that in the case of Uniform Linear Arrays (ULA), the bulk of the Mean-Square-Error (MSE) of ESPRIT is due to the sensor phase errors as opposed to the sensor gain errors.

- An approach based on a signal subspace constraint is proposed for array signal processing under model errors. This approach yields asymptotically unbiased estimates of the sensor gains and phases when the DOA angles are known *a-priori*. When both sensor gains/phases and DOA angles are unknown, an iterative version of the approach is given.

- A novel approach using blind identification is developed for the source estimation problem under model errors and uncertainties. By using clustering techniques in conjunction with blind identification, it is shown that the proposed

approach is *robust* against the *silmutaneous* presence of such uncertainties such as unknown sensor or channel gains, unknown combinations of near-field and far-field sources, unknown combinations of wideband and narrowband sources, unknown source spectral charateristics and unknown number of sources. As such, it shows promising potential in such application areas as speech separation/processing and mobile communications.

Bibliography

[1] H. Akaike, "A New Look at the Statistical Model Identification," *IEEE Trans. Auto. Contr.* , vol. 19, no. 6, pp. 716-723, December 1974.

[2] W. J. Bangs, Array Processing with Generalized Beamformers, PhD Dissertation, Yale University, New Haven CT, 1971.

[3] A. J. Barabell, J. Capon, D. F. Delong, J. R. Johnson and K. Senne. "Performance Comparison of Superresolution Array Processing Algorithms." Tech. Rpt TST-72, Lincoln Lab., MIT, 1984.

[4] Y. Bresler and A. Macovski, "Exact Maximum Likelihood Parameter Estimation of Superimposed Exponential Signals in Noise," *IEEE Trans. Acoust., Speech and Sig.*, vol. ASSP-34, no. 10, Oct. 1986, pp. 1081-1089.

[5] Y. Bresler and A. H. Delaney, "Resolution of Overlapping Echoes of Unknown Shape," *Proc. IEEE Intl. Conf. Acoust. , Speech, Sig. Proc.*, Glasgow, Scotland, 1989, pp. 2657-2660.

[6] G. C. Brown, J. H. McClellan and E. J. Holder, "Eigenstructure Approach for Array Processing and Calibration with General Phase and Gain Perturbations," *Proc. IEEE Intl. Conf. Acoust. , Speech, Sig. Proc.*, Toronto, pp. 3037-3040, 1991.

[7] A. Bruckstein, T. J. Shan and T. Kailath, "The Resolution of Overlapping Echoes," *IEEE Trans. Acoust. Speech Sig.*, vol. 33, no. 6, pp. 1357-1367, Dec. 1985.

[8] K. Buckley and L. J. Griffiths, "Broad-band Signal Subspace Spatial Spectrum (BASS-ALE) Estimation," *IEEE Trans. Acoust., Speech and Sig.*, vol. ASSP-36, no. 7, July 1988, pp. 953-964.

[9] L. Camp, *Underwater Acoustics*, Wiley-Interscience, NY, 1970.

[10] J. Cardoso, "Source Separation using Higher Order Moments," *Proc. IEEE Intl. Conf. Acoust. Speech Sig. Proc.*, pp. 2109-2112, Scotland, 1989.

[11] R. T. Compton, *Adaptive Antennas: Concepts and Performance*. Prentice-Hall, NJ, 1988.

[12] K. Farrell, R. J. Mammone and J. L. Flanagan, "Beamforming Microphone Arrays for Speech Enhancement," *Proc. IEEE Intl. Conf. Acoust. , Speech, Sig. Proc.*, San Francisco CA, pp. 285 - 288, vol. I, 1992.

[13] B. Friedlander, "A Sensitivity Analysis of the MUSIC Algorithm," *Proc. IEEE Intl. Conf. Acoust. , Speech, Sig. Proc.*, Glasgow, Scotland, pp. 2811-2814, 1989.

[14] D. R. Fuhrmann, "Estimation of Sensor Gains and Phases Using Known Field Covariance," *Proc. IEEE Intl. Conf. Acoust. , Speech, Sig. Proc.*, Toronto, pp. 1369-1372, 1991.

[15] G. H. Golub and C. F. VanLoan, *Matrix Computations*, Johns Hopkins University Press, Baltimore, MD: 1983.

[16] Y. Grenier, "A Microphone Array for Car Environments," *Proc. IEEE Intl. Conf. Acoust. , Speech, Sig. Proc.*, San Francisco CA, pp. 305 - 308, vol. I, 1992.

[17] S. Haykin (ed.), *Array Signal Processing*, Prentice-Hall, NJ, 1988.

[18] S. Haykin, *Adaptive Filter Theory*, Prentice-Hall, NJ, 1986.

[19] S. D. Hodges and P. G. Moore, "Data Uncertainties and Least Squares Regression," *Applied Statistics*, vol. 21, pp. 185-195, 1972.

[20] H. Hung and M. Kaveh, "Focusing Matrices for Coherent Signal Subspace Processing," *IEEE Trans. Acoust., Speech and Sig.*, vol. ASSP-36, no. 8, Aug. 1988, pp. 1272-1281.

[21] H. Hung and M. Kaveh, "Coherent Wideband ESPRIT method for Directions of Arrival Estimation of Multiple Wideband Sources," *IEEE Trans. Acoust., Speech and Sig.*, vol. ASSP-38, no. 2, Feb. 1990, pp. 354-356.

[22] Y. Kaneda and J. Ohga, "Adaptive Microphone-Array System for Noise Reduction," *IEEE Trans. Acoust. Speech and Sig. Proc.*, vol. ASSP-34, No. 6, Dec. 1986, pp. 1391-1400.

[23] M. Kaveh and A. J. Barabell, "The Statistical Performance of MUSIC and the Minimum-Norm Algorithms in Resolving Plane Waves in Noise," *IEEE Trans. Acoust. , Speech, Sig.*, vol. ASSP-36, pp. 331-340, Apr. 1986.

[24] S. M. Kay, *Modern Spectral Estimation: Theory and Application*, Prentice-Hall, NJ, 1988.

[25] W. Kellermann, "A Self-Steering Digital Microphone Array," *Proc. IEEE Intl. Conf. Acoust. Speech Sig. Proc.*, pp. 3581-3583, Toronto, 1991.

[26] K. Konstantinides and K. Yao, "Statistical Analysis of Effective Singular Values in Matrix Rank Determination," *IEEE Trans. Acoust., Speech and Sig. Proc.*, vo. ASSP-36, 1988, pp. 757-763.

[27] J. Krolik and D. Swingler, "Multiple Broad-band Source Location using Steered Covariance Matrices," *IEEE Trans. Acoust. , Speech, Sig.*, vol. ASSP-37, no. 10, pp. 1481-1494, Oct. 1989.

[28] R. Kumaresan, L. L. Scharf and A. K. Shaw, "An Algorithm for Pole-Zero Modeling and Spectral Analysis," *IEEE Trans. Acoust., Speech and Sig. Proc.*, vol. ASSP-34, no. 6, June 1986, pp. 637-640.

[29] E. L. Lehman, *Theory of Point Processes*, Wiley, 1983.

[30] F. Li and R. J. Vaccaro. "Statistical Comparison of Subspace Based DOA Estimation Algorithms in the Presence of Sensor Errors," *Proc. 5th ASSP Work. on Spect. Est. and Mod.*, pp. 327 - 331, Oct. 1990.

[31] J. T. Lo and S. L. Marple, "Eigenstructure Methods for Array Sensor Localization,", *Proc. IEEE Intl. Conf. Acoust. , Speech, Sig. Proc.*, Dallas TX, pp. 2260-2263, 1987.

[32] S. Oh, V. Viswanathan and P. Papamichalis, "Hands-Free Voice Communication in an Automobile with a Microphone Array," *Proc. IEEE Intl. Conf. Acoust. , Speech, Sig. Proc.*, San Francisco CA, pp. 281 - 284, vol. I, 1992.

[33] B. Ottersten and T. Kailath, "Direction-of-Arrival Estimation for Wideband Signals using the ESPRIT Algorithm," *IEEE Trans. Acoust., Speech and Sig. Proc.*, vol. ASSP-38, no. 2, Feb. 1990, pp. 317-327.

[34] B. E. Ottersten, Parameter Subspace Fitting Methods for Array Signal Processing, PhD. Dissertation, Stanford Univ. , Stanford CA, Dec. 1989.

[35] B. Ottersten, M. Viberg and T. Kailath, "Performance Analysis of the Total Least Squares ESPRIT Algorithm," *IEEE Trans. Sig. Proc.*, vol. SP-39, pp. 1122-1135, May 1991.

[36] J. Parry, "Microphone Arrays for Desktop Computers and Speech Recognition," *Proc. IEEE Intl. Conf. Acoust. Speech Sig. Proc.*, pp. 1149-1152, Alburqueque NM, 1990.

[37] E. A. Patrick, *Fundamentals of Pattern Recognition*, Englewood Cliffs, NJ, 1972.

[38] A. Paulraj and T. Kailath, "Direction of Arrival Estimation by Eigenstructure Methods with Unknown Sensor Gains and Phases," *Proc. IEEE Intl. Conf. Acoust. , Speech, Sig. Proc.*, Tampa FL, pp. 640-643, 1985.

[39] A. Paulraj, T. J. Shan, V. U. Reddy and T. Kailath, "A Subspace Approach to Determining Sensor Gain and Phase with Application to Array Processing," *Proc. SPIE*, vol. 696 (Adv. Algor. and Arch. for Sig. Proc.), pp. 102-109, 1986.

[40] J. Pierre and M. Kaveh, "Experimental Performance of Calibration and Direction-Finding Algorithms," *Proc. IEEE Intl. Conf. Acoust. , Speech, Sig. Proc.*, Toronto, pp. 1365-1368, 1991.

[41] S. U. Pillai, *Array Signal Processing*, Springer Verlag, NY, 1989.

[42] B. Porat and B. Friedlander, "Analysis of the Asymptotic Relative Efficiency of the MUSIC Algorithm," *IEEE Trans. Acoust., Speech and Sig.*, vol. ASSP-36, no. 4, Apr. 1988, pp. 532-543.

[43] B. D. Rao and K. V. S. Hari, "Performance Analysis of Root MUSIC," *IEEE Trans. Acoust. , Speech, Sig. Proc.*, vol. ASSP-37, pp. 1939-1949, Dec. 1989.

[44] B. D. Rao and K. V. S. Hari, "Performance Analysis of ESPRIT and TAM in Determining the Direction of Arrival of Plane Waves in Noise," *IEEE Trans. Acoust. , Speech, Sig. Proc.*, vol. ASSP-37, pp. 1990-1995, Dec. 1989.

[45] S. S. Reddi, "Multiple Source Location - A Digital Approach," *IEEE Trans. Aerosp. Elec. Sys.*, vol. 15, no. 1, pp. 95-105, January 1979.

[46] J. Rissanen, "Modeling by Shortest Data Description," *Automatica*, vol. 14, pp. 465-471, 1978.

[47] Y. Rockah and P. M. Schultheiss, "Array Shape Calibration Using Sources in Unknown Locations - Part I: Far Field Sources," *IEEE Trans. Acoust. Speech Sig. Proc.* , vol. 35, no. 3, pp. 286-299, March 1987.

[48] Y. Rockah and P. M. Schultheiss, "Array Shape Calibration Using Sources in Unknown Locations - Part II: Near Field Sources and Estimation Implementation", *IEEE Trans. Acoust. Speech Sig. Proc.* , vol. 35, no. 6, pp. 724-735, June 1987.

[49] M. Rossi, *Acoustics and Electroacoustics*, Artech House, Norwood MA, 1988.

[50] R. Roy and T. Kailath, "ESPRIT - Estimation of Signal Parameters via Rotational Invariance Techniques," *IEEE Trans. Acoust. , Speech, Sig. Proc.*, vol. ASSP-37, pp. 984-993, July 1989.

[51] L. L. Scharf, *Statistical Signal Processing*, Prentice-Hall, NJ, 1991.

[52] R. O. Schmidt, "Multiple Emitter Location and Signal Parameter Estimation," *Proc. RADC Spectral Est. Work.*, Griffiths AFB, Rome NY, pp. 243-256, 1977.

[53] R. O. Schmidt, "Multiple Emitter Location and Signal Parameters Estimation," *IEEE Trans. Antenn. Propag.* vol. AP-34, pp. 276-280, March 1986.

[54] G. Schwartz, "Estimating the Dimensions of a Model," *Ann. Stat.*, vol. 6, pp. 461-464, 1978.

[55] W. W. Seto, *Acoustics, Schaum's Outline Series in Engineering*, McGraw Hill, NY 1971.

[56] T. J. Shan, M. Wax and T. Kailath, "On Spatial Smoothing for Direction-of-Arrival Estimation of Coherent Signals," *IEEE Trans. Acoust. Speech and Sig. Proc.*, vol. ASSP-27, No. 6, June. 1985, pp. 527-536.

[57] H. F. Silverman, "Some Analysis of Microphone Arrays for Speech Data Acquisition," *IEEE Trans. Acoust. Speech and Sig. Proc.*, vol. ASSP-35, No. 12, Dec. 1987, pp. 1699-1712.

[58] M. L. Skolnik, *Introduction to Radar Systems*, McGraw-Hill, NY, 1980.

[59] J. O. Smith and J. S. Abel, "Closed-Form Least-Squares Source Location Estimation from Range-Difference Measurements," *IEEE Trans. Acoust. Speech and Sig. Proc.*, vol. ASSP-35, No. 12, Dec. 1987, pp. 1661-1669.

[60] V. C. Soon and Y. F. Huang, "An Analysis of ESPRIT under Random Sensor Uncertainties," *Proc. of the 28th Annual Allerton Conf. on Comm. , Contr. and Comp.*, Urbana-Champaign, pp. 334-343, 1990.

[61] V. C. Soon, L. Tong, Y. F. Huang and R. Liu, "An Extended Fourth Order Blind Identification Algorithm in Spatially Correlated Noise," *Proc. IEEE Intl. Conf. Acoust. , Speech, Sig. Proc.*, Alburquque NM, 1990.

[62] P. Stoica and A. Nehorai, "MUSIC, Maximum Likelihood and Cramer-Rao Bound," *IEEE Trans. Acoust. , Speech. Sig. Proc.*, vol. ASSP-37, pp. 720-741, May 1989.

[63] P. Stoica and A. Nehorai, "Performance Comparison of Subspace Rotation and MUSIC Methods for Direction Estimation," *Proc. 5th ASSP Work. on Spect. Est. and Mod.*, pp. 357-361, Oct. 1990.

[64] P. Stoica and A. Nehorai, "Performance Study of Conditional and Unconditional Direction-of-Arrival Estimation," *IEEE Trans. Acoust. Speech Sig.*, vol. 38, no. 10, pp. 1783-1795, October 1990.

[65] G. Su and M. Morf, "Modal Decomposition Signal Subspace Algorithms," *IEEE Trans. Acoust., Speech and Sig.*, vol. ASSP-34, no. 3, June 1986, pp. 585-602.

[66] B. P. Suard, *Spatial Diversity in Cellular Networks*, MS Thesis, MIT, Cambridge, May 1992.

[67] A. Swindlehurst and T. Kailath, "A Performance Analysis of Subspace-Based Methods in the Presence of Model Errors - Part I: The MUSIC Algorithm," *IEEE Trans. Sig. Proc.*, in review.

[68] A. L. Swindlehurst and T. Kailath, "An Analysis of the Subspace Fitting Algorithm in the Presence of Sensor Errors," *Proc. IEEE Intl. Conf. Acoust. , Speech, Sig. Proc.*, Alburqueque NM, pp. 2647-2650, 1990.

[69] A. L. Swindlehurst and T. Kailath, "On the Sensitivity of the ESPRIT Algorithm to Non-Identical Subarrays," *Sadhana, Proc. Indian Acad. Sci. in Eng.*, 1991.

[70] L. Tong, R. Liu, V. C. Soon and Y. F. Huang, "The Indeterminacy and Identifiability of Blind Identification," *IEEE Trans. Circ. Sys.*, vol. CAS-38, no. 5, May 1991, pp. 499-509.

[71] L. Tong, V. C. Soon, Y. F. Huang and R. Liu, "Multiple Source Signal Separation in Noise," *Proc. of the 27th Annual Allerton Conf. on Comm. , Contr. and Comp.*, Urbana-Champaign, 1989.

[72] L. Tong, Blind Channel Identification and Blind Signal Estimation, PhD Dissertation, University of Notre Dame, Notre Dame IN, 1990.

[73] L. Tong and Y. Inouye and R. Liu, "A Finite-Step Global Convergence Algorithm for the Parameter Estimation of Multichannel MA Processes", *IEEE Trans. Signal Processing*, to appear.

[74] L. Tong and Y. Inouye and R. Liu, "Waveform Preserving Blind Estimation of Multiple Independent Sources", *IEEE Trans. Signal Processing*, to appear.

[75] H. Wang and M. Kaveh, "Coherent Signal-Subspace Processing for the Detection and Estimation of Angles of Arrival of Multiple Wideband Sources" *IEEE Trans. Acoust., Speech and Sig. Proc.*, vol. ASSP-33, no. 4, Aug. 1985, pp. 823-831.

[76] M. Wax and I. Ziskind, "On Unique Localization of Multiple Sources by Passive Sensor Arrays," *IEEE Trans. Acoust. Speech Sig.* , vol. 37, no. 7, pp. 996-1000, July 1989.

[77] M. Wax and T. Kailath, "Detection of Signals by Information Theoretic Criterion," *IEEE Trans. Acoust. Speech Sig.*, vol. 33, no. 2, pp. 387-392, April 1985.

[78] M. Wax, T. J. Shan and T. Kailath, "Spatio-temporal Spectral Analysis by Eigenstructure Methods," *IEEE Trans. Acoust., Speech and Sig. Proc.*, vo. ASSP-32, Aug. 1984, pp. 817-827.

[79] A. J. Weiss and B. Friedlander, "Eigenstructure Methods for Direction Finding with Sensor Gain and Phase Uncertainties," *J. Circ. Sys. Sig. Proc.*, vol. 9, pp. 271-300, 1990.

[80] A. J. Weiss and B. Friedlander, "Array Shape Calibration Using Sources in Unknown Locations - A Maximum Likelihood Approach," *IEEE Trans. Acoust. Speech Sig. Proc.* , vol. 37, no. 12, pp. 1958-1966, December 1989.

[81] A. J. Weiss, A. S. Willsky and B. C. Levy, "Eigenstructure Approach for Array Processing with Unknown Intensity Coefficients," *IEEE Trans. Acoust., Speech and Sig. Proc.*, vol. ASSP-36, no. 10, Oct. 1988, pp. 1613-1617.

[82] K. M. Wong, R. S. Walker and G. Niezgoda, "Effects of Random Sensor Motion on Bearing Estimation by the MUSIC Algorithm," *Proc. Inst. Elec. Eng.* , vol. 135, pt. F, pp. 233-250, June 1988.

[83] B. D. Van Veen and K. M. Buckley, "Beamforming: A Versatile Approach to Spatial Filtering," *IEEE ASSP Mag.*, pp. 4 - 24, Apr. 1986.

[84] I. Ziskind and M. Wax, "Maximum Likelihood Localization of Multiple Sources by Alternating Projection," *IEEE Trans. Acoust., Speech and Sig.*, vol. ASSP-36, no. 10, Oct. 1988, pp. 1553-1560.